Um sobrevoo do problema da fadiga

Paulo M. S. Tavares de Castro

Faculdade de Engenharia Universidade do Porto
Rua Dr. Roberto Frias
4200-465 Porto
Portugal

Introdução – exs. de casos

- **Haste**
- **Ligação soldada**

Referência a conceitos básicos

- **Bibliografia de autores do DEMec da FEUP**

Propagação de fendas

- **Expansão de furos**

Propagação de fendas em modo misto

- **O caso da flexão em 4 pontos**

Métodos numéricos – o XFEM

Introdução – exs. de casos

- Haste
- Ligação soldada

Referência a conceitos básicos

- Bibliografia de autores do DEMec da FEUP

Propagação de fendas

- Expansão de furos

Propagação de fendas em modo misto

- O caso da flexão em 4 pontos

Métodos numéricos – o XFEM

technical drawing and fracture location

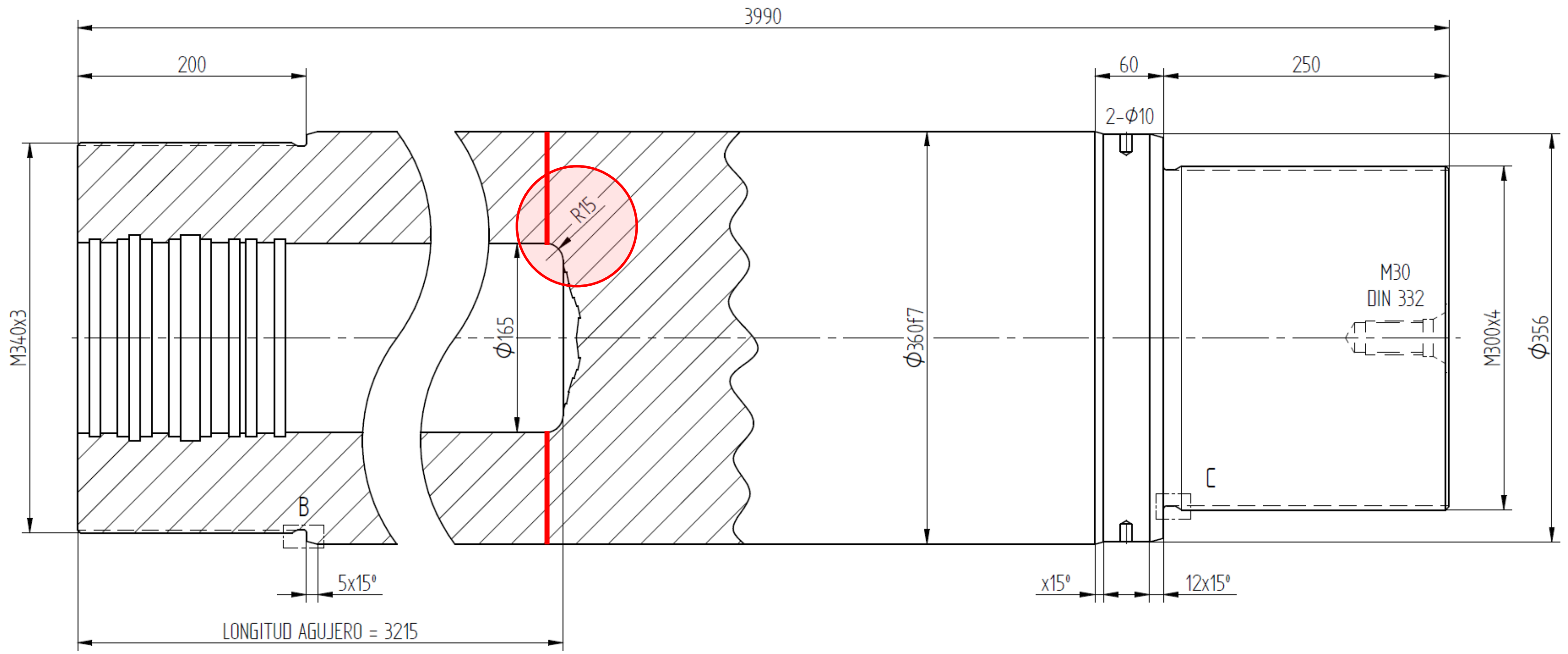

S.M.O. Tavares, N. Viriato, M. Vaz, P.M.S.T. de Castro, ‘Failure analysis of the rod of a hydraulic cylinder’, *Procedia Structural Integrity*, vol.1, pp.173-180, 2016

S.M.O. Tavares, N. Viriato, M. Vaz, P.M.S.T. de Castro, ‘Failure analysis of the rod of a hydraulic cylinder’, *Procedia Structural Integrity*, vol.1, pp.173-180, 2016

fatigue testing machine for large cables for marine applications

Lankhorst, Maia, Portugal; >1500 t capacity

4m long rod, ext. diam. 340mm

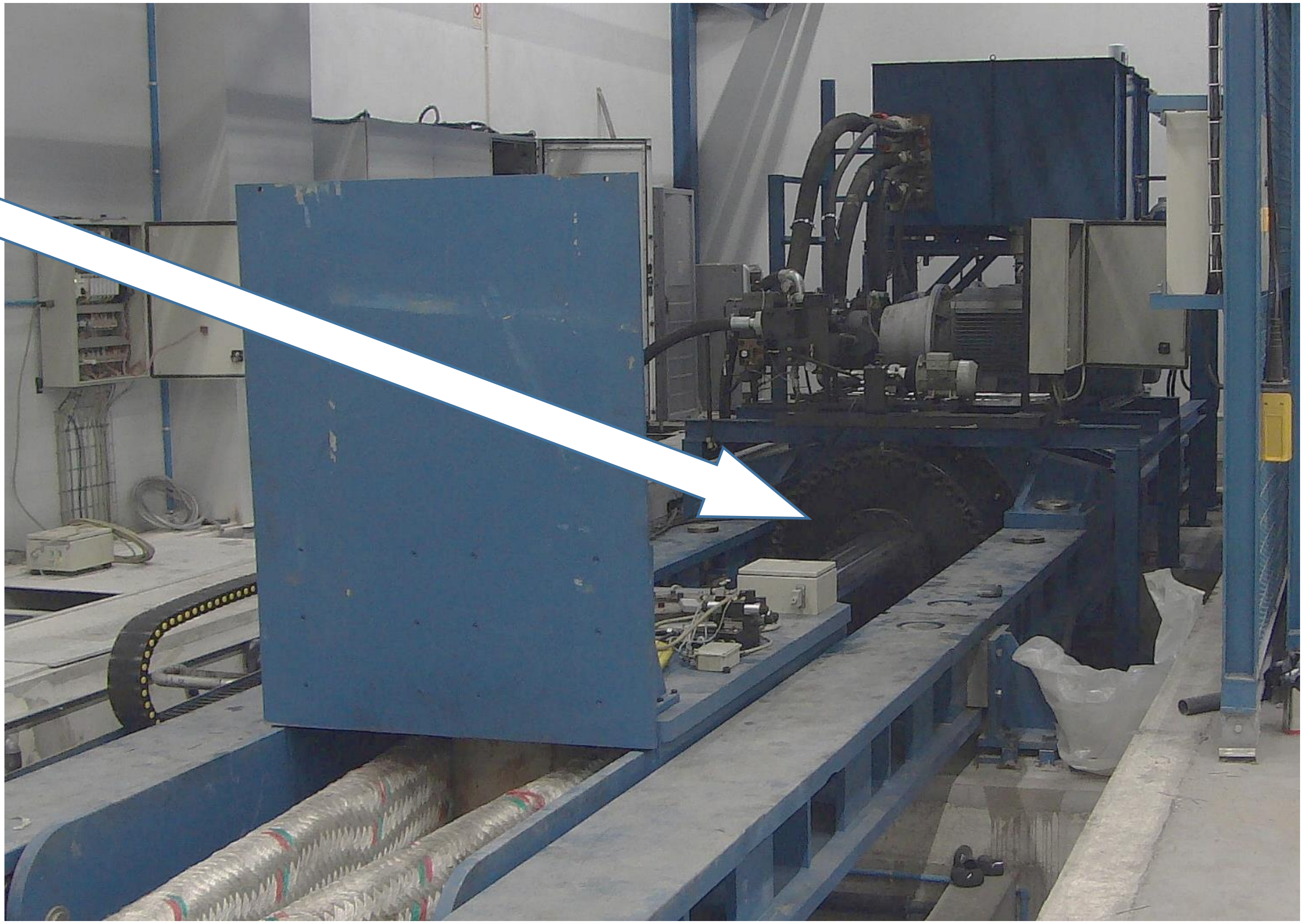

Welding and Cutting, vol.14, 2015, (2), p.80

another example of high capacity fatigue testing
TWI, Abington, UK; max. load ~600 t

S.M.O. Tavares, N. Viriato, M. Vaz, P.M.S.T. de Castro, 'Failure analysis of the rod of a hydraulic cylinder', *Procedia Structural Integrity*, vol.1, pp.173-180, 2016

fractured rod of the hydraulic cylinder

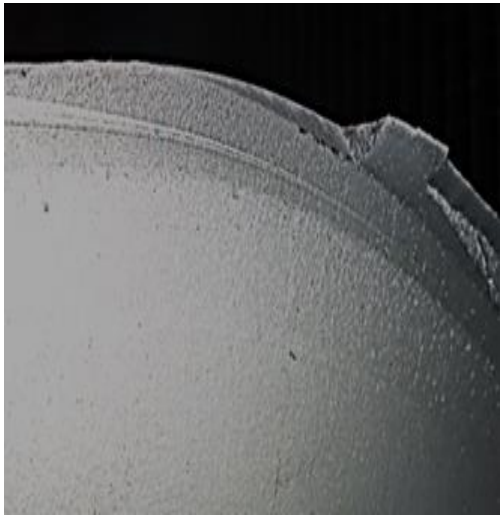

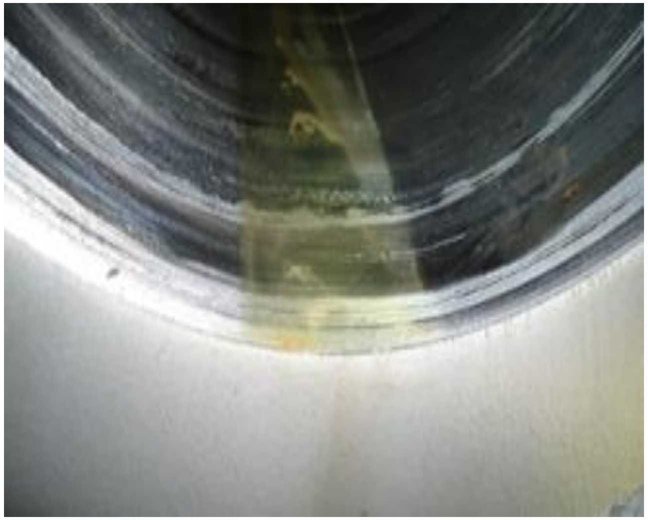

- 42CrMo4 steel (σ_{UTS}=830 MPa; σ_{YS}=621 MPa)
- length: 3990 mm
- external diameter: 340 mm
- internal diameter: 165 mm

S.M.O. Tavares, N. Viriato, M. Vaz, P.M.S.T. de Castro, 'Failure analysis of the rod of a hydraulic cylinder', *Procedia Structural Integrity*, vol.1, pp.173-180, 2016

fractured rod of the hydraulic cylinder

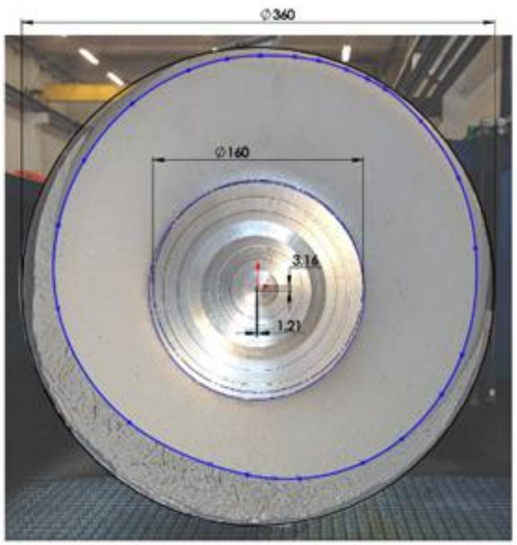

fatigue and final rupture surface

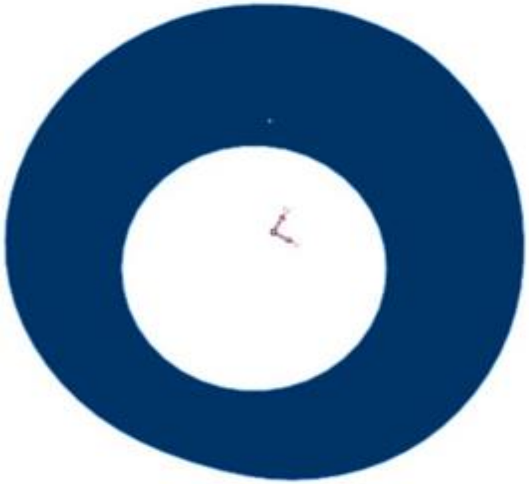

fatigue surface area

final rupture area

it was noticed that the hollow cylinder is not precisely concentric and fatigue surface area indicates that the cylinder was loaded with some bending stress (study performed using Solidworks)

S.M.O. Tavares, N. Viriato, M. Vaz, P.M.S.T. de Castro, 'Failure analysis of the rod of a hydraulic cylinder', *Procedia Structural Integrity*, vol.1, pp.173-180, 2016

two common approaches that have been employed to design shafts based on standards are:

(i) ANSI/ASME B106.1M, "Design of Transmission Shafting", last edition in 1984

(ii) DIN 743, "Calculation of load capacity of shafts and axles" (German standard), last edition in 2012

the ASME approach is based upon a concept of static equivalent stress using Soderberg's criterion

the DIN procedure for shaft fatigue design is based upon the amplitude of the normal stress and the amplitude of the shear stress. The normal stress is separated into its components resulting from axial load and from bending

S.M.O. Tavares, N. Viriato, M. Vaz, P.M.S.T. de Castro, 'Failure analysis of the rod of a hydraulic cylinder', *Procedia Structural Integrity*, vol.1, pp.173-180, 2016

Stress concentration factor

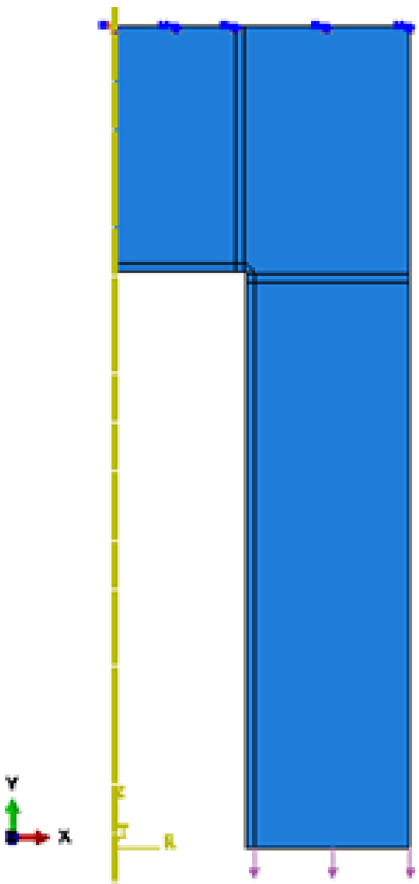

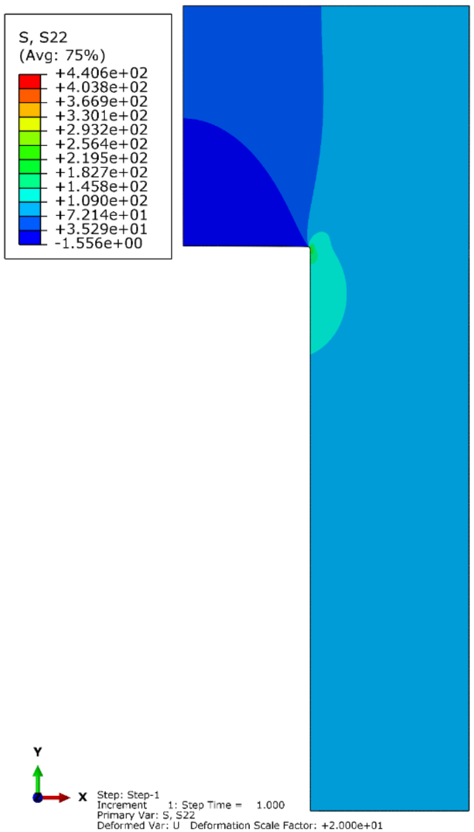

- **for the stress concentration factor determination, finite elements were performed in Abaqus with axisymmetric elements**

- **in the different rod radius analyses, different element sizes were evaluated in order to study the mesh sensitivity in the stress concentration factor**

S.M.O. Tavares, N. Viriato, M. Vaz, P.M.S.T. de Castro, 'Failure analysis of the rod of a hydraulic cylinder', *Procedia Structural Integrity*, vol.1, pp.173-180, 2016

Stress concentration factor

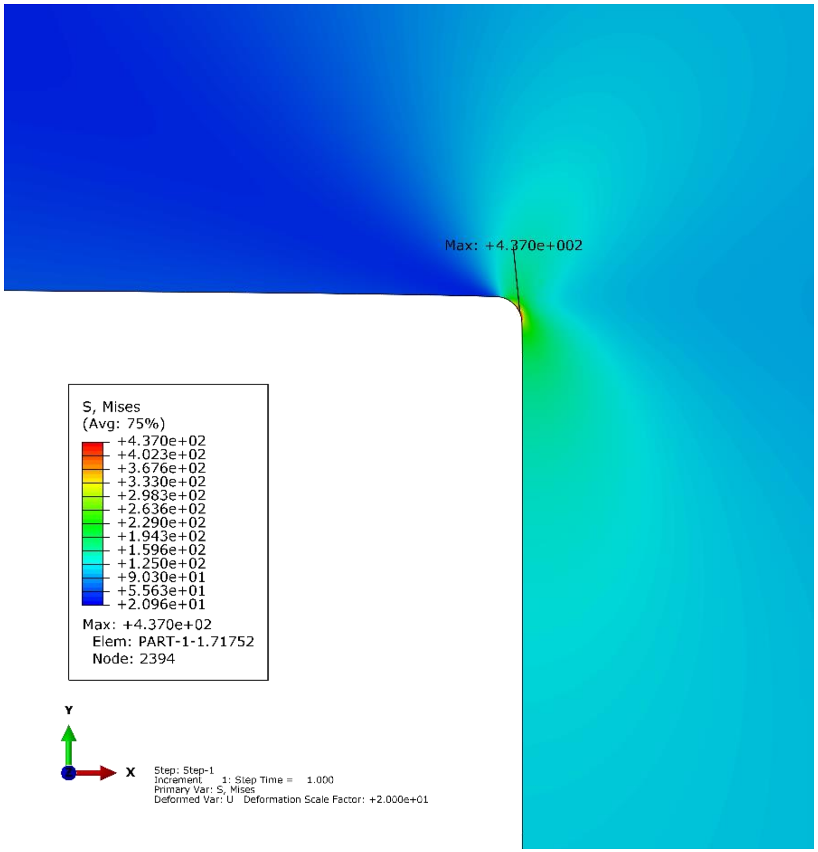

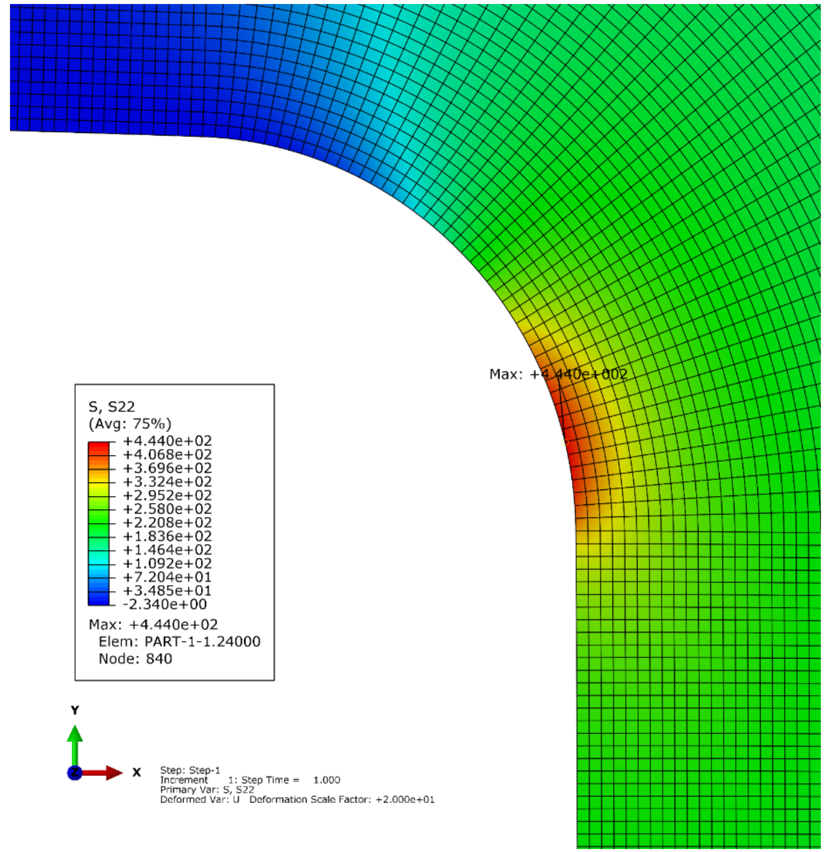

von Mises stress field and σ_{yy} in the critical point

S.M.O. Tavares, N. Viriato, M. Vaz, P.M.S.T. de Castro, 'Failure analysis of the rod of a hydraulic cylinder', *Procedia Structural Integrity*, vol.1, pp.173-180, 2016

Stress concentration factor

stress concentration factor calibration

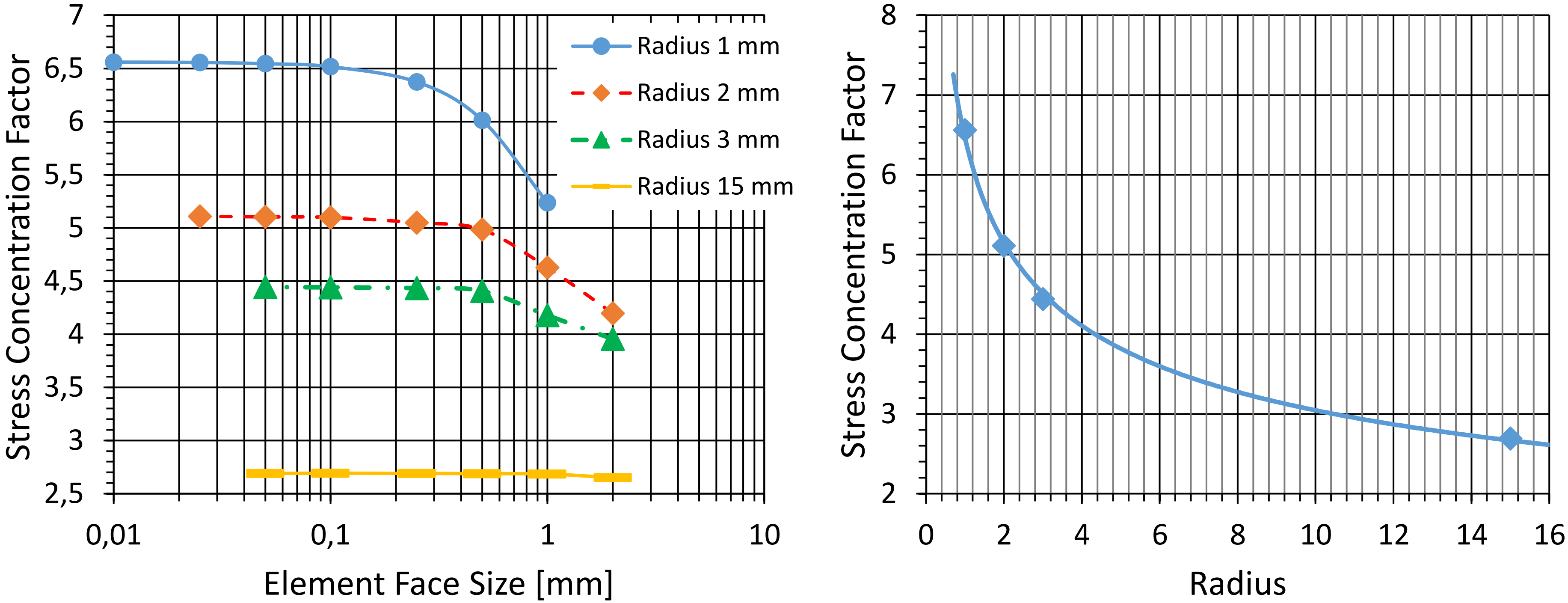

the evolution of the concentration factor for the different radii shows that using quadratic elements, the element face width should be 10 times less than the radius

S.M.O. Tavares, N. Viriato, M. Vaz, P.M.S.T. de Castro, ‘Failure analysis of the rod of a hydraulic cylinder’, *Procedia Structural Integrity*, vol.1, pp.173-180, 2016

Stress concentration factor

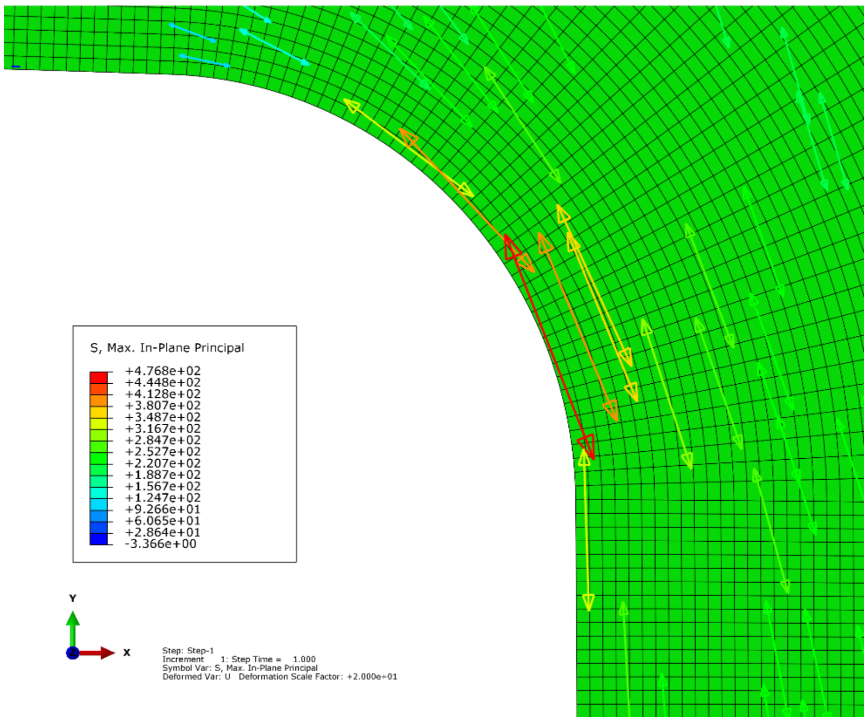

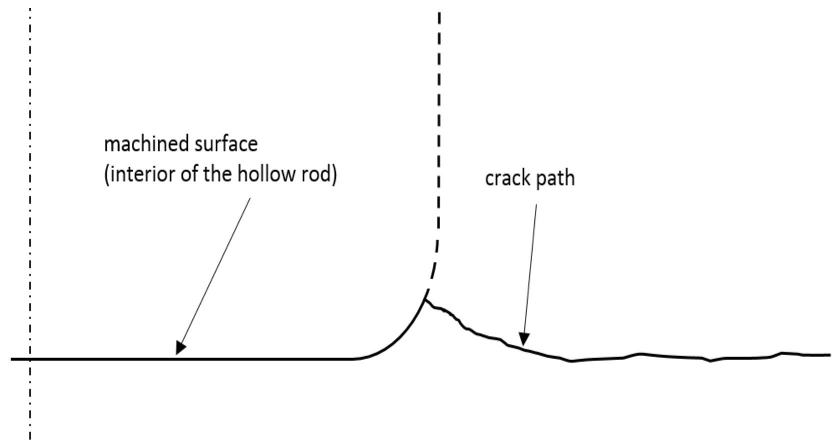

the direction of maximum stress and the ledge on the fracture and the respective positions are in accordance

Bernardo F. de Mendonça, Paulo M.S.T. de Castro, 'Rupture of the girth gear / kiln shell connection at an expanded clay factory', *Anales de Mecánica de la Fractura*, 2020

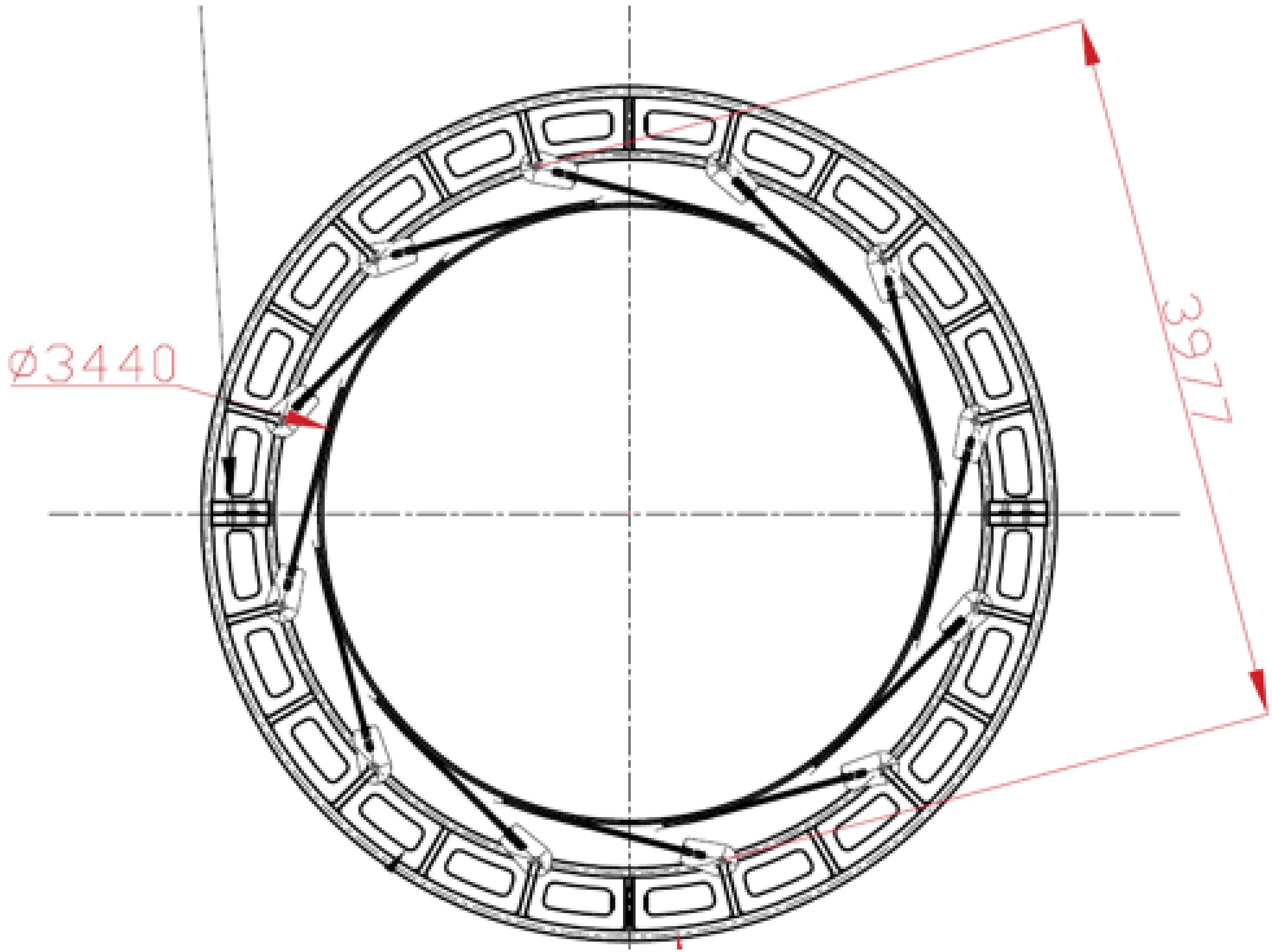

Bernardo F. de Mendonça, Paulo M.S.T. de Castro, 'Rupture of the girth gear / kiln shell connection at an expanded clay factory', *Anales de Mecánica de la Fractura*, 2020

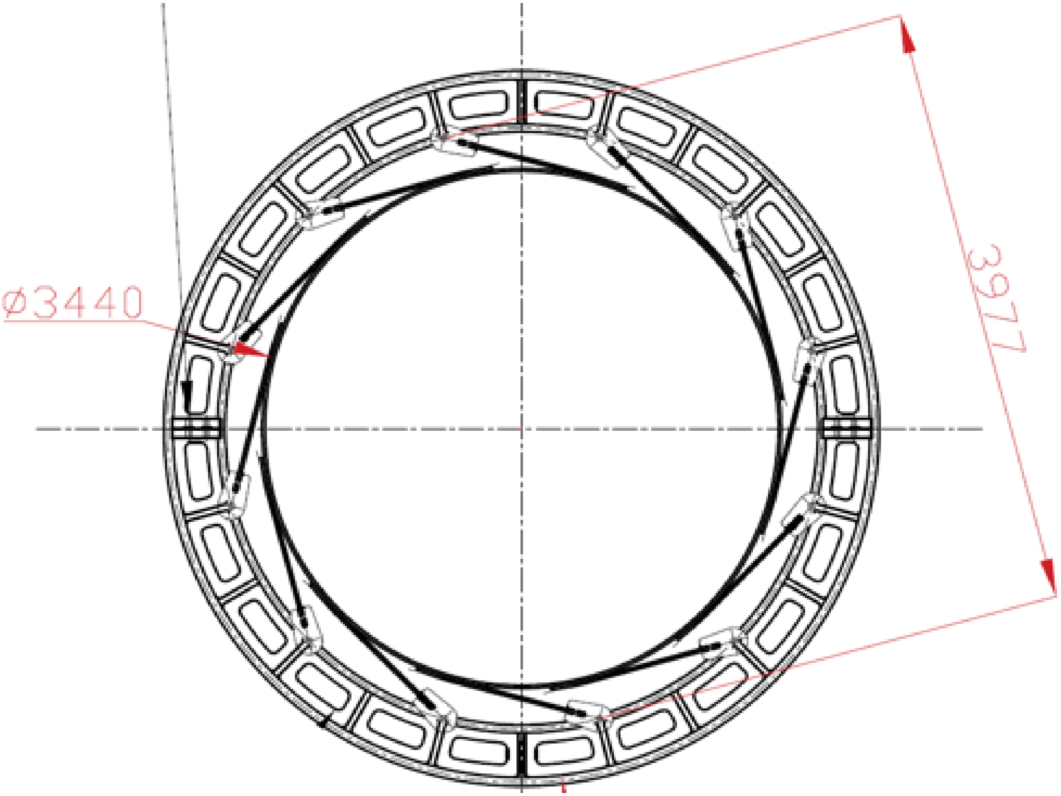

Bernardo F. de Mendonça, Paulo M.S.T. de Castro, 'Rupture of the girth gear / kiln shell connection at an expanded clay factory', *Anales de Mecánica de la Fractura*, 2020

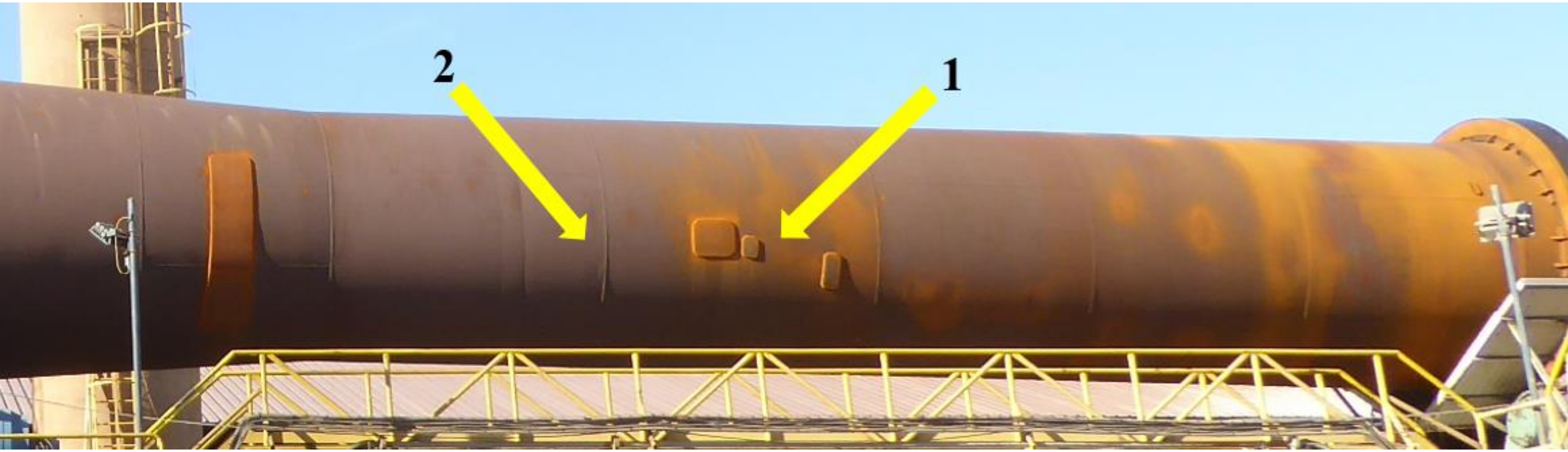

Bernardo F. de Mendonça, Paulo M.S.T. de Castro, 'Rupture of the girth gear / kiln shell connection at an expanded clay factory', *Anales de Mecánica de la Fractura*, 2020

Bernardo F. de Mendonça, Paulo M.S.T. de Castro, ‘Rupture of the girth gear / kiln shell connection at an expanded clay factory’, *Anales de Mecánica de la Fractura*, 2020

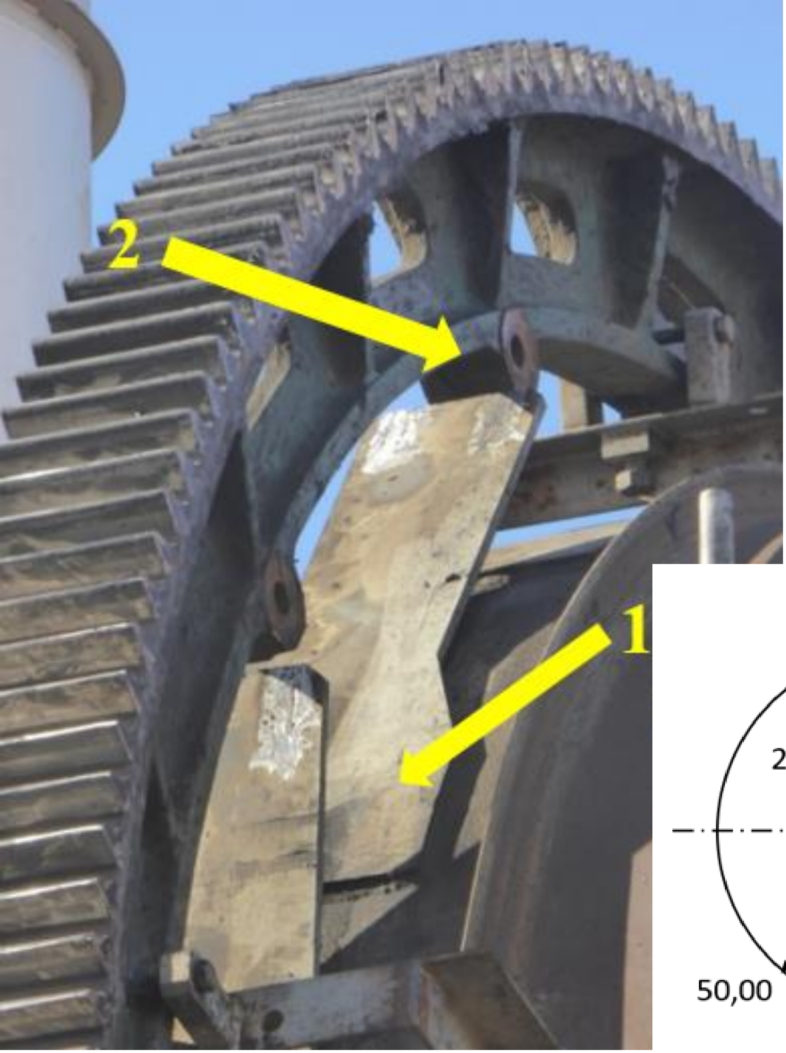

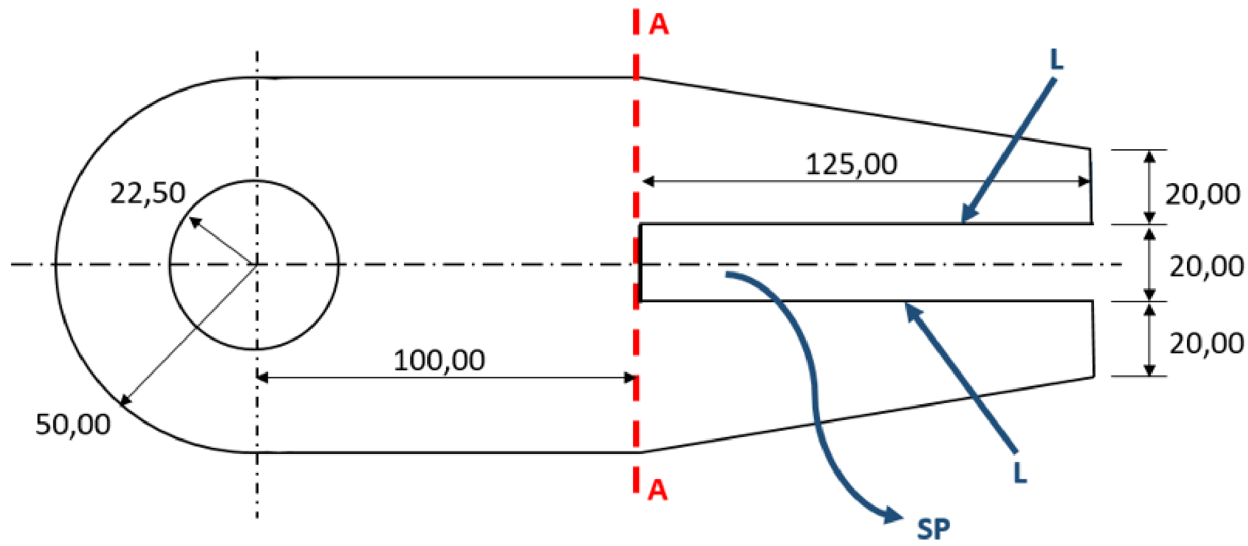

Bernardo F. de Mendonça, Paulo M.S.T. de Castro, ‘Rupture of the girth gear / kiln shell connection at an expanded clay factory’, *Anales de Mecánica de la Fractura*, 2020

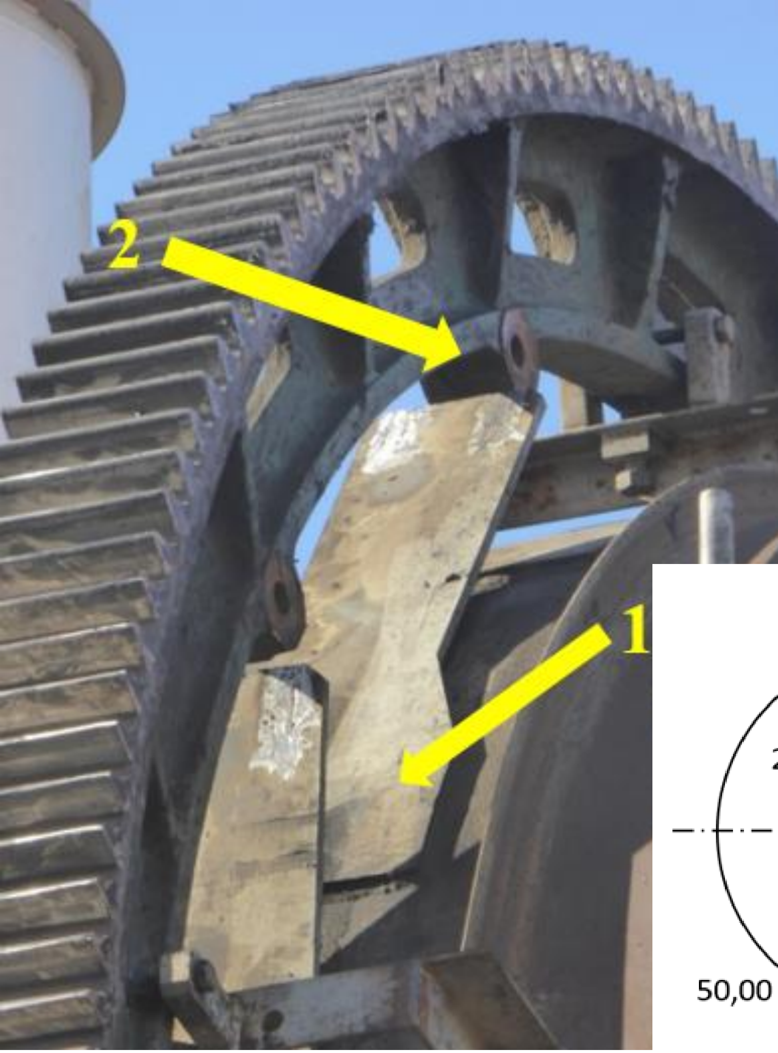

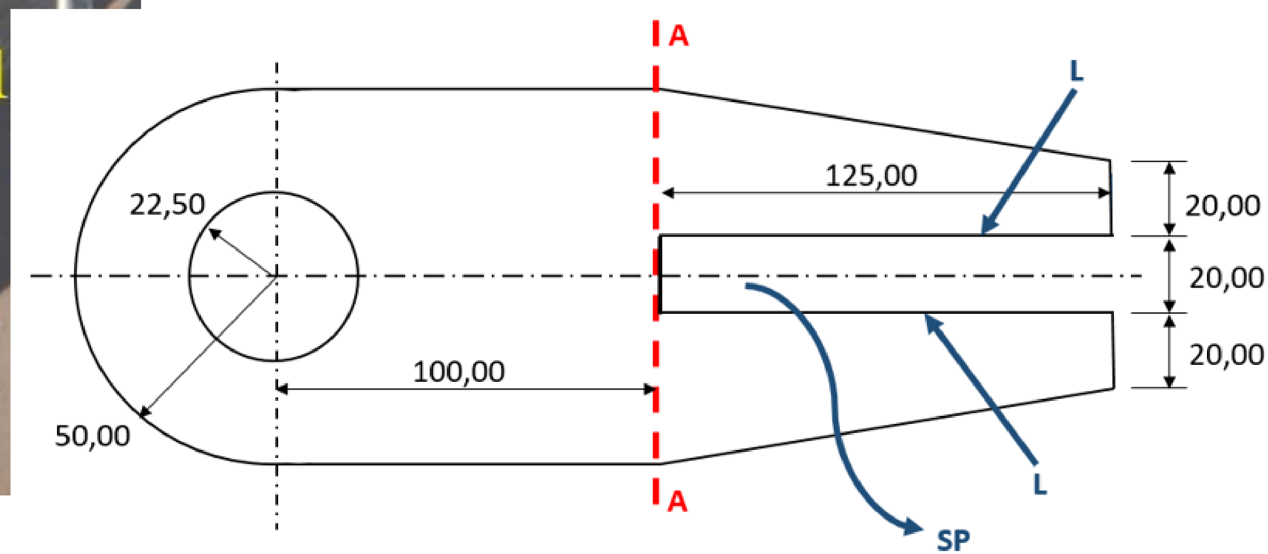

Bernardo F. de Mendonça, Paulo M.S.T. de Castro, 'Rupture of the girth gear / kiln shell connection at an expanded clay factory', *Anales de Mecánica de la Fractura*, 2020

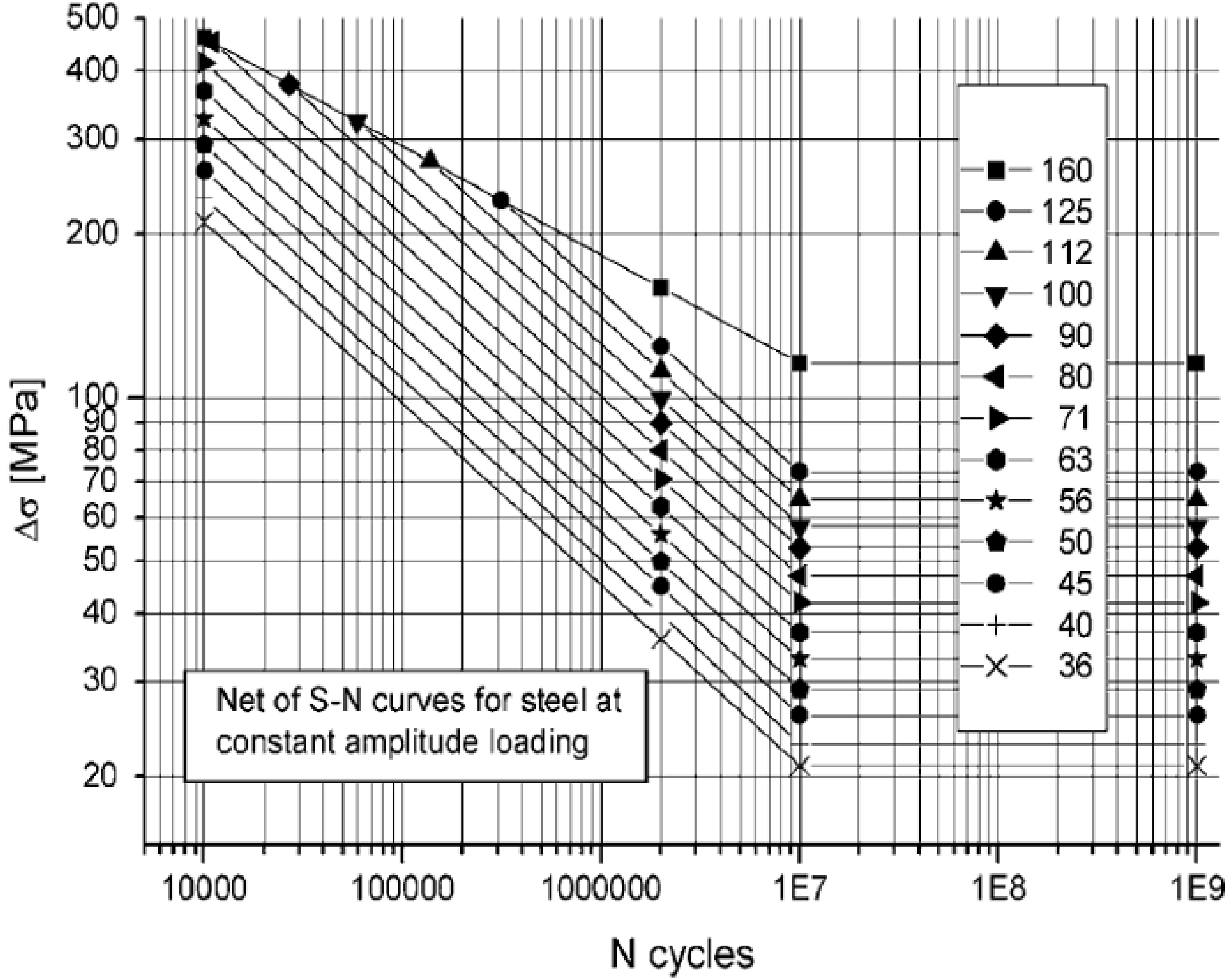

Bernardo F. de Mendonça, Paulo M.S.T. de Castro, ‘Rupture of the girth gear / kiln shell connection at an expanded clay factory’, *Anales de Mecánica de la Fractura*, 2020

Bernardo F. de Mendonça, Paulo M.S.T. de Castro, 'Rupture of the girth gear / kiln shell connection at an expanded clay factory', *Anales de Mecánica de la Fractura*, 2020

Introdução – exs. de casos

- **Haste**
- **Ligação soldada**

Referência a conceitos básicos

- Bibliografia de autores do DEMec da FEUP

Propagação de fendas

- Expansão de furos

Propagação de fendas em modo misto

- O caso da flexão em 4 pontos

Métodos numéricos – o XFEM

estudos a várias escalas

- provete
- ligação estrutural
- módulo estrutural
- estrutura completa

………..

e com vários objectivos

- iniciação de fendas
- propagação de fendas
- resistência residual

…….

M. Zimmermann, 'Very High Cycle Fatigue', chapter #57 of C.-H. Hsueh et al. (eds.), Handbook of Mechanics of Materials, Springer 2019, pp.1879-1916 – see Figure 3, p.1884

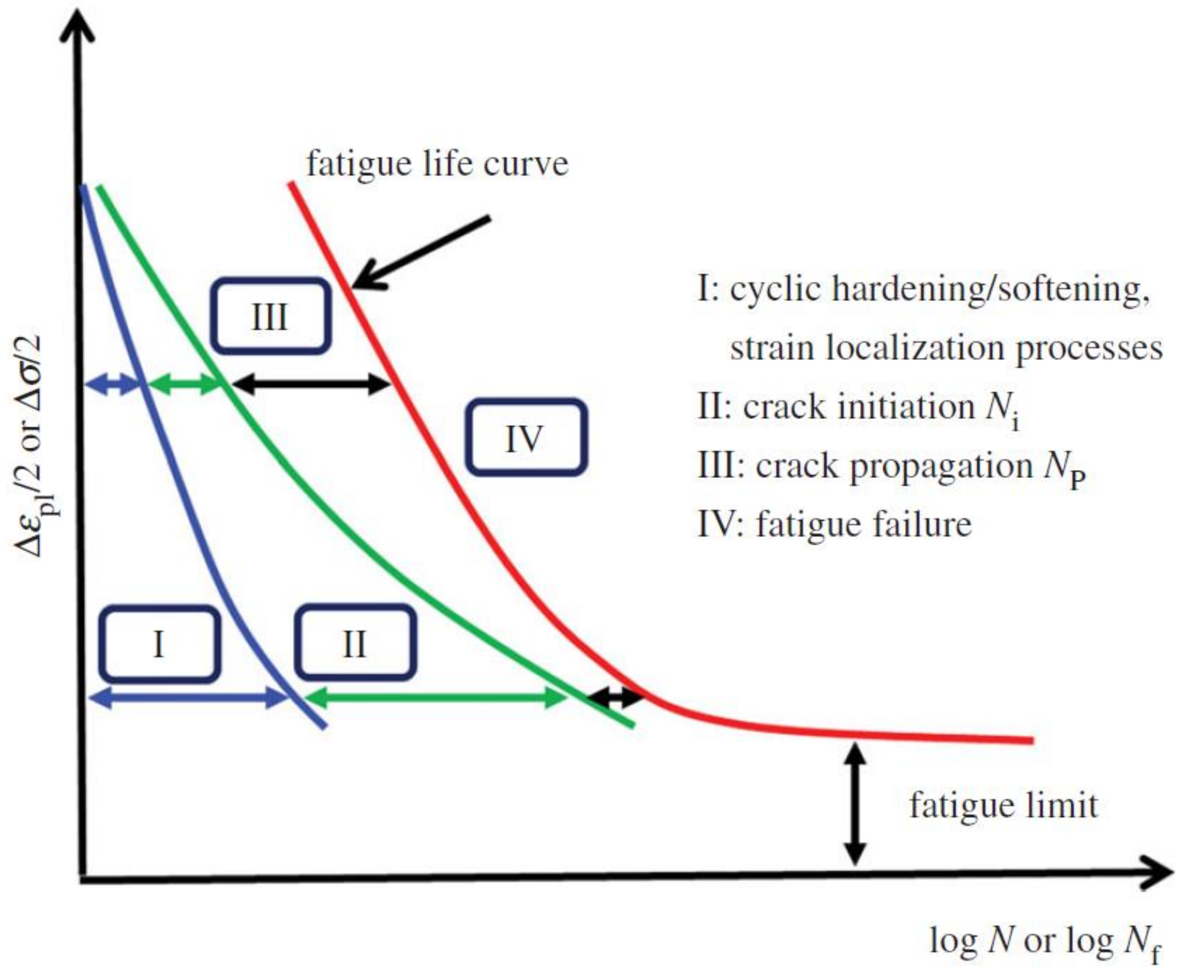

H. Mughrabi, 'Microstructural mechanisms of cyclic deformation, fatigue crack initiation and early crack growth', *Philosophical Transactions of the Royal Society A*, vol.373, (2038), 2015

problemas

iniciação

• Wöhler, curvas SN baseadas em tensões elásticas

propagação

• lei de Paris

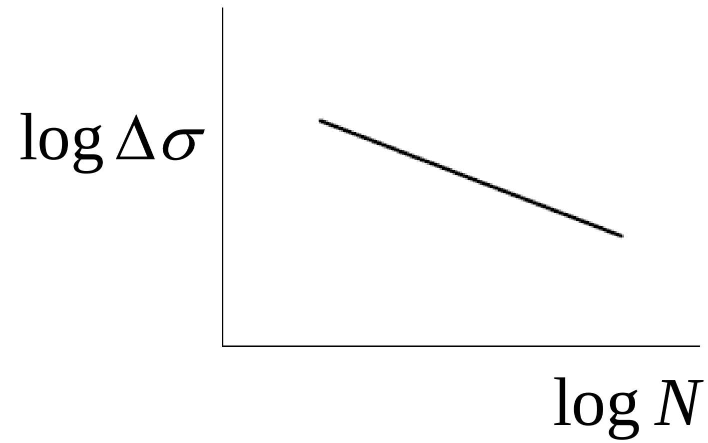

entre outros desenvolvimentos

iniciação

• estudos elasto-plásticos: Coffin-Manson,
Neuber, ...

propagação

• razão de carga R = carga max load/carga min, limiare de propagação, ...

Acumulação de dano

• Miner, ...

....

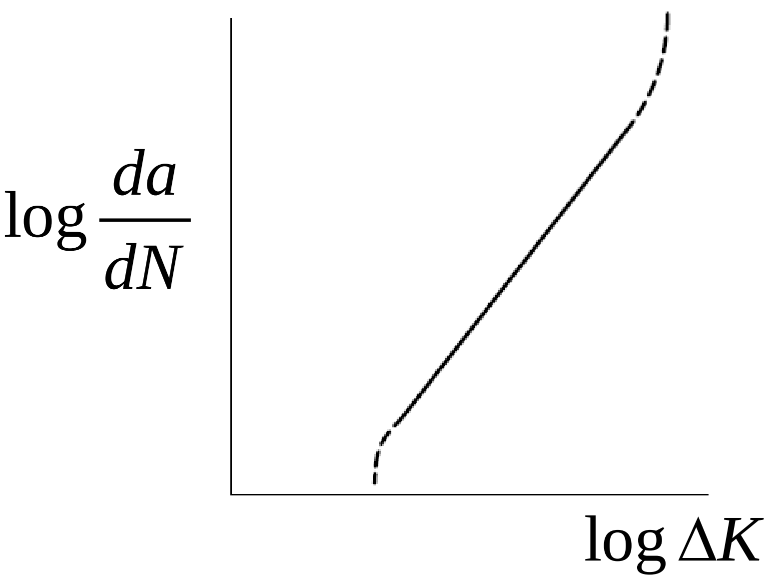

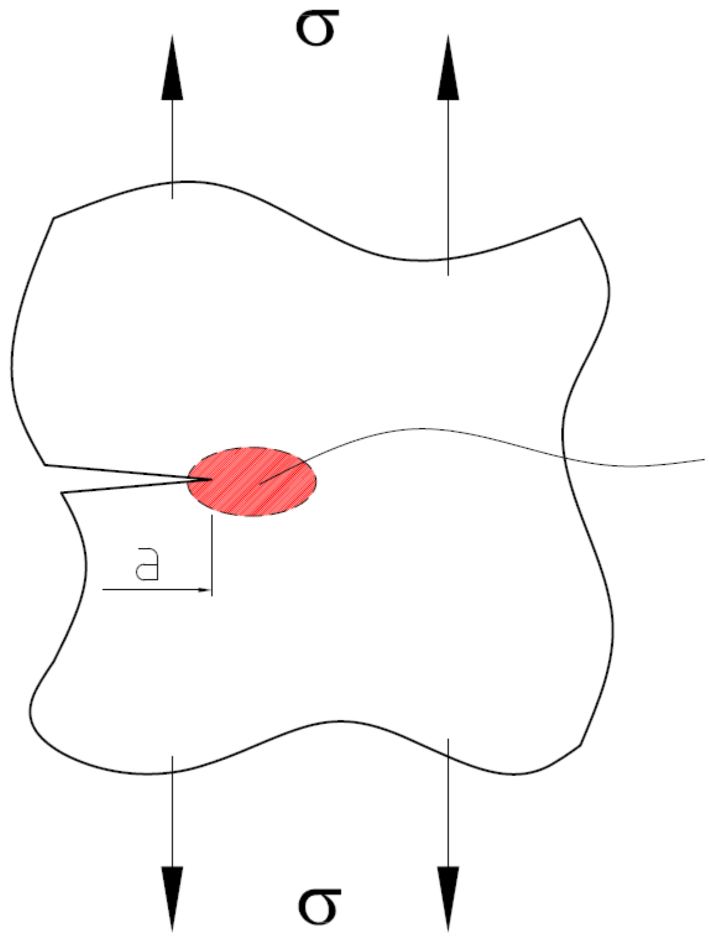

$$\sigma_{local} = f(K)$$

$$K = Y\sigma\sqrt{\pi a}$$

$$\sigma_x = \frac{K_I}{\sqrt{2\pi r}} \cos\frac{\theta}{2}\left(1-\sin\frac{\theta}{2}\sin\frac{3\theta}{2}\right)$$

$$\sigma_y = \frac{K_I}{\sqrt{2\pi r}} \cos\frac{\theta}{2}\left(1+\sin\frac{\theta}{2}\sin\frac{3\theta}{2}\right)$$

$$\tau_{xy} = \frac{K_I}{\sqrt{2\pi r}} \cos\frac{\theta}{2}\sin\frac{\theta}{2}\cos\frac{3\theta}{2}$$

$$\sigma_z = 0 \quad , \quad \text{ou} \quad \sigma_z = \nu\left(\sigma_x + \sigma_y\right)$$

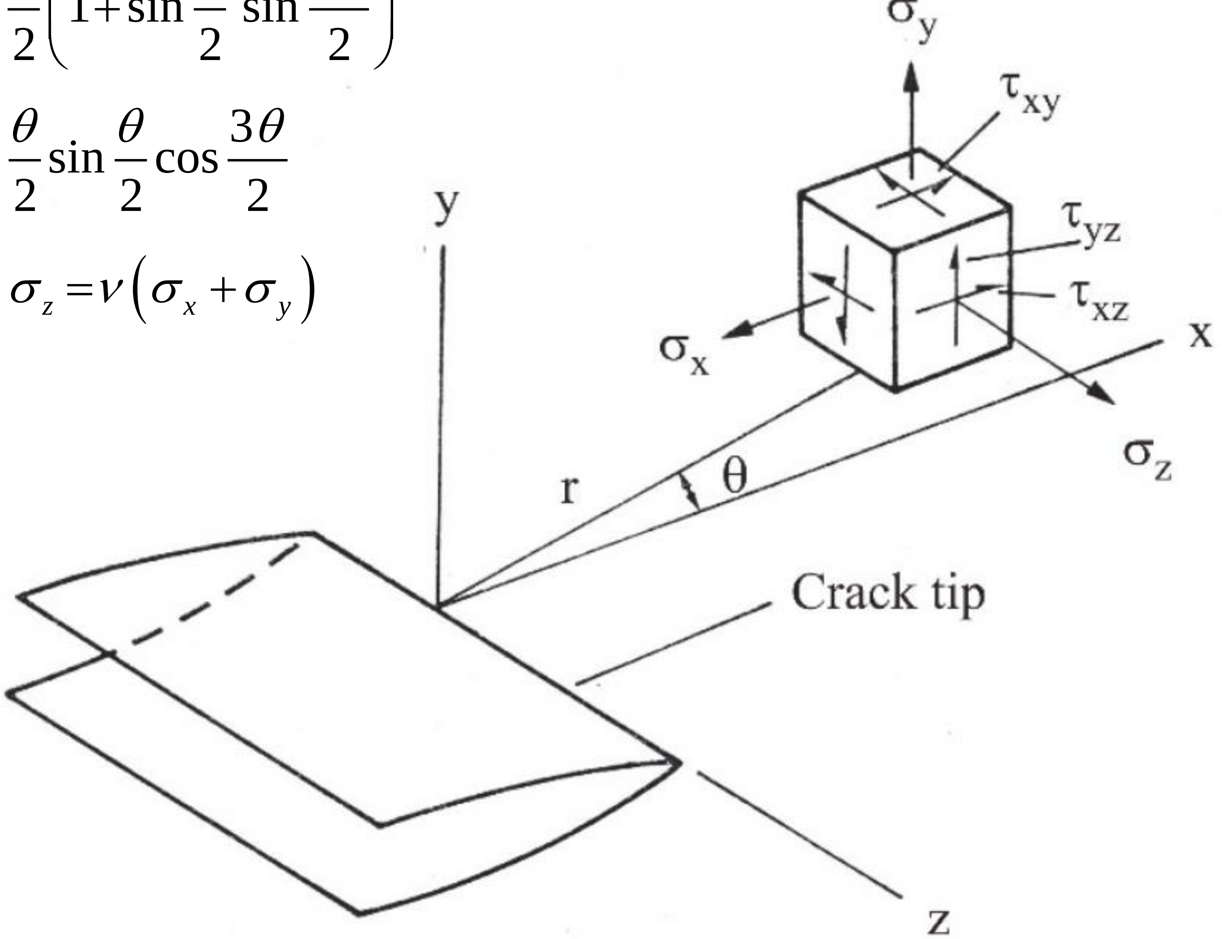

carregamentos:

forças, deslocamentos, condições fronteira

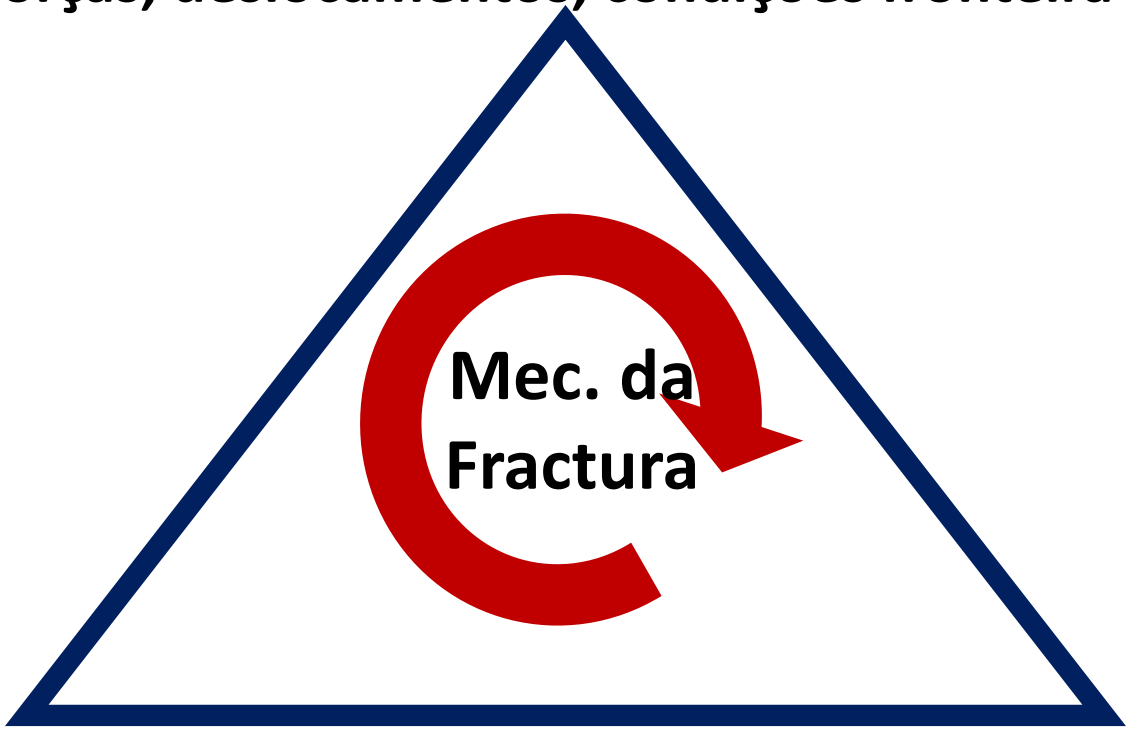

fendas

comp. ‘*a*’, ou geometria…

propriedades mecânicas

tensão de ced., tenacidade,

…

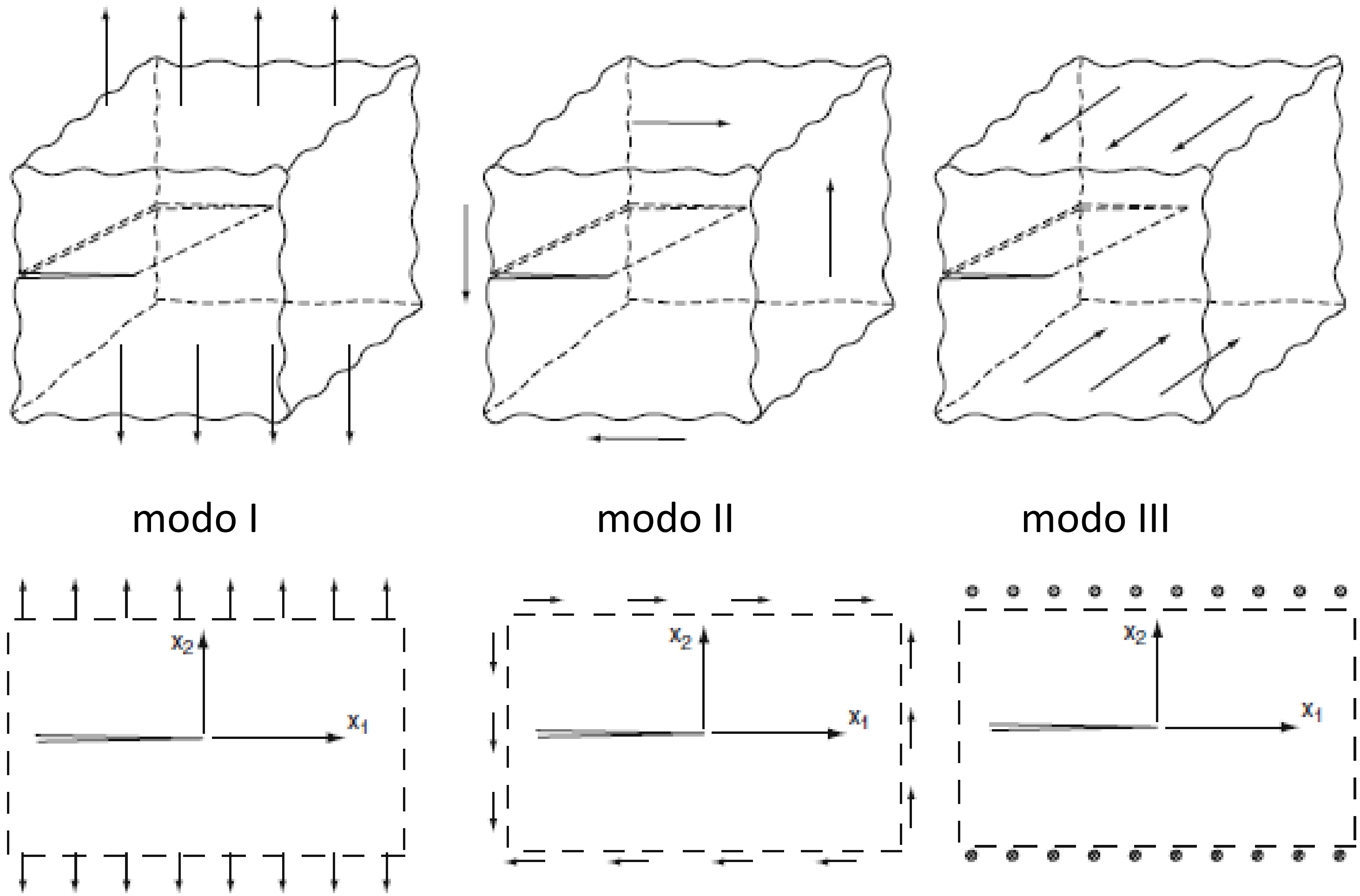

A.T. Zehnder, 'Modes of fracture', in: Q.J. Wang, Y.-W. Chung, eds., 'Encyclopedia of Tribology', Springer, pp.2292-2295, 2013

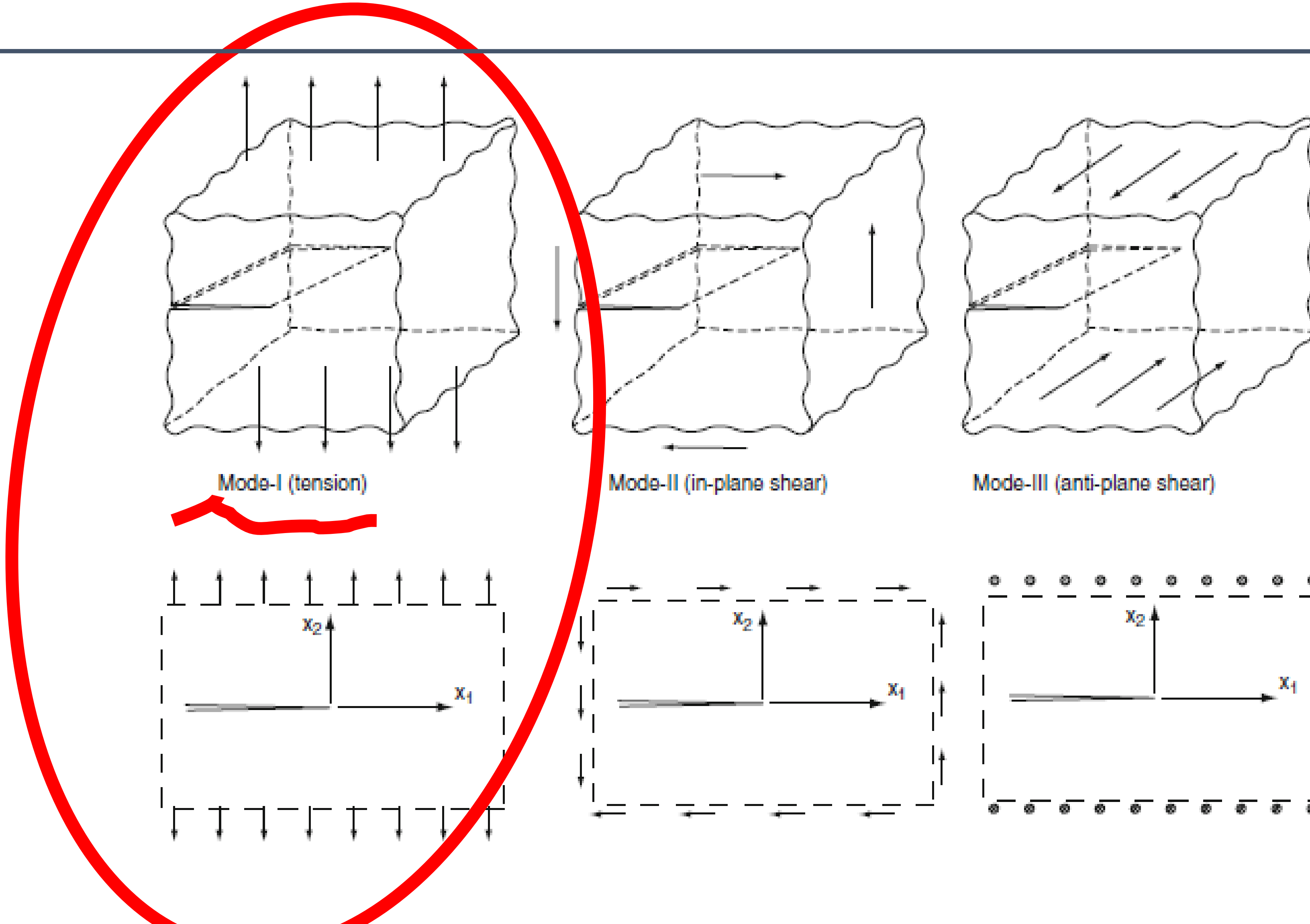

A.T. Zehnder, 'Modes of fracture', in: Q.J. Wang, Y.-W. Chung, eds., 'Encyclopedia of Tribology', Springer, pp.2292-2295, 2013

$$K = f\left(\sigma, a, \ldots\right) = Y\sigma\sqrt{\pi a}$$

$$\Delta K = f\left(\Delta\sigma, a, \ldots\right) = Y\Delta\sigma\sqrt{\pi a}$$

$$\frac{da}{dN} = f\left(\Delta K, \ldots\right)$$

$$N = \int_{a_i}^{a_f} \frac{da}{f\left(\Delta K\right)}$$

sendo aplicável a lei de Paris: $\dfrac{da}{dN} = C\left(\Delta K\right)^m$, e com $Y \simeq const$

$$N = \int_{a_i}^{a_f} \frac{da}{C\left(\Delta K\right)^m} = \int_{a_i}^{a_f} \frac{da}{C\left(\Delta K\right)^m} = \frac{1}{C\left(Y\Delta\sigma\sqrt{\pi}\right)^m} \int_{a_i}^{a_f} \frac{da}{a^{m/2}} =$$

$$= \frac{2\left(a_f^{\frac{2-m}{2}} - a_i^{\frac{2-m}{2}}\right)}{\left(2-m\right)C\left(Y\Delta\sigma\sqrt{\pi}\right)^m}$$

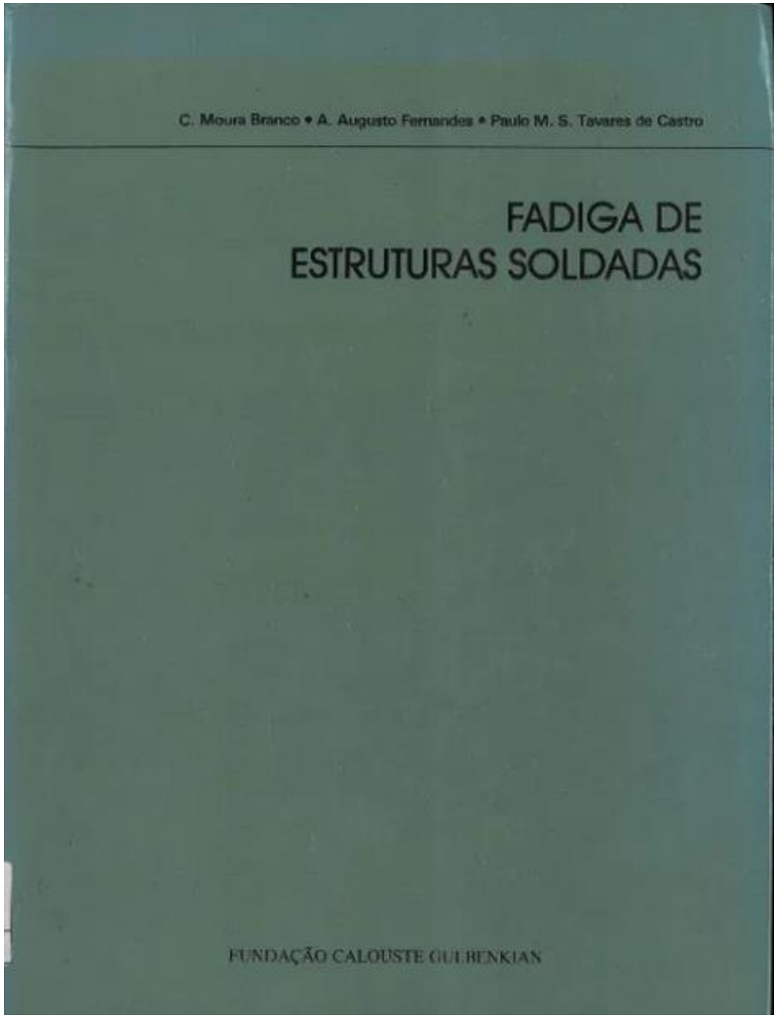
C. Moura Branco • A. Augusto Fernandes • Paulo M. S. Tavares de Castro
FADIGA DE
ESTRUTURAS SOLDADAS
FUNDAÇÃO CALOUSTE GULBENKIAN

1986

C. Moura Branco • A. Augusto Fernandes • Paulo M. S. Tavares de Castro
ESTRUTUR
FUNDAÇÃO CALOUSTE G
C. MOURA BRANCO ▪ A. AUGUSTO FERNANDES
PAULO M. S. TAVARES DE CASTRO
FADIGA
DE ESTRUTURAS
SOLDADAS
2.ª edição
SERVIÇO DE EDUCAÇÃO
FUNDAÇÃO CALOUSTE GULBENKIAN

2nd ed
1999

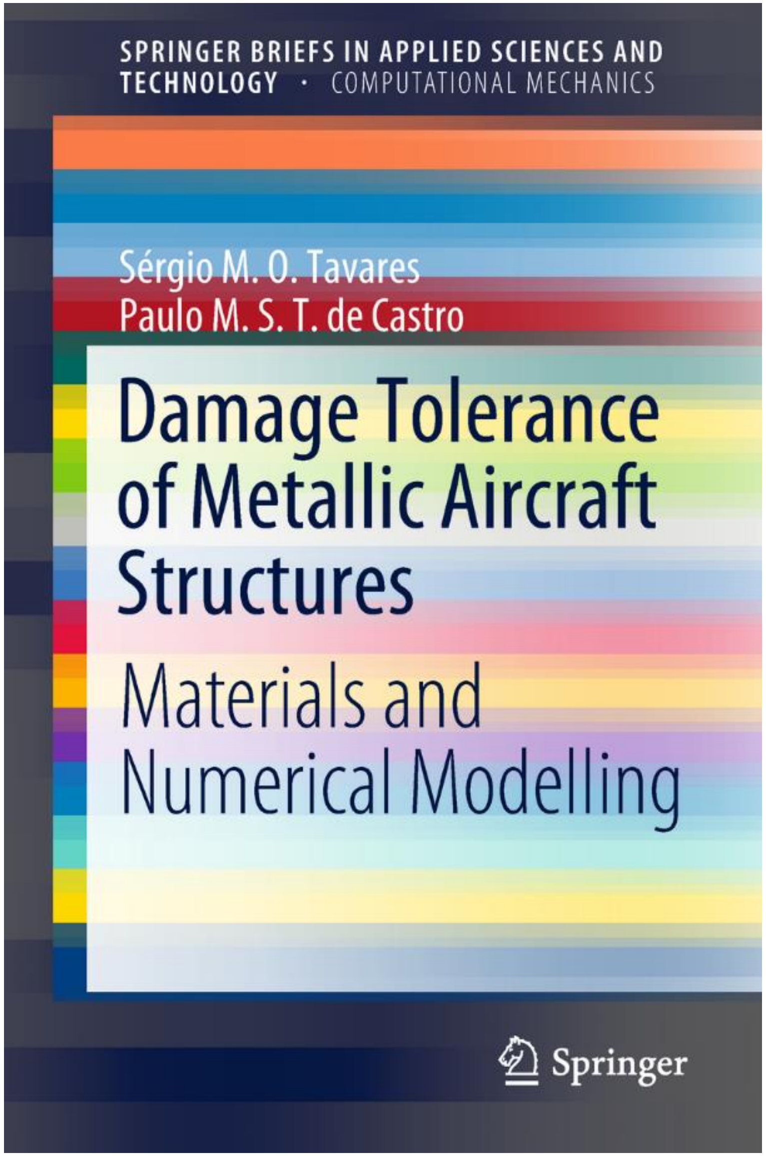
SPRINGER BRIEFS IN APPLIED SCIENCES AND TECHNOLOGY · COMPUTATIONAL MECHANICS
Sérgio M. O. Tavares
Paulo M. S. T. de Castro
Damage Tolerance of Metallic Aircraft Structures
Materials and Numerical Modelling
Springer

2019

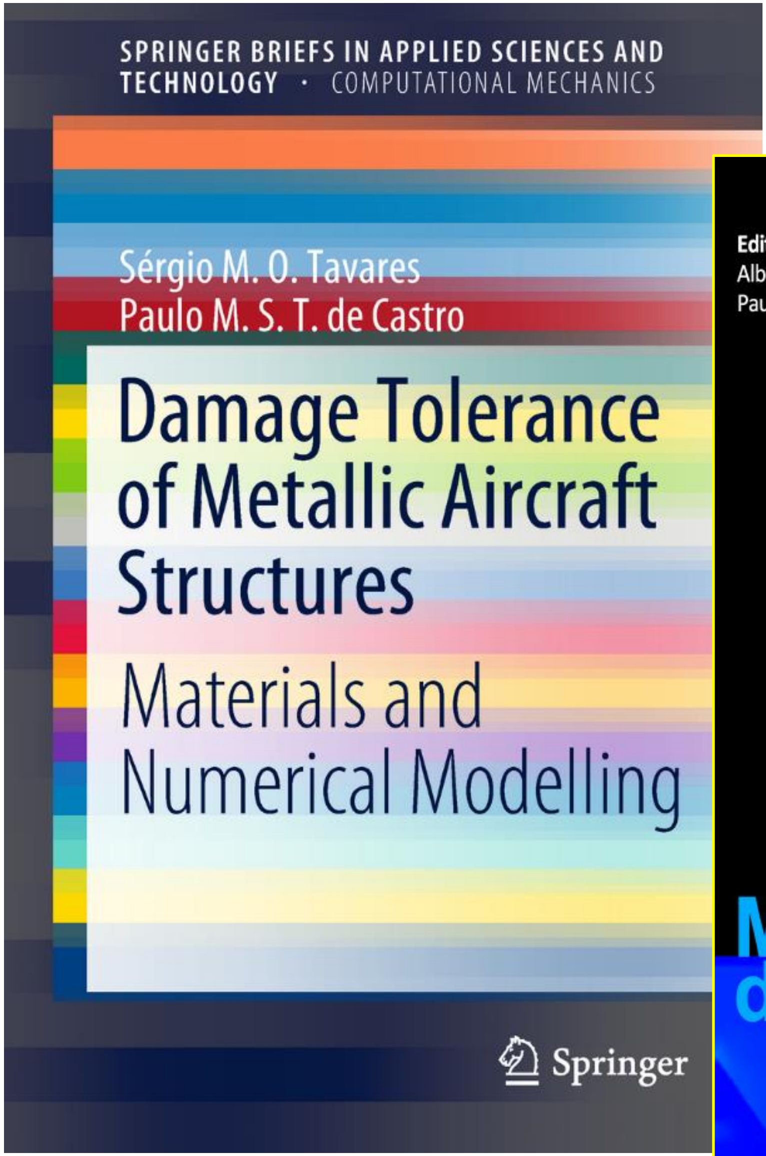
SPRINGER BRIEFS IN APPLIED SCIENCES AND TECHNOLOGY · COMPUTATIONAL MECHANICS
Sérgio M. O. Tavares
Paulo M. S. T. de Castro
Damage Tolerance of Metallic Aircraft Structures
Materials and Numerical Modelling
Springer

2019


FEUP edições
Editado por
Albertino J. C. Arteiro
Paulo M. S. Tavares de Castro
Mecânica da Fratura e Fadiga
Exemplos de cálculo e aplicação
2014

2014

colegas da FEUP
trabalhando
nestes temas
incluem,
entre outros,

Abílio de Jesus
Albertino Arteiro
António A Fernandes
António T. Marques
Lucas da Silva
Marcelo de Moura
Pedro Camanho
Rui Calçada
…………

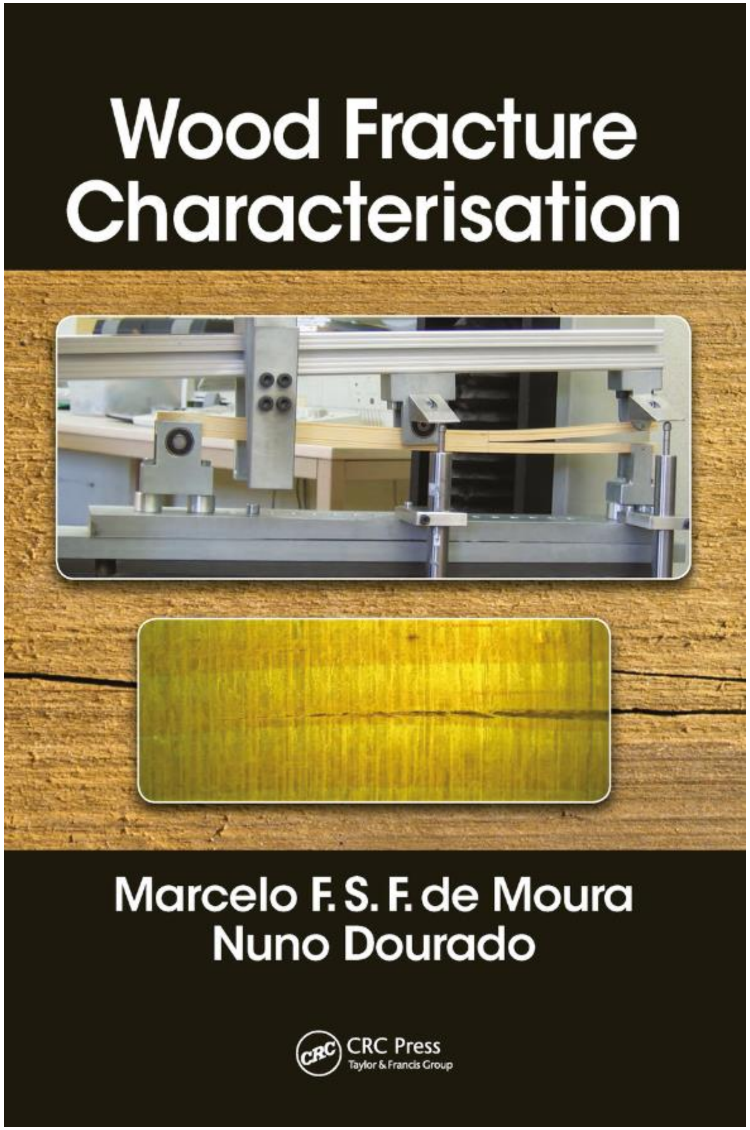

colegas da FEUP
trabalhando
nestes temas
incluem,
entre outros,

Abílio de Jesus
Albertino Arteiro
António A Fernandes
António T. Marques
Lucas da Silva
Marcelo de Moura
Pedro Camanho
Rui Calçada
…………

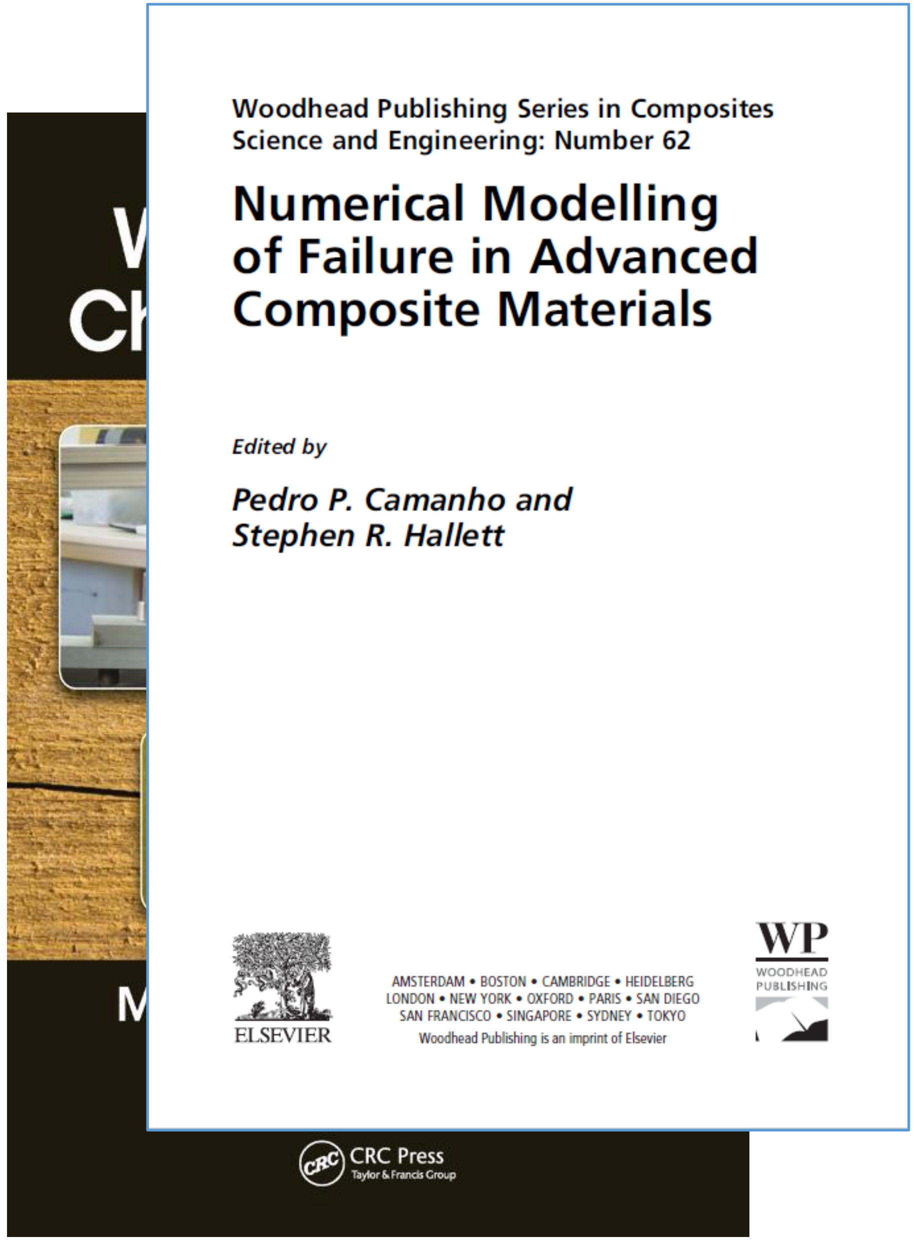

colegas da FEUP
trabalhando
nestes temas
incluem,
entre outros,

Abílio de Jesus
Albertino Arteiro
António A Fernandes
António T. Marques
Lucas da Silva
Marcelo de Moura
Pedro Camanho
Rui Calçada
....

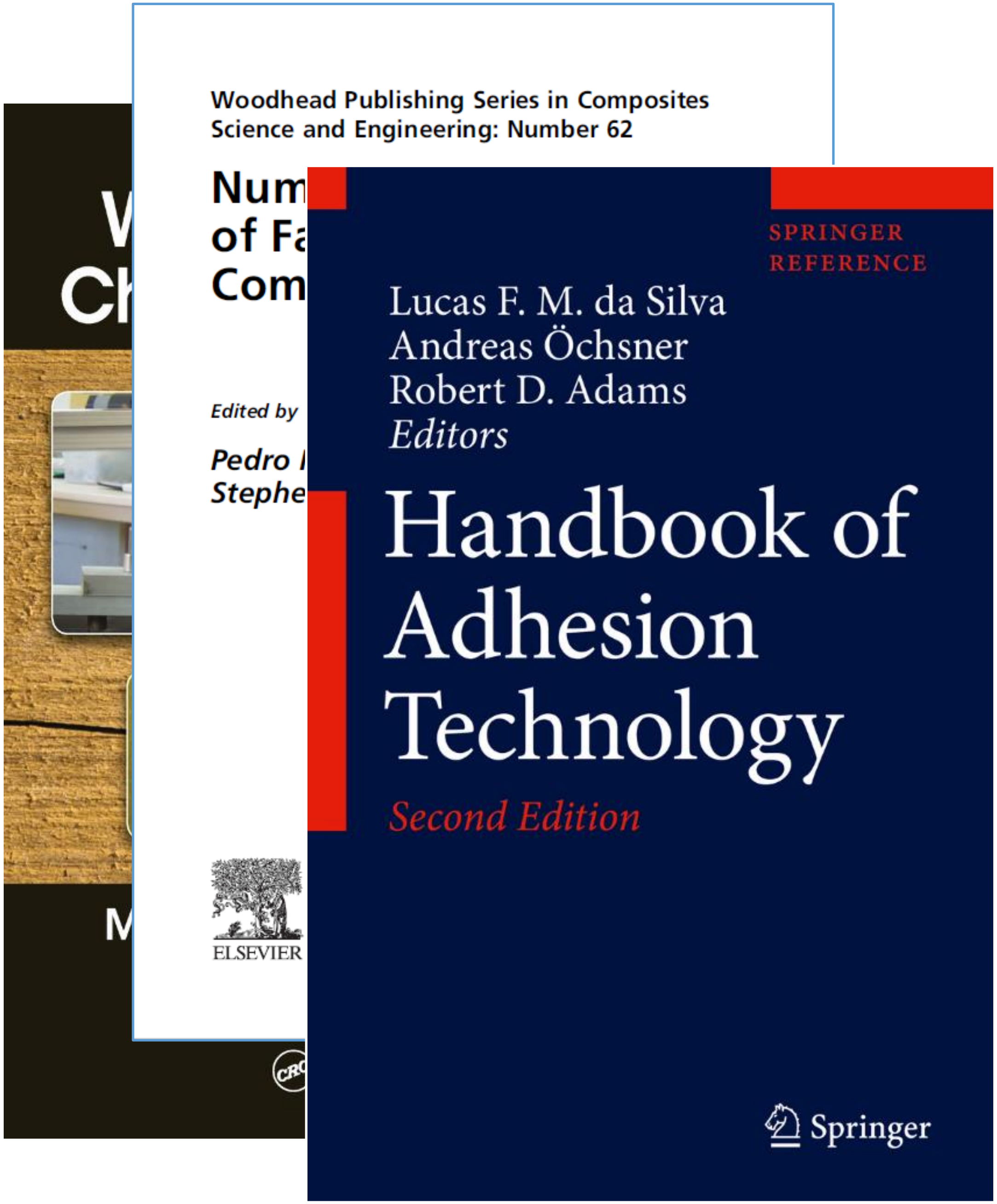

colegas da FEUP
trabalhando
nestes temas
incluem,
entre outros,

Abílio de Jesus
Albertino Arteiro
António A Fernandes
António T. Marques
Lucas da Silva
Marcelo de Moura
Pedro Camanho
Rui Calçada
…………

Introdução – exs. de casos

- **Haste**
- **Ligação soldada**

Referência a conceitos básicos

- Bibliografia de autores do DEMec da FEUP

Propagação de fendas

- Expansão de furos

Propagação de fendas em modo misto

- O caso da flexão em 4 pontos

Métodos numéricos – o XFEM

National Transportation Safety Board

Washington, D.C. 20594

Accident Number: DCA11MA039
Operator/Flight Number: Southwest Airlines, Flight 812
Aircraft and Registration: Boeing 737-3H4, N632SW
Location: Yuma, Arizona
Date: April 1, 2011
Adopted: September 24, 2013

HISTORY OF FLIGHT

On April 1, 2011, about 1558 mou
N632SW, operating as Southwest Airlines fli
climbing through flight level 340. The flight c
to Yuma International Airport (NYL), Yuma, A
on board, one crewmember and one nonreve
minor injuries. The airplane sustained substan
section of fuselage skin about 60 inches long t
the upper left side above the wing. The flight
Federal Regulations (CFR) Part 121 as a re
Phoenix Sky Harbor International Airport,
Airport, Sacramento, California.

According to the flight crew and recor
At 1558:05, an unidentified sound was re
2 seconds later, the captain announced that th
for oxygen masks on; sounds consistent wit
voice recording. The captain declared an emer
altitude. The air traffic controller provided
descended the airplane to 11,000 feet within 5
1605, the cabin crew began relaying conditio
in the fuselage and one broken-nose injury of
further descent to 9,000 feet, and the capta
airport (NYL). The airplane landed about 162
The passengers deplaned via airstairs.

[1] Unless otherwise noted, all times in this brief are

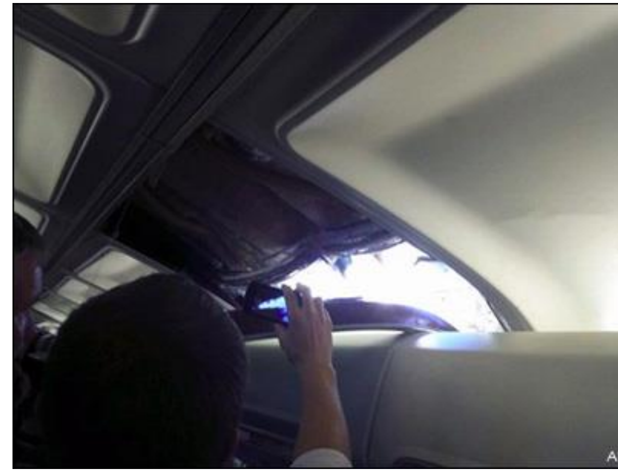

http://www.airsafenews.com/2011/04/bbc-interview-about-southwest-737.html

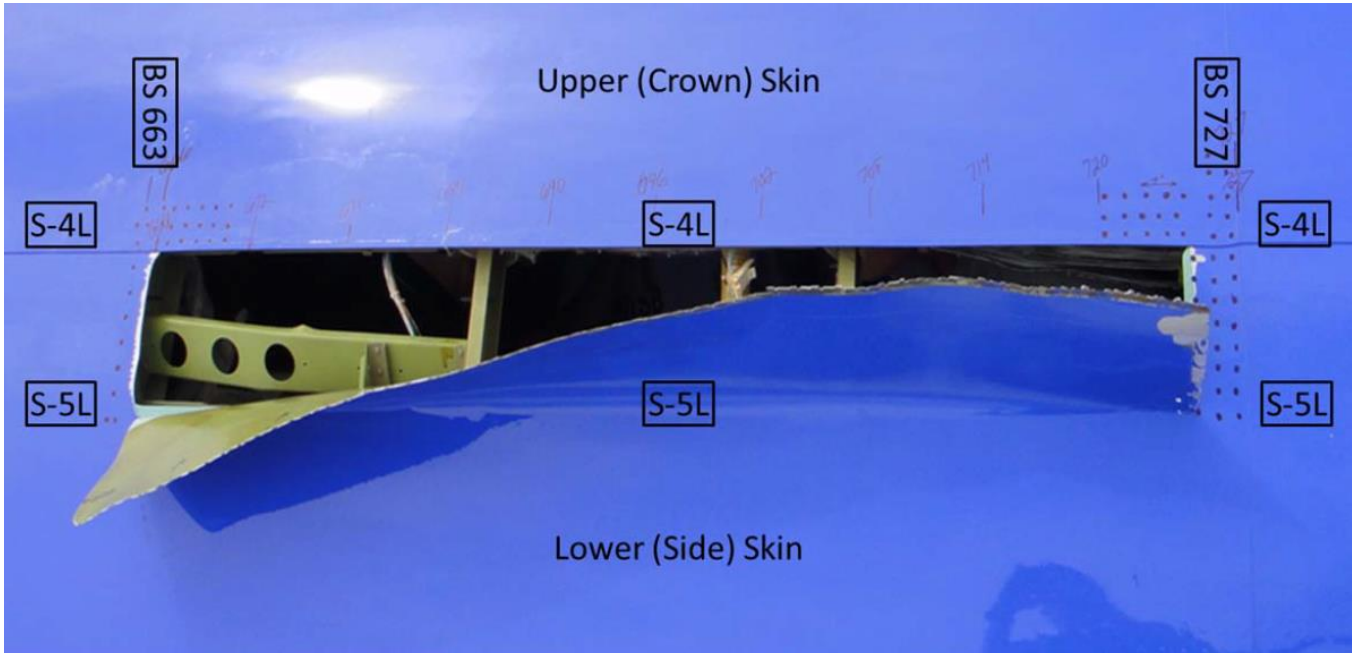
Upper (Crown) Skin
BS 663
BS 727
S-4L
S-4L
S-4L
S-5L
S-5L
S-5L
Lower (Side) Skin

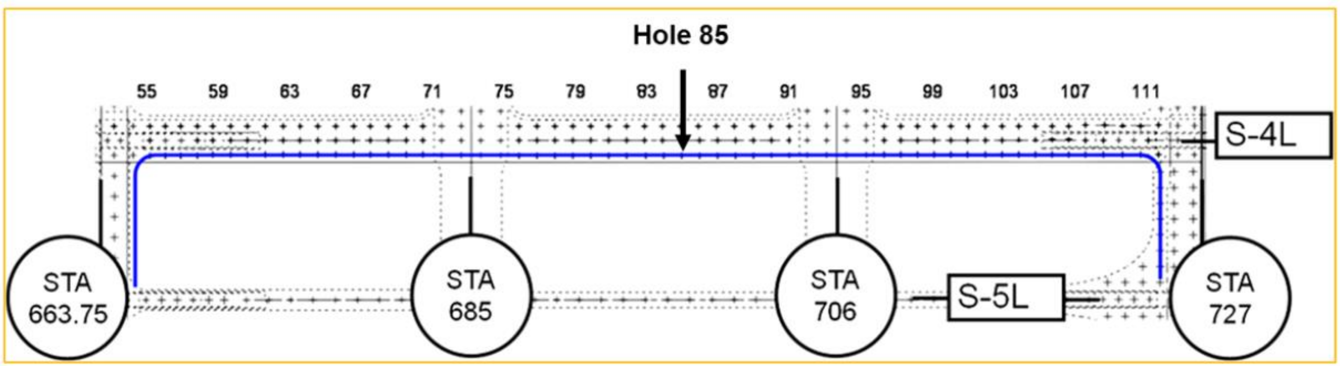
Hole 85
55
59
63
67
71
75
79
83
87
91
95
99
103
107
111
S-4L
S-5L
STA 663.75
STA 685
STA 706
STA 727

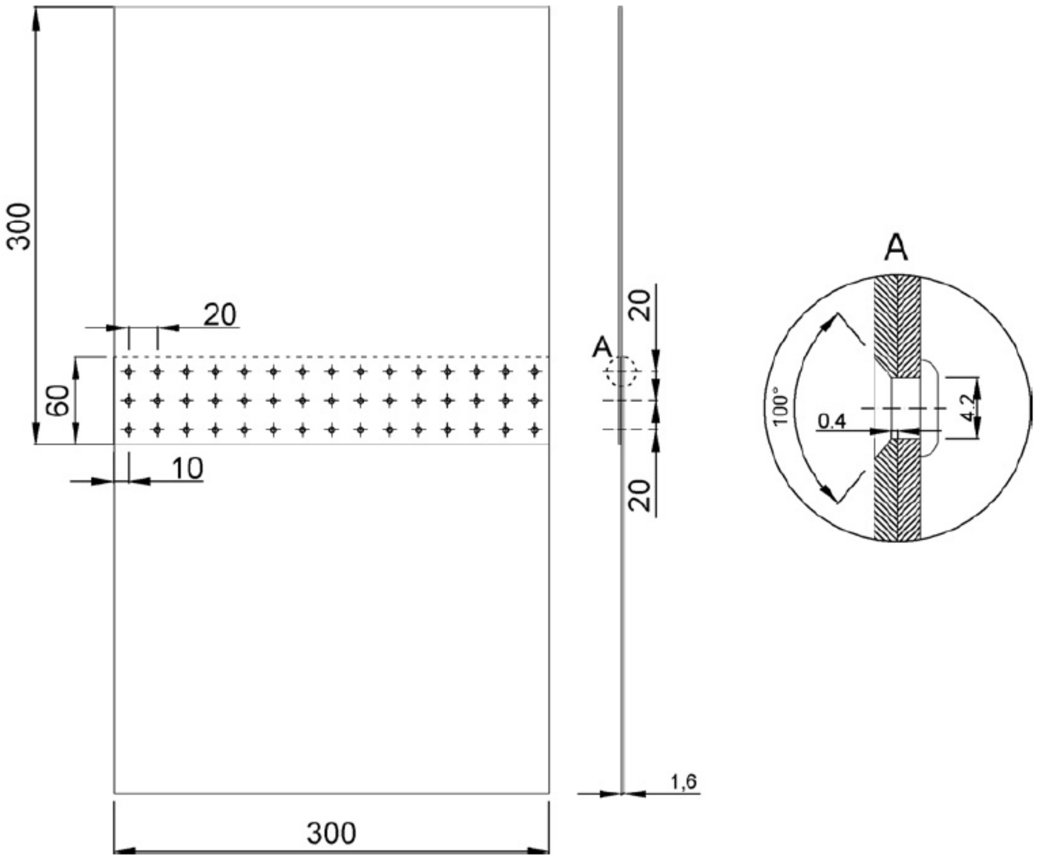

P.M.S.T. de Castro *et al.*, 'An overview on fatigue analysis of aeronautical structural details: Open hole, single rivet lap-joint, and lap-joint panel', *Materials Science and Engineering A*, vol.468–470, pp.144–157, 2007

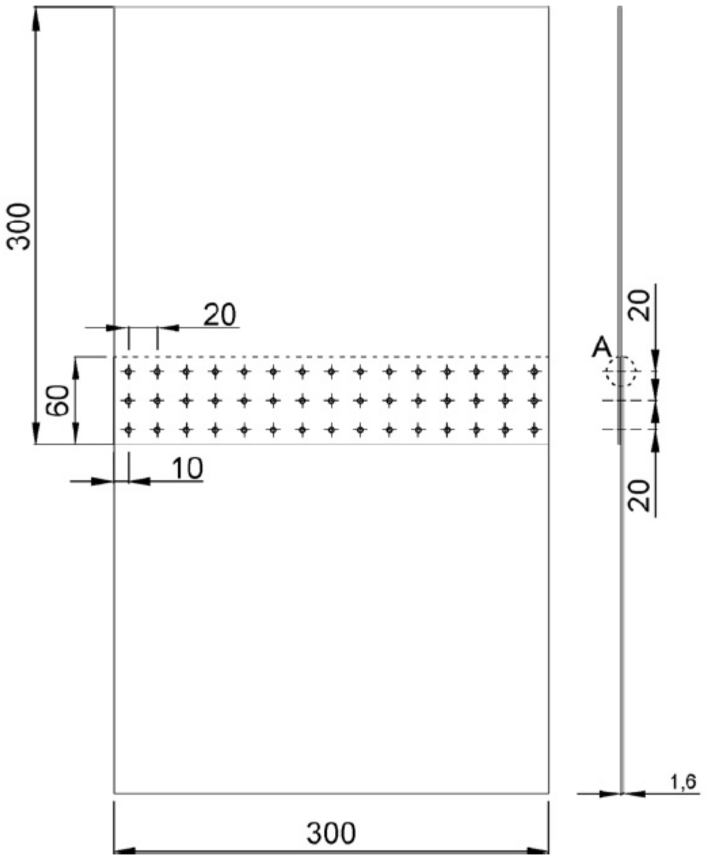

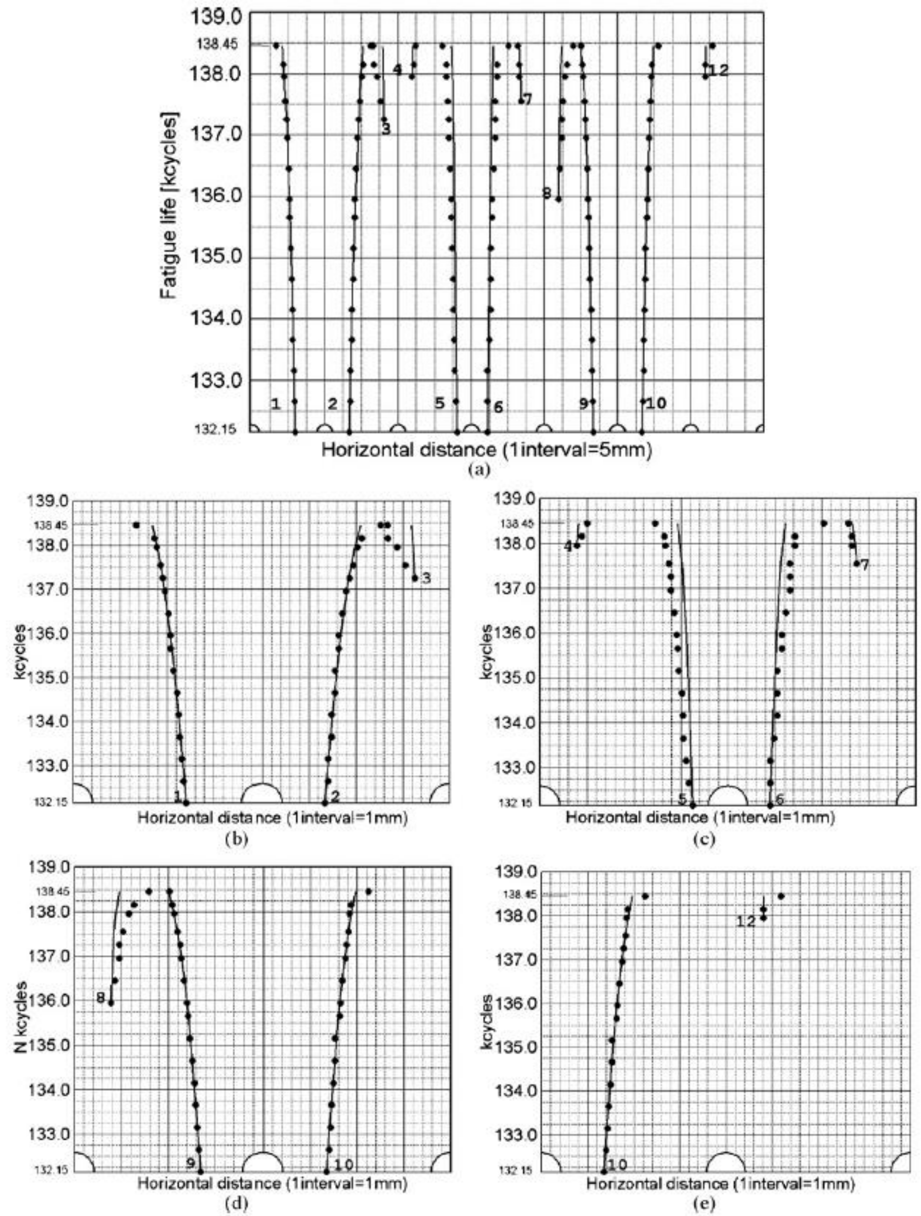

P.M.S.T. de Castro *et al.*, ‘An overview on fatigue analysis of aeronautical structural details: Open hole, single rivet lap-joint, and lap-joint panel’, *Materials Science and Engineering A*, vol.468–470, pp.144–157, 2007

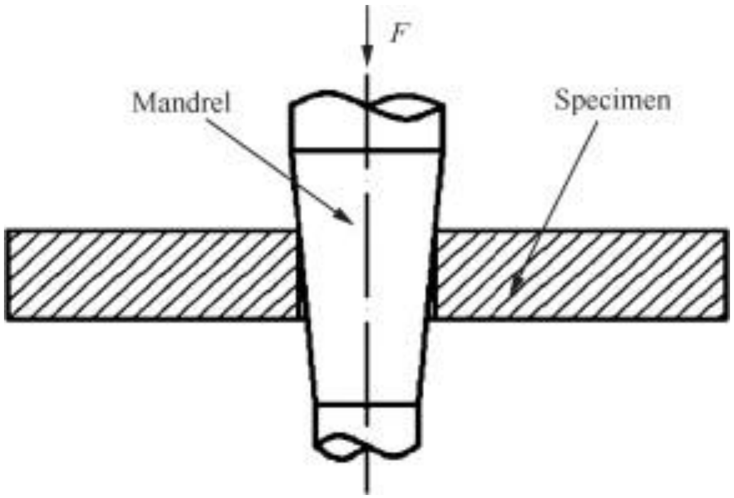

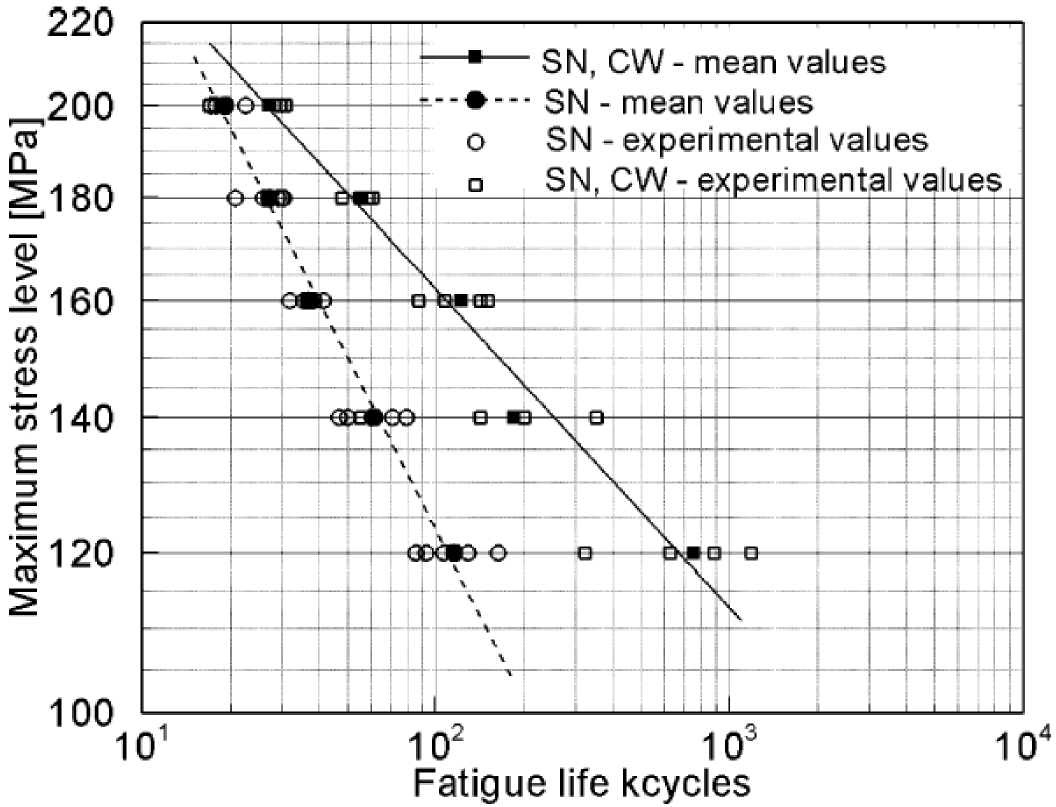

Fu Yucan *et al.*, 'Cold expansion technology of connection holes in aircraft structures: A review and prospect', *Chinese Journal of Aeronautics*, vol.28, (4), pp.961–973, 2015

P.M.S.T. de Castro *et al.*, 'An overview on fatigue analysis of aeronautical structural details: Open hole, single rivet lap-joint, and lap-joint panel', *Materials Science and Engineering A*, vol.468–470, pp.144–157, 2007

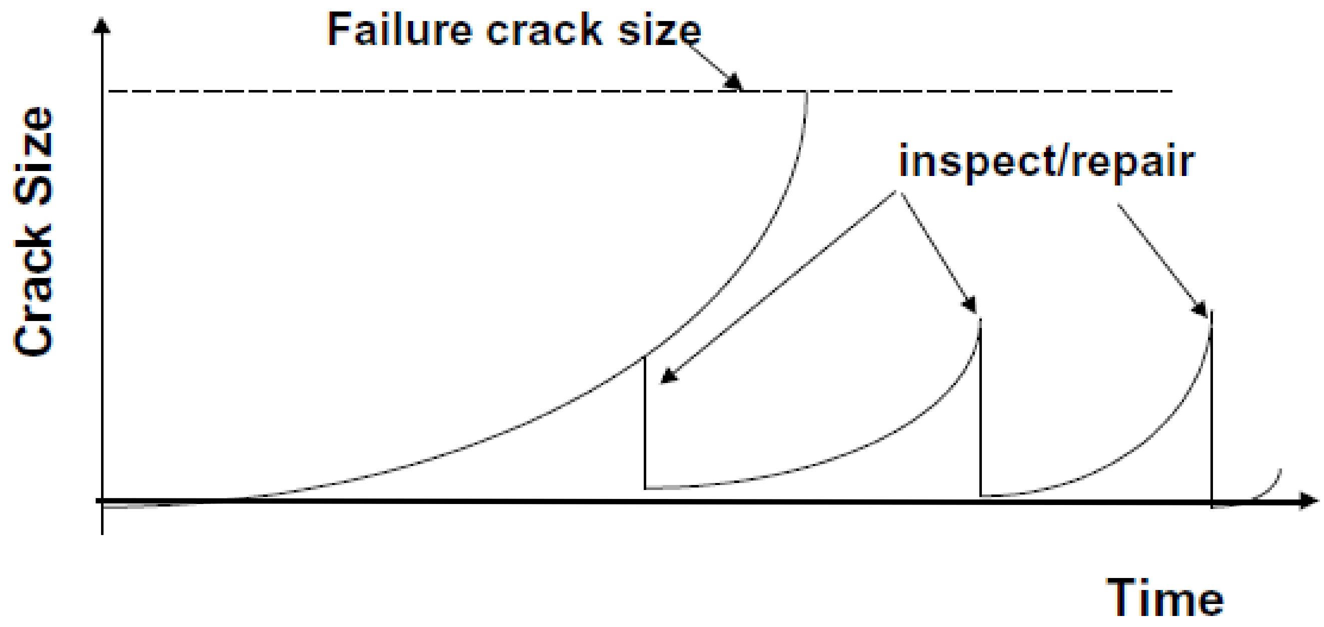

the damage tolerance philosophy as used in aeronautical engineering
tolerância ao dano, como usada em aeronáutica

M. Chajes *et al.*, 'Steel Girder Fracture on Delaware's I-95 Bridge over the Brandywine River', Structures Congress 2005, April 20-24, 2005, NY, USA, American Society of Civil Engineers

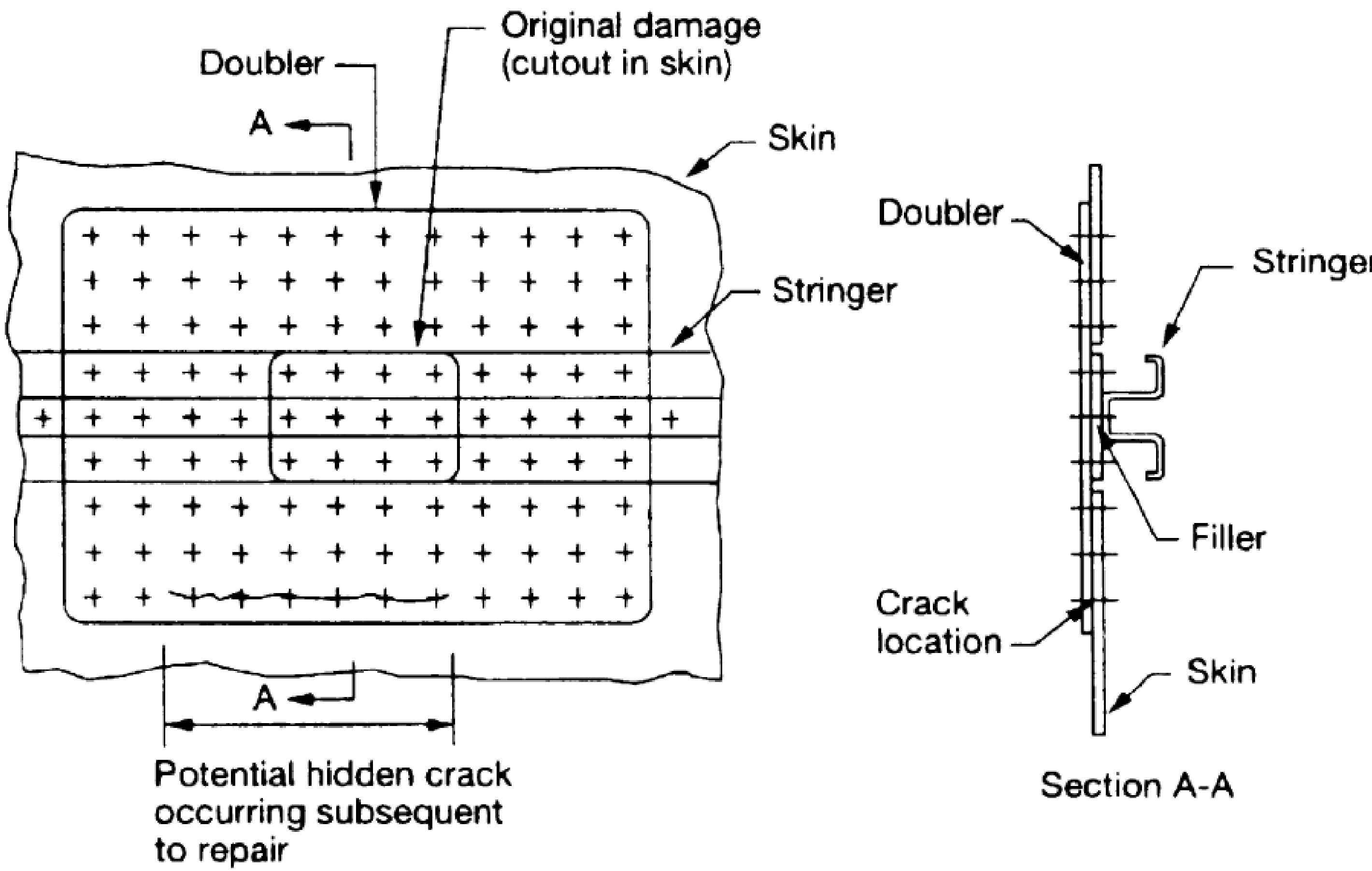

Figure 48 Typical fuselage external skin repair

U.G. Goranson, 'Fatigue issues in aircraft maintenance and repairs', *International Journal of Fatigue*, vol.19, supp. no.1, pp.S3–S21, 1997

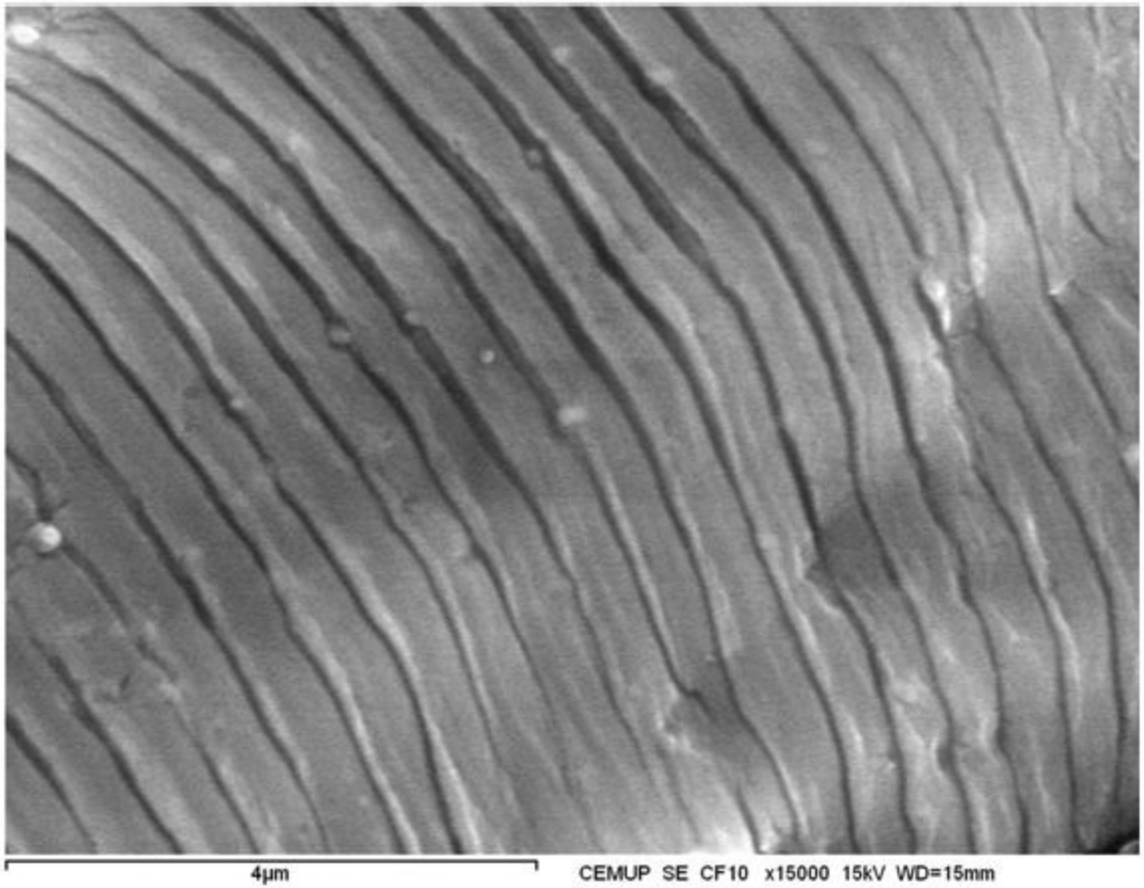

P. Moreira, M. Figueiredo, P.M.S.T. de Castro, ‘Fatigue behaviour of FSW and MIG weldments for two aluminium alloys’, *Theoretical and Applied Fracture Mechanics,* vol.48, pp.169–177, 2007

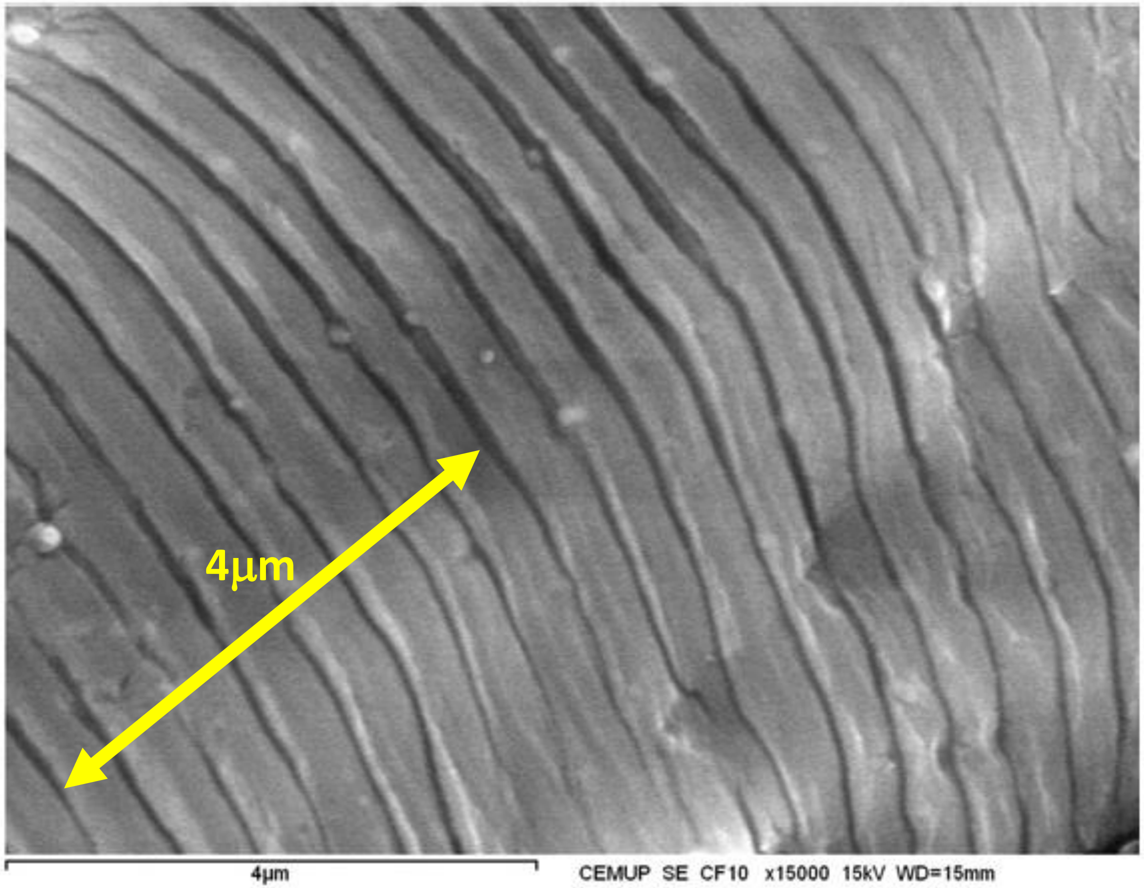

P. Moreira, M. Figueiredo, P.M.S.T. de Castro, ‘Fatigue behaviour of FSW and MIG weldments for two aluminium alloys’, *Theoretical and Applied Fracture Mechanics,* vol.48, pp.169–177, 2007

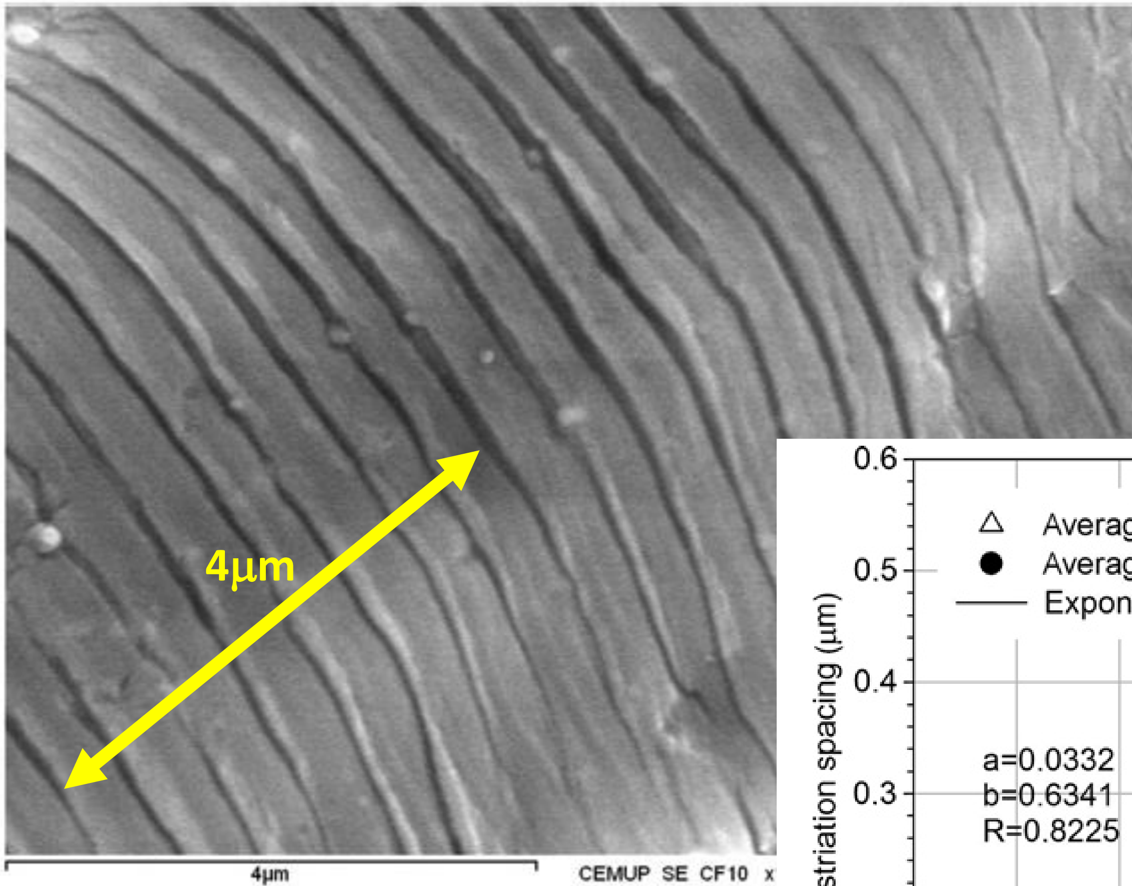

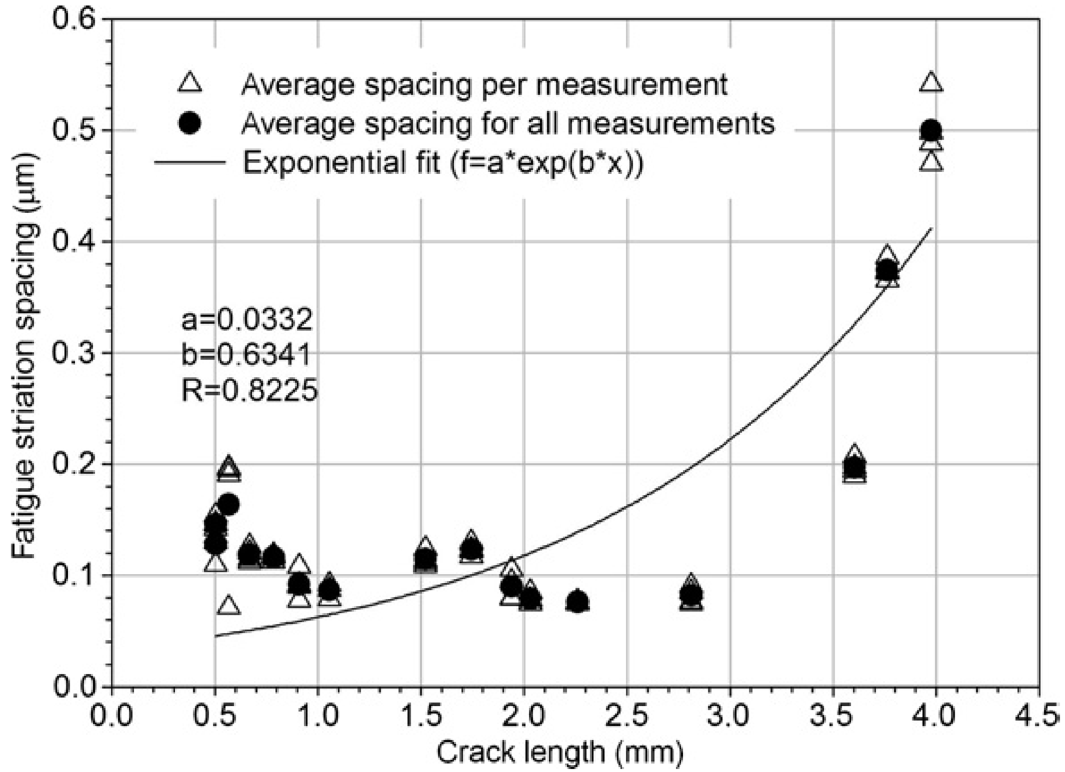

estria: $4\ \mu m / 8 \simeq 0.5\ \mu m$

Fig. 8. Fatigue striation spacing *vs.* crack length for specimen of Al6082-T6.

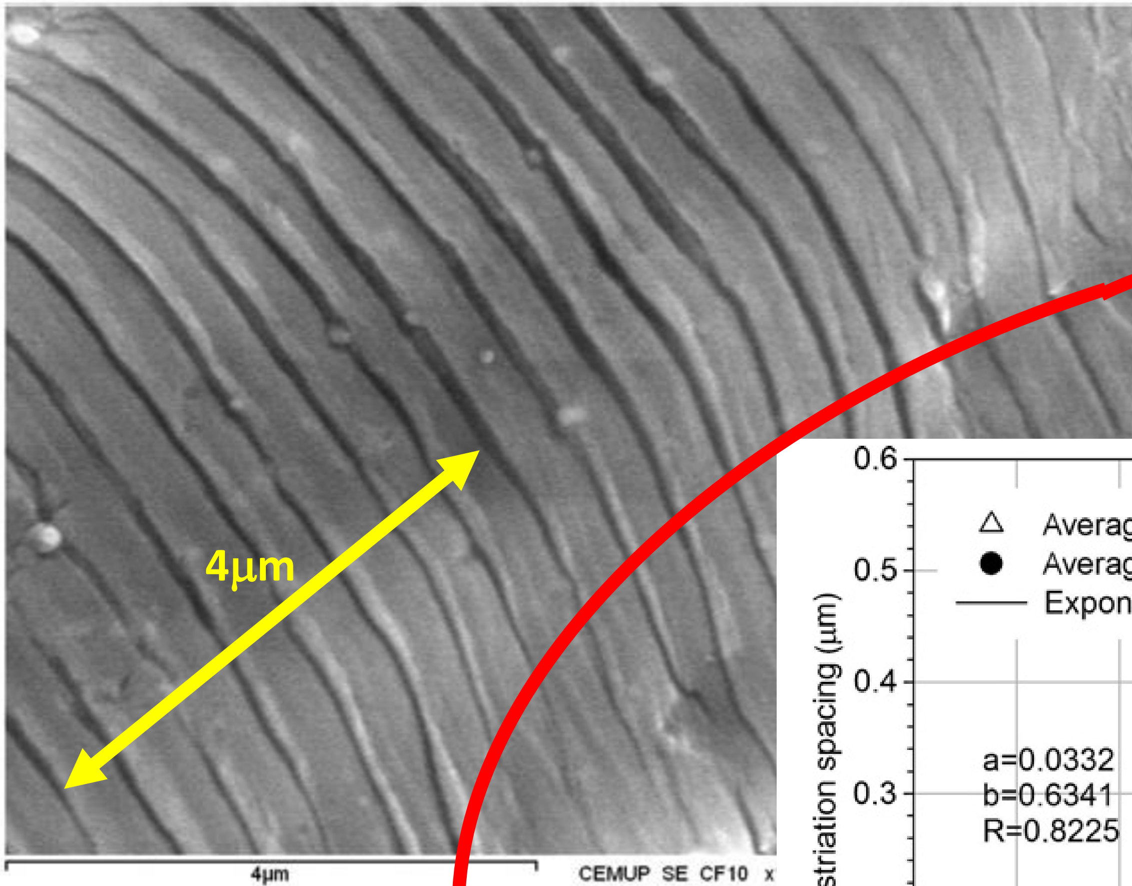

estria: 4 μm /8 ≃ 0.5 μm

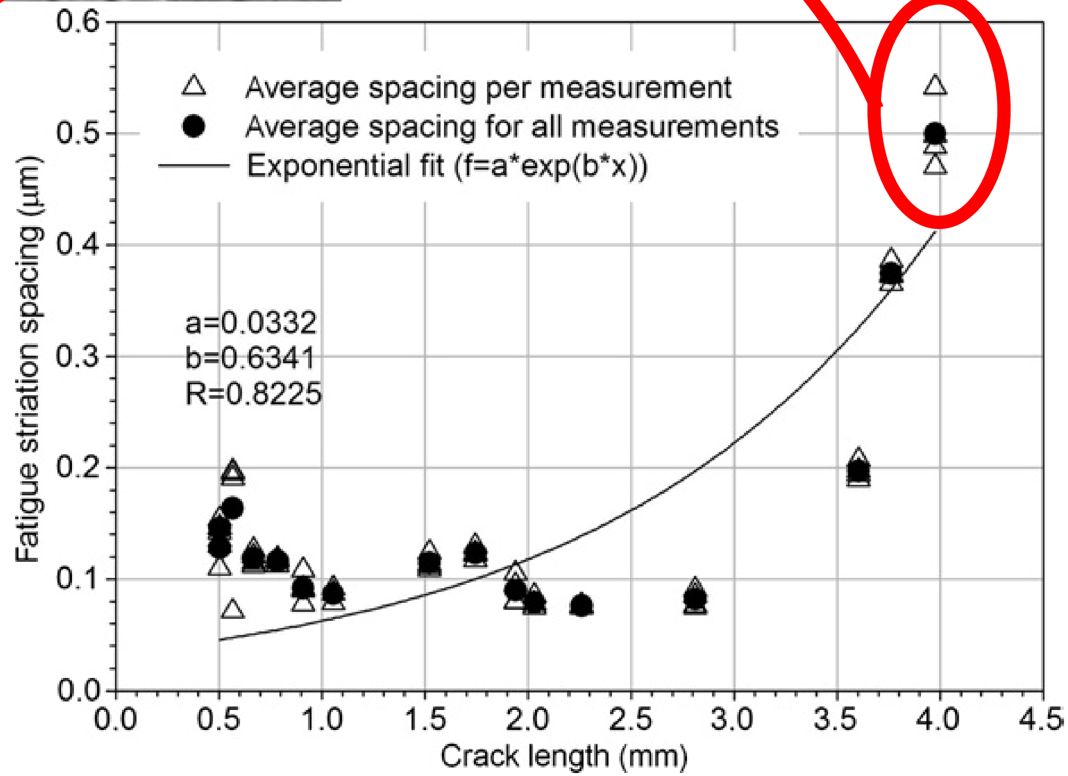

Fig. 8. Fatigue striation spacing *vs.* crack length for specimen of Al6082-T6.

Introdução – exs. de casos

- **Haste**
- **Ligação soldada**

Referência a conceitos básicos

- Bibliografia de autores do DEMec da FEUP

Propagação de fendas

- Expansão de furos

Propagação de fendas em modo misto

- O caso da flexão em 4 pontos

Métodos numéricos – o XFEM

$$\sigma_r = \frac{K_I}{\sqrt{2\pi r}} \cos\frac{\psi}{2}\left(3 - \cos\psi\right)$$

$$\sigma_\psi = \frac{K_I}{\sqrt{2\pi r}} \frac{1}{2} \cos\frac{\psi}{2}\left(1 + \cos\frac{\psi}{2}\right)$$

$$\tau_{r\psi} = \frac{K_I}{\sqrt{2\pi r}} \frac{1}{2} \sin\frac{\psi}{2}\left(1 + \cos\psi\right)$$

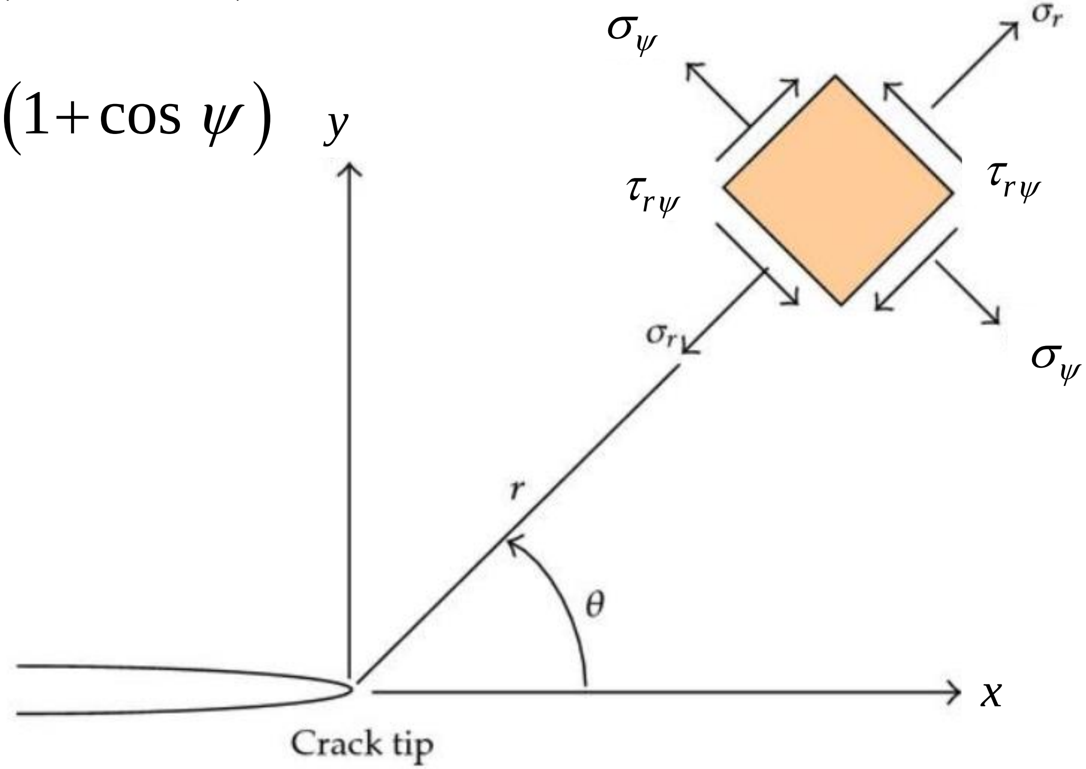

Notation used in crack propagation direction studies from an initial pre-crack. In this figure σ it is the remote load applied, *a* it is the semi crack length, ψ_0 is the angle between the remote load direction and the crack plane, and β is the angle of crack propagation in relation to the pre-crack direction.

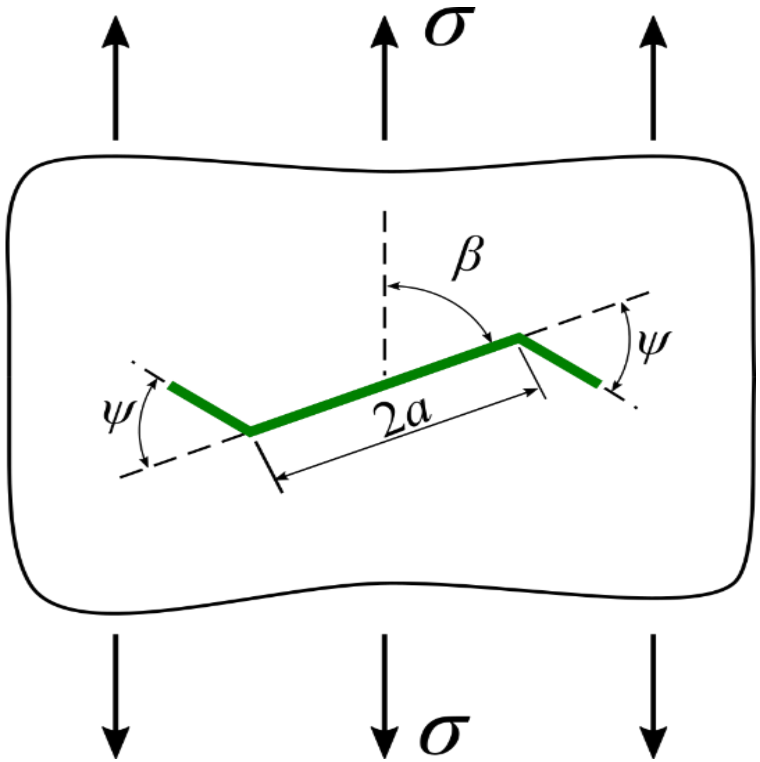

Notation used in studies of the direction of crack propagation from an initial pre-crack of length 2*a*

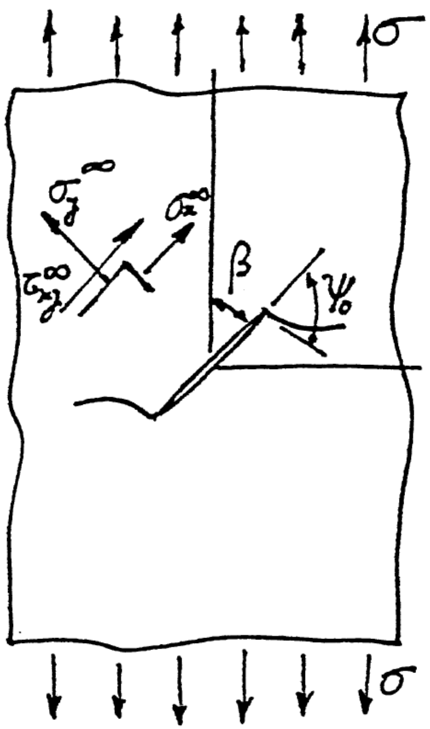

$$\sigma_r = \frac{K_I}{\sqrt{2\pi r}} \cos\frac{\psi}{2}(3-\cos\psi)$$

$$\sigma_\psi = \frac{K_I}{\sqrt{2\pi r}} \frac{1}{2} \cos\frac{\psi}{2}\left(1+\cos\frac{\psi}{2}\right)$$

$$\tau_{r\psi} = \frac{K_I}{\sqrt{2\pi r}} \frac{1}{2} \sin\frac{\psi}{2}(1+\cos\psi)$$

recall that principal stresses are

$$\sigma_{1,2} = \frac{\sigma_r + \sigma_\psi}{2} + \sqrt{\left(\frac{\sigma_r - \sigma_\psi}{2}\right)^2 + \tau_{r\psi}^2}$$

$$\rightarrow \sigma_{1,2} = \frac{K_I}{\sqrt{2\pi r}} \cos\frac{\psi}{2}\left(1 \pm \sin\frac{\psi}{2}\right)$$

Based on the experimentally confirmed hypothesis that a crack propagates along a path perpendicular to the direction of the highest principal stress, (therefore the shear stress component in the expected crack propagation path is zero), Sih *et al*. obtained

$$\tau_{r\psi} = 0 = \frac{K_I}{\sqrt{2\pi r}} \frac{1}{2} \sin\frac{\psi}{2}(1+\cos\psi) - \frac{K_{II}}{\sqrt{2\pi r}} \frac{1}{2} \cos\frac{\psi}{2}(1-3\cos\psi)$$

$$\tau_{r\psi}=0=\frac{K_I}{\sqrt{2\pi r}}\,\frac{1}{2}\sin\frac{\psi}{2}\left(1+\cos\psi\right)-\frac{K_{II}}{\sqrt{2\pi r}}\,\frac{1}{2}\cos\frac{\psi}{2}\left(1-3\cos\psi\right)$$

$$0=K_I\sin\frac{\psi}{2}\left(1+\cos\psi\right)-K_{II}\cos\frac{\psi}{2}\left(1-3\cos\psi\right)$$

$$0=K_I\,\frac{\sin\frac{\psi}{2}}{\cos\frac{\psi}{2}}\left(1+\cos\psi\right)-K_{II}\,\frac{\cos\frac{\psi}{2}}{\cos\frac{\psi}{2}}\left(1-3\cos\psi\right)$$

$$0=K_I\tan\frac{\psi}{2}\left(1+\cos\psi\right)-K_{II}\,\left(1-3\cos\psi\right)$$

but

$$\tan\frac{\psi}{2}=\sqrt{\frac{1-\cos\psi}{1+\cos\psi}}\rightarrow$$

$$0=K_I\sqrt{\frac{1-\cos\psi}{1+\cos\psi}}\left(1+\cos\psi\right)-K_{II}\,\left(1-3\cos\psi\right)=$$

$$=K_I\sqrt{\left(1-\cos\psi\right)\left(1+\cos\psi\right)}-K_{II}\,\left(1-3\cos\psi\right)$$

$$0 = K_I \sqrt{1-\cos^2\psi} + K_{II}\ \left(3\cos\ \psi - 1\ \right)$$

$$K_I \sin\psi_o + K_{II}\left(3\cos\ \psi_o - 1\right) = 0$$

in the present case,

$$\sigma_y^\infty = \sigma \sin^2\beta \quad ; \quad \sigma_x^\infty = \sigma\cos^2\beta \quad ; \quad \tau_{xy}^\infty = \sigma\sin\beta\cos\beta$$

and

$$K_I = \sigma\ \sin^2\beta\sqrt{\pi\, a} \quad ; \quad K_{II} = \sigma\sin\beta\ \cos\beta\sqrt{\pi\, a}$$

$$\rightarrow \cot\beta = \frac{-\sin\psi_o}{3\cos\ \psi_o - 1}$$

when $0 < \beta < \dfrac{\pi}{2}$, ψ_o is negative.

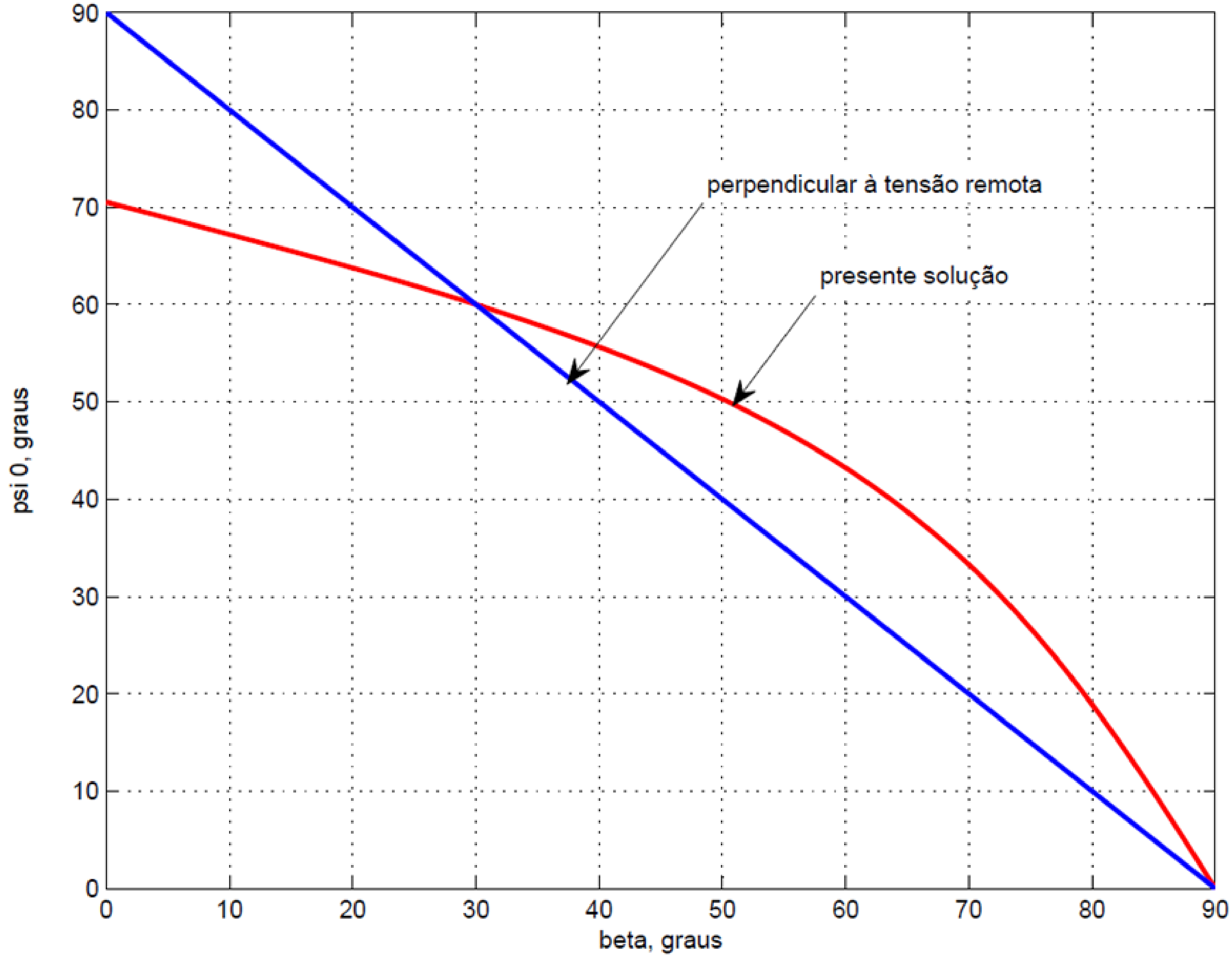

Relationship ψ_0 *versus* β, figure of previous slide. Note ψ_0 <0. The straight line represents the direction perpendicular to remote stress

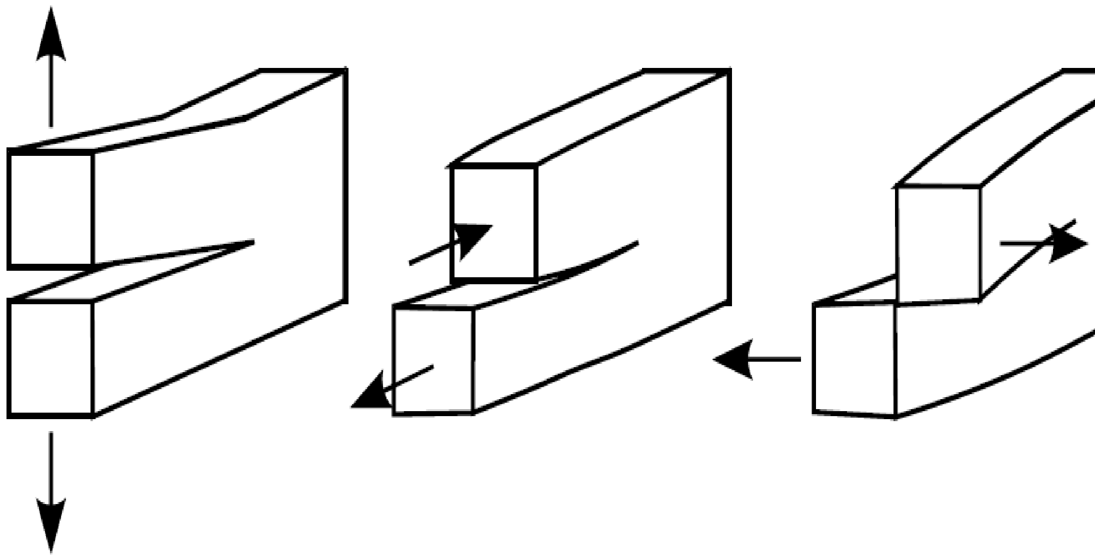

Mode I Mode II Mode III

3 basic fracture modes

Most of the work on fatigue involves mode I situations, but in practice, mixed mode situations are often encountered.

bending tests are routine in characterizing the mechanical behavior of materials. The most common configuration is 3 point bending, which implies that the test takes place in the presence of shear or shear stress, and 4 point bending, eliminating shear stress

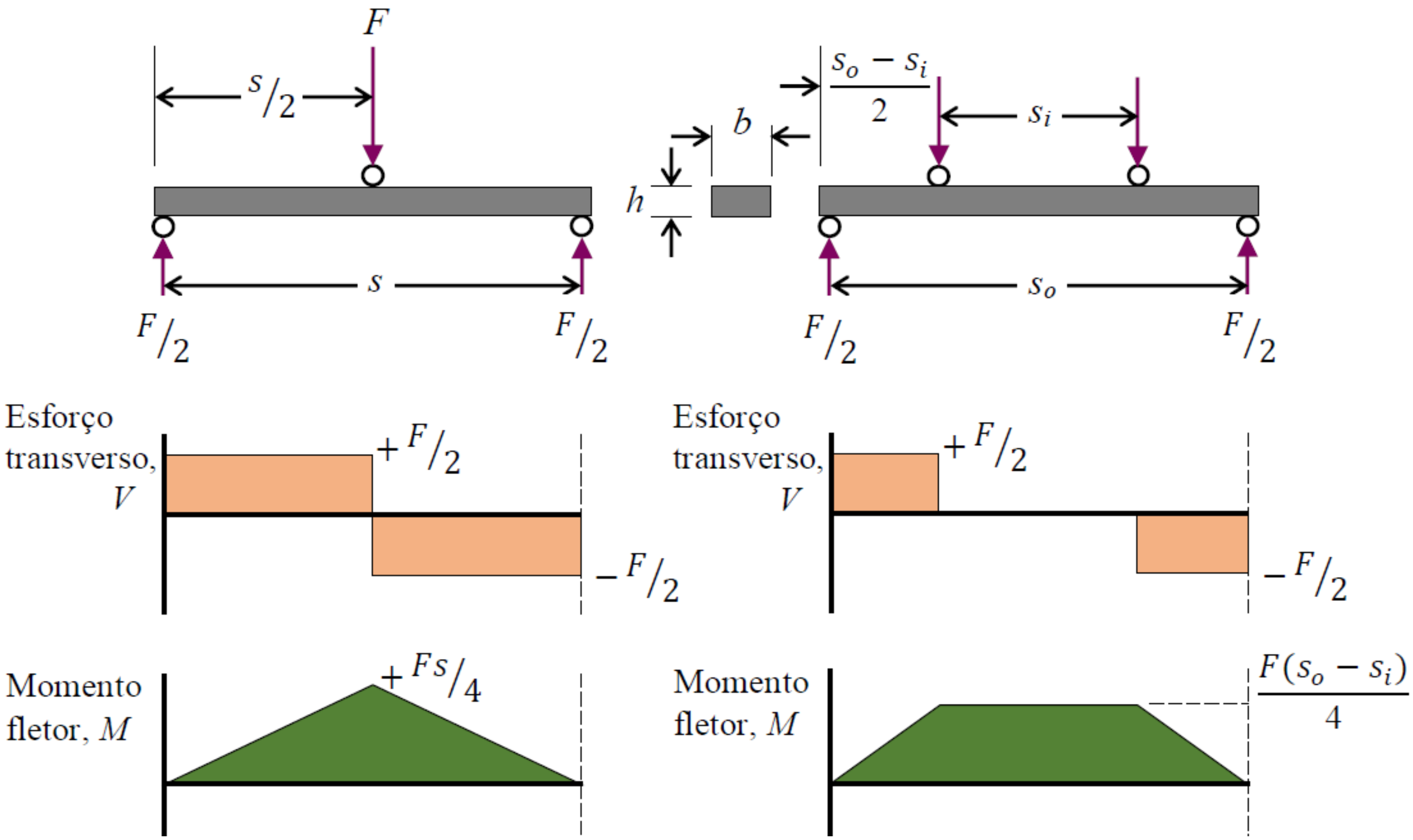

L. Guerra Rosa, 'Caracterização Mecânica de Cerâmicos', 2017

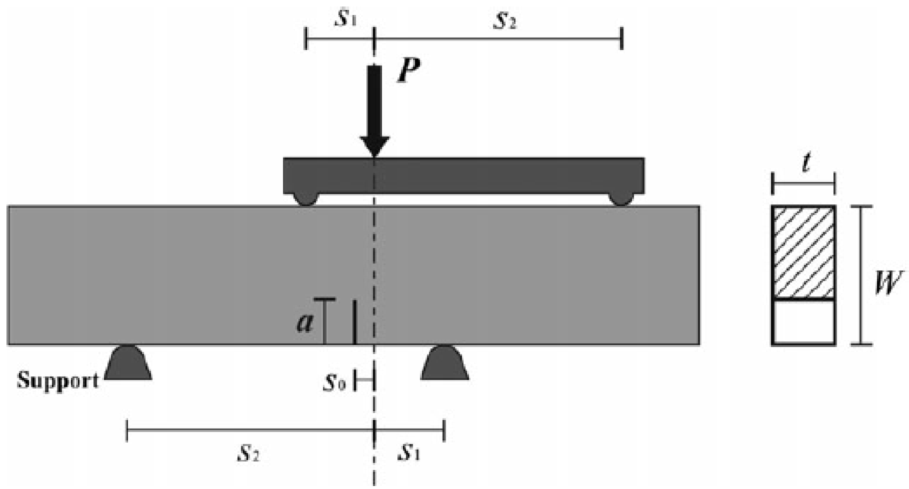

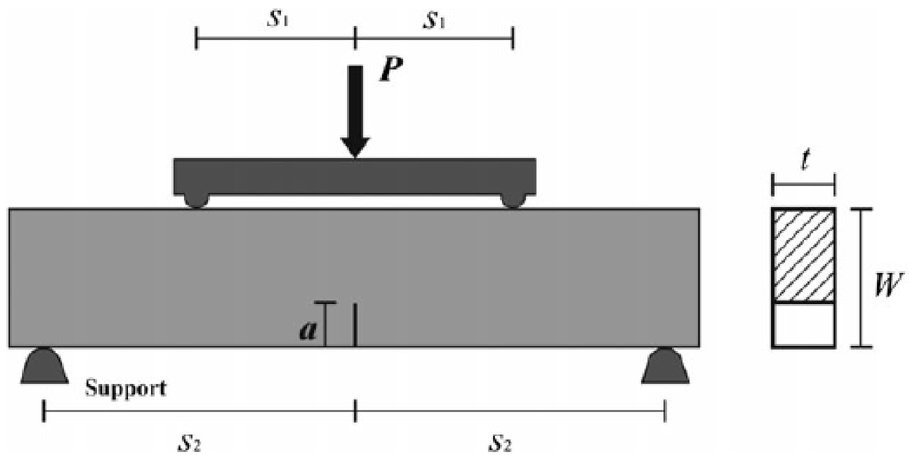

C. Wang, *et al.*, *Fatigue and Fracture of Engineering Materials and Structures*, vol.39, pp.1193–1203, 2016

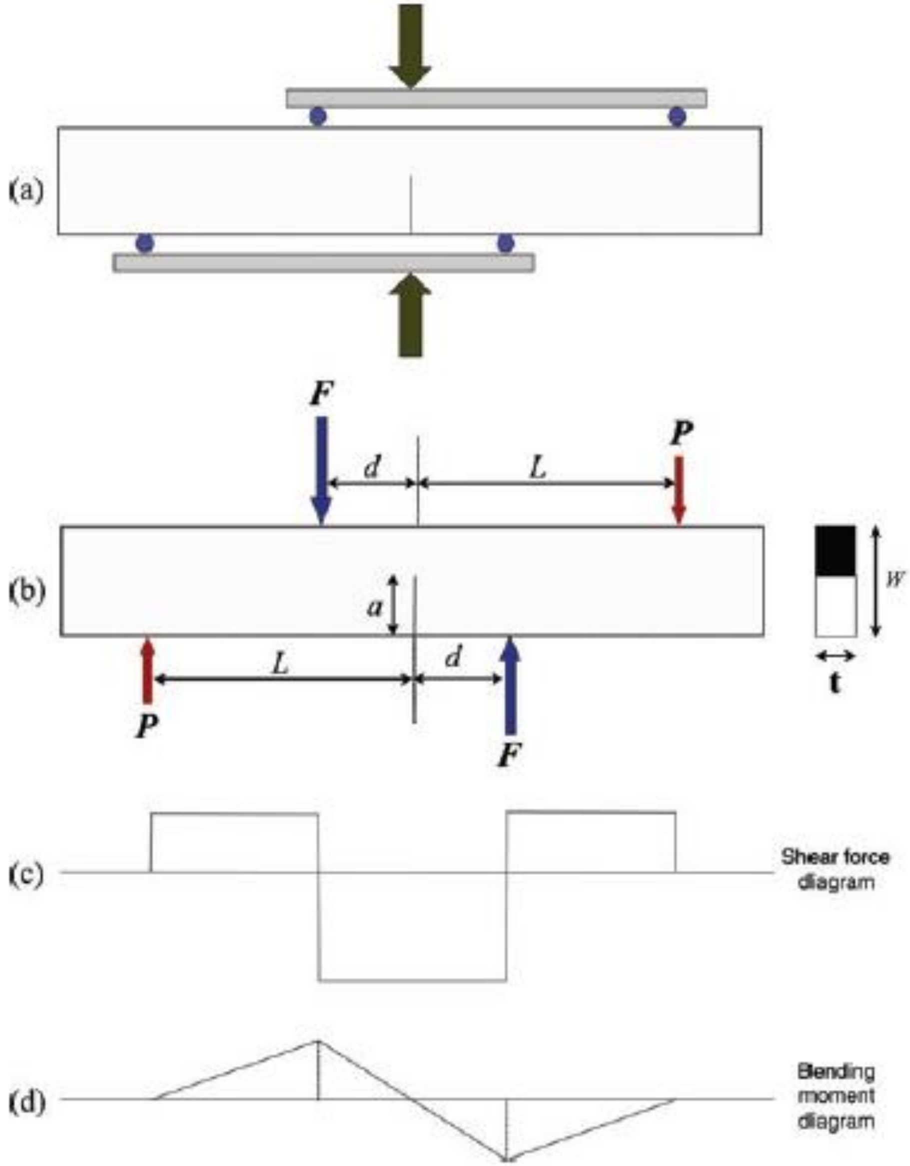

M.R. Ayatollahi, M.R.M. Aliha, Fatigue and Fracture of Engineering Materials and Structures, vol.34, (11), pp.898–907, 2011

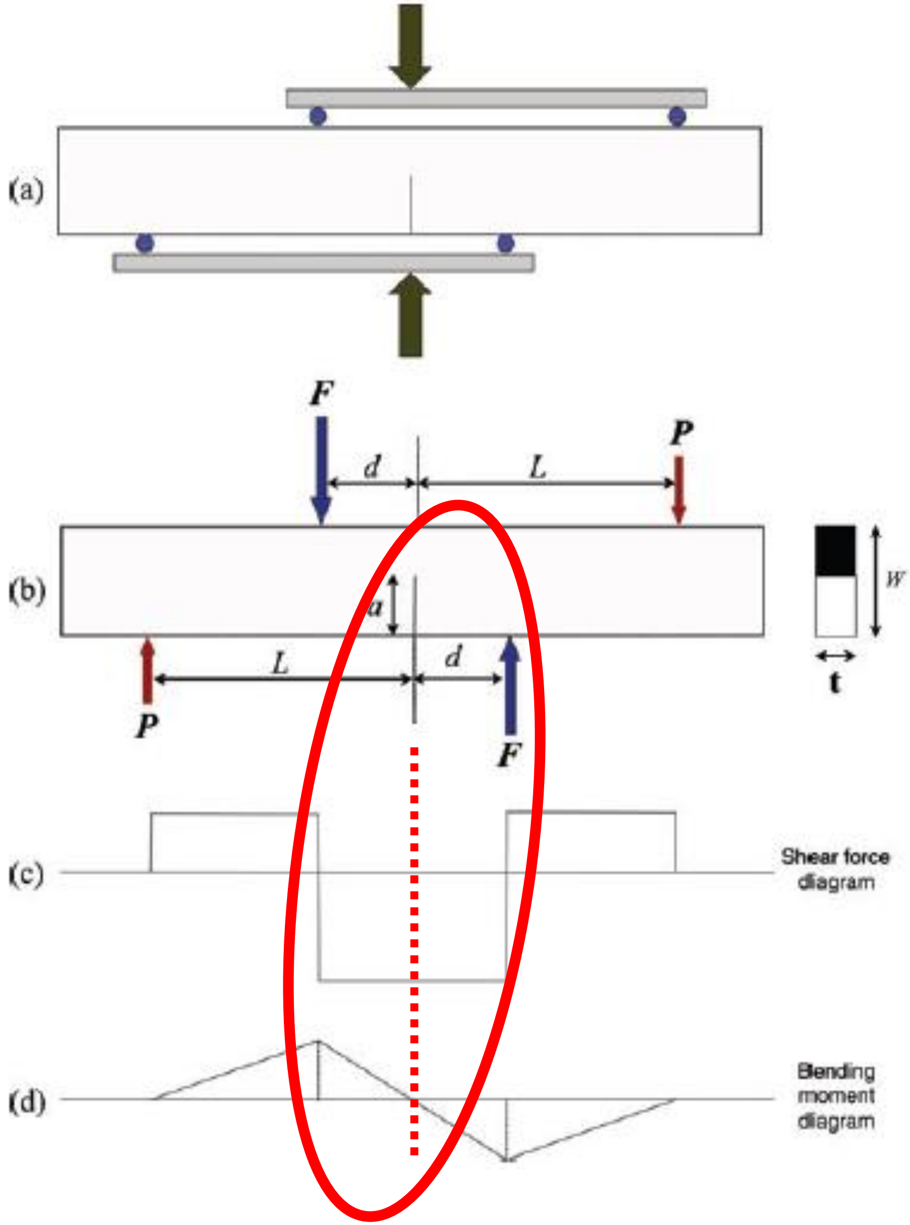

M.R. Ayatollahi, M.R.M. Aliha, Fatigue and Fracture of Engineering Materials and Structures, vol.34, (11), pp.898–907, 2011

The last type of specimen mentioned (4-point bending specimen) allows to test a range of values of the mode I / mode II ratio (mixity value), and, in certain circumstances, allows evaluations of pure mode II (similarly to the Iosipescu notched specimen). Figure shows a notch machined in an AA6082 T6 Aluminum alloy specimen tested in 4-point bending, with cyclic loading and load ratio *R*=0. A pre-crack in mode I was initially made from the machined notch. The clearly visible sudden change in the direction of propagation was caused by the creation of a pure mode II situation, which in this type of test pieces is done changing the position of the load application points.

Example of deviation from the direction of propagation of a crack due to a change in the ratio I mode / mode II (mode mixity): detail of a flexion specimen in 4 points of AA 6082 T6 tested at FEUP by L. Gicquel, 2017

Work by Baganha Marques *et al*. at FEUP shows an AA6082 T6 4-point bending specimen. In one side of the test pieces several auxiliary markings of the test are visible. Again, the change in direction of propagation occurred when a pure mode II situation was created.

Example of deviation from the direction of propagation of a crack due to a change in the ratio of mode I / mode II: 4-point bending tests of AA 6082 T6, FEUP, J. Baganha Marques, 2017.

J. Baganha Marques, FEUP, 2018

Work by Baganha Marques *et al*. at FEUP shows an AA6082 T6 4-point bending specimen. In one side of the test pieces several auxiliary markings of the test are visible. Again, the change in direction of propagation occurred when a pure mode II situation was created.

Example of deviation from the direction of propagation of a crack due to a change in the ratio of mode I / mode II: 4-point bending tests of AA 6082 T6, FEUP, J. Baganha Marques, 2017.

J. Baganha Marques, FEUP, 2018

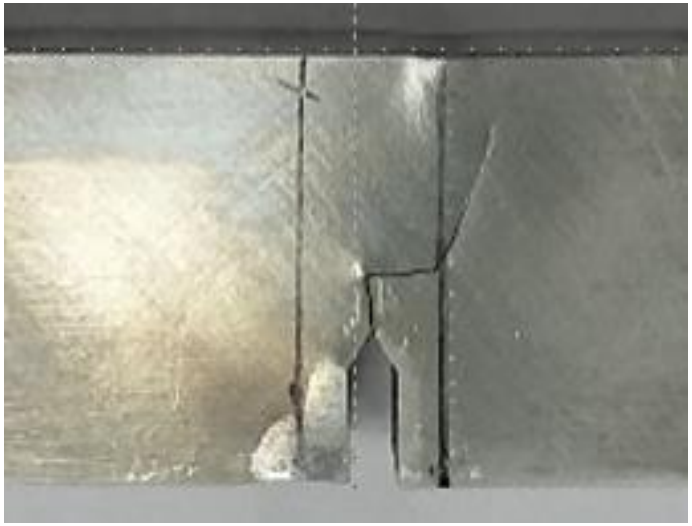

J. Baganha Marques, FEUP, 2018

Next Figure presents experimental values of the angle ψ_0 as a function of the ratio K_I/K_{II}. The K_I/K_{II} ratio is related to the angle β of the basic situation (previous slide) through the relationship:

$$\beta = \arctan\left(\frac{K_I}{K_{II}}\right)$$

The experimental data was compared with theoretical predictions using the MTS and SED (strain energy density) criteria. The figure illustrates the good agreement between the prediction of the SED criterion for the angles of propagation direction at the onset of crack growth from the pre-crack (ψ_0 versus β).

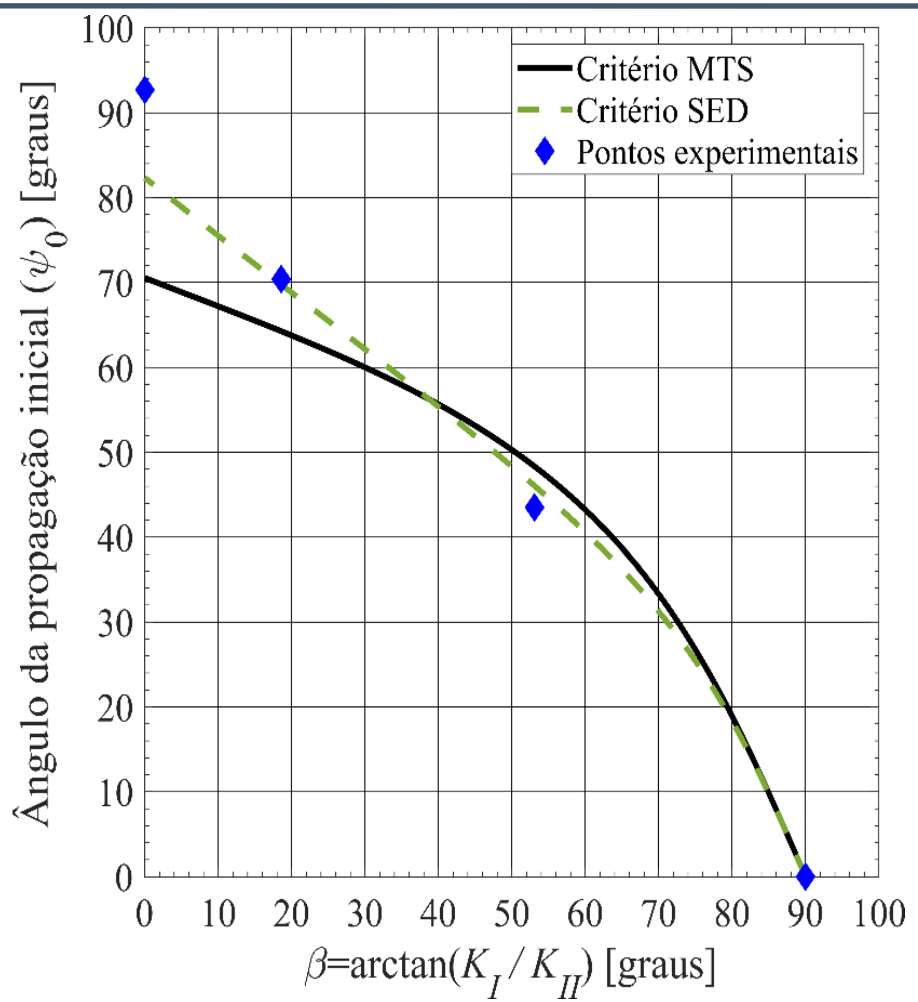

J. Baganha Marques, FEUP, 2018

Paulo C. M. Azevedo, 'Evaluation of the propagation of an inclined crack for the DaToN stiffened panel under uniaxial loading using 3D FE analysis', FEUP, 2008

1. Introduction and Procedure

The finite element (FE) method was used to predict the propagation of an inclined central through crack in the DaToN stiffened panel under uniaxial tensile loading. The 3D analyses were carried out using ABAQUS.
The stress intensity factors (SIFs) were determined using the *J* integral method. After obtaining K_I and K_{II} for the initial inclined crack, subsequent FE analyses were carried out for successive crack increments.

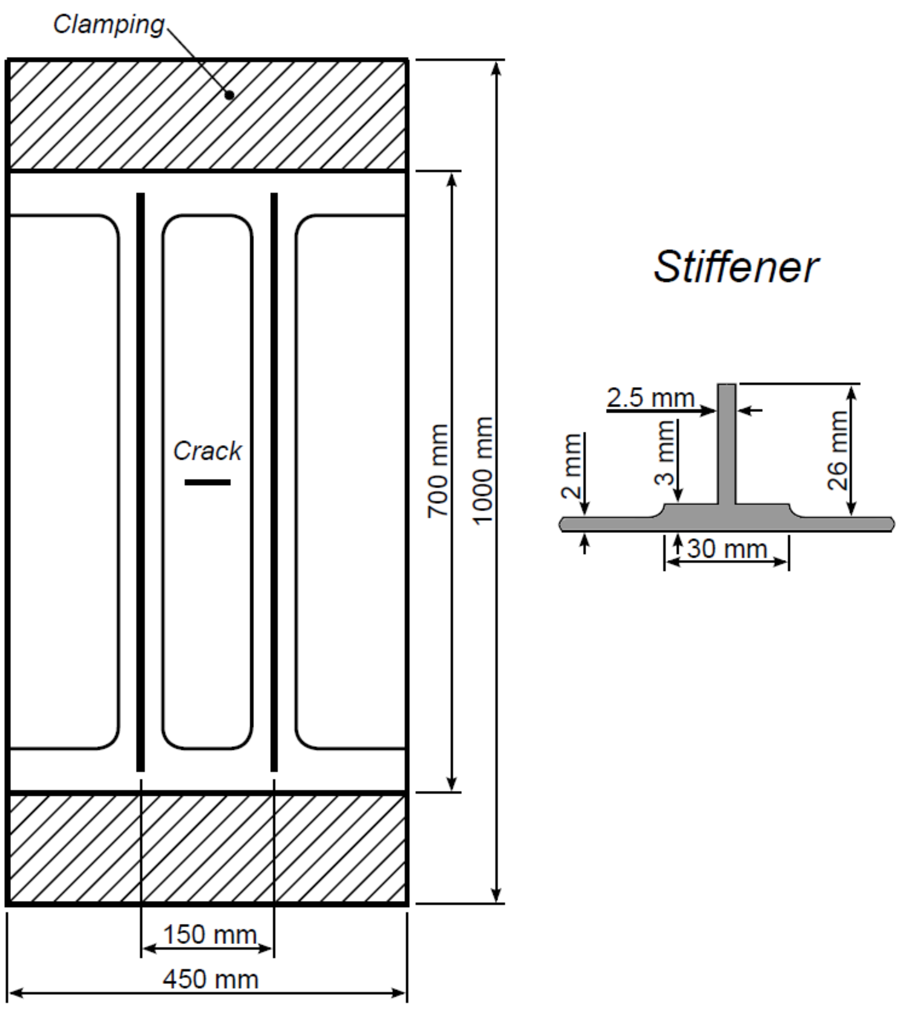

DaToN stiffened panel (specimen geometry)

Paulo C. M. Azevedo, FEUP, 2008

1. Introduction and Procedure

The direction of propagation was predicted based on K_I and K_{II}. The crack increment was the same for all the steps considered, and it was not small enough for this work to serve as a faithful prediction of the crack propagation behavior. All FE simulations are linear elastic.

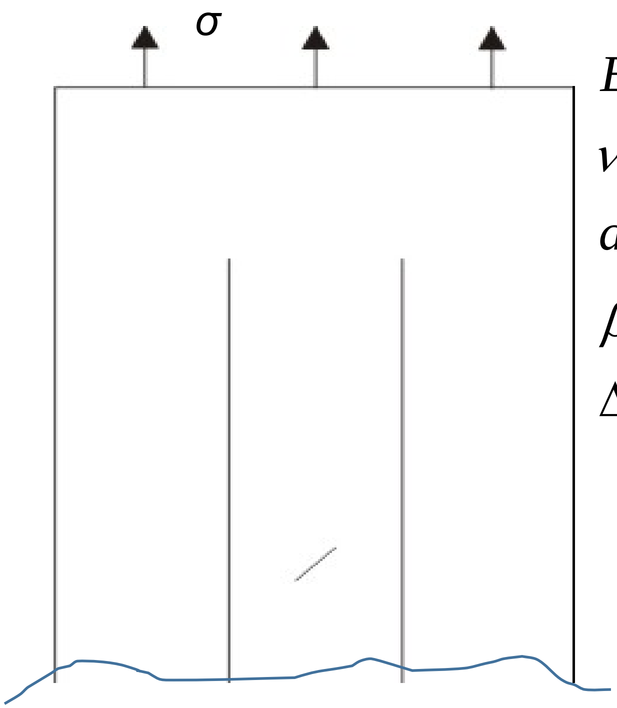

$$E_{Al} = 70 \text{ GPa}$$
$$\nu = 0.33$$
$$a_0 = 25 \text{ mm}$$
$$\beta_0 = 45^{\circ}$$
$$\Delta a = 4 \text{ mm}$$

Loaded panel with initial inclined crack

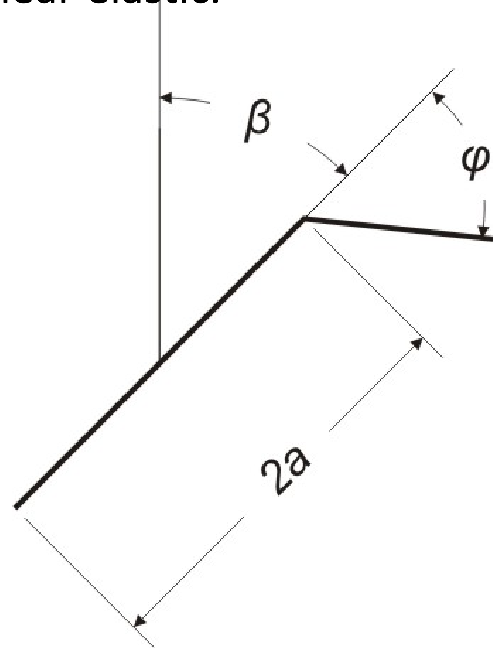

$$K_I \sin\varphi + K_{II}\left(3\cos\varphi - 1\right) = 0$$

Scheme of crack propagation; notation

Paulo C. M. Azevedo, FEUP, 2008

1. Introduction and Procedure

The calculation of the number of cycles is performed considering a dynamic load, even though the FE analyses were static. Since these simulations are carried out for $\sigma = \sigma_{\max} = 110$ MPa the resultant SIFs and *R* are used to determine ΔK_{eq}.

$$\Delta N = \frac{\Delta a}{C\left(\Delta K\right)^m}$$

$$C = 1.371 \times 10^{-11}$$

$$m = 2.744$$

$$R = \frac{\sigma_{\min}}{\sigma_{\max}} = 0.1$$

$$\Delta K_{eq} = \left(1 - R\right) \times \left[K_I \left(\cos\frac{\varphi}{2} \right)^3 - 3K_{II} \left(\cos\frac{\varphi}{2} \right)^2 \left(\sin\frac{\varphi}{2} \right) \right]$$

Paulo C. M. Azevedo, FEUP, 2008

1. Introduction and Procedure

$E_{st} = 210 \text{ GPa} \quad ; \quad \nu_{st} = 0.29$

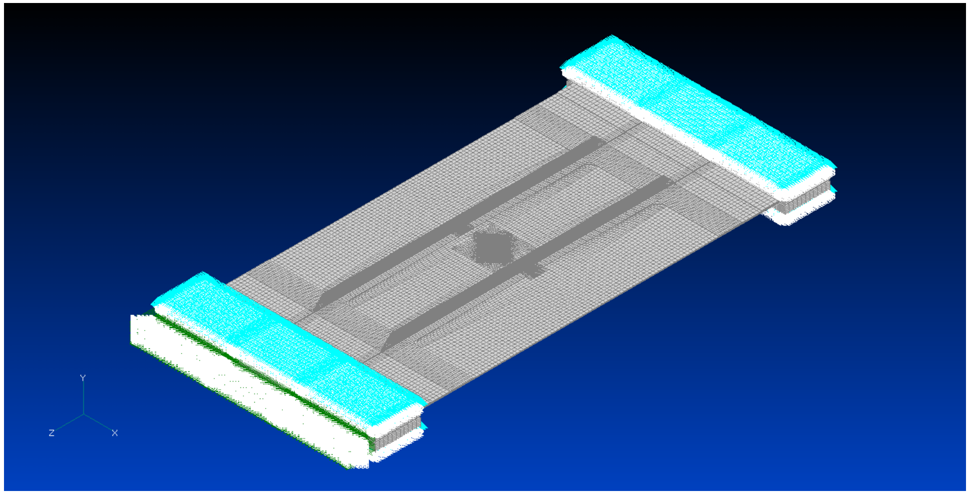

Meshed DaToN panel with load and constraints

Four FE analyses were performed. The distance between each crack tip and the closer mid-side nodes is reduced to half of its original length, for all elements along the thickness of the panel.

Five elements are defined along the thickness of the panel. Therefore, eleven nodes define each crack tip.

The value of φ that defines the direction of the crack increment is the average of all the angles determined for both crack tips, except for the ones that correspond to the surfaces of the panel.

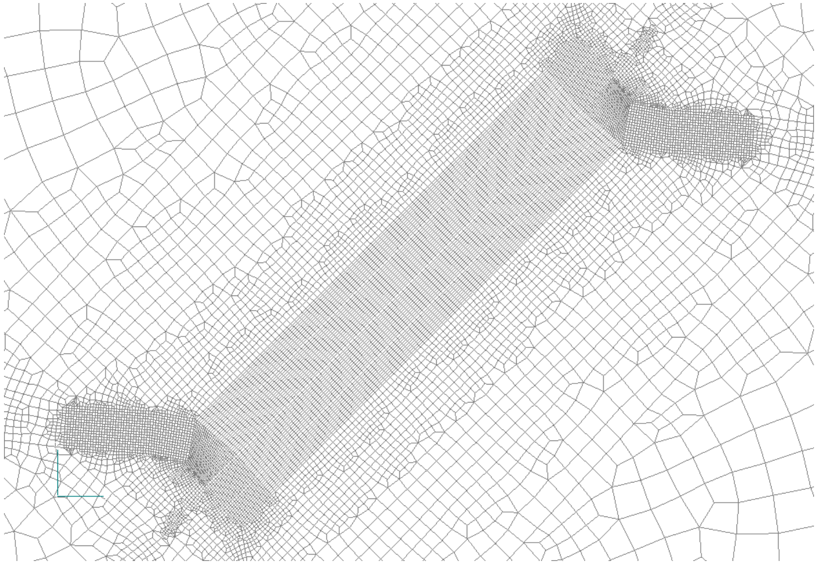

Mesh detail: region of the crack

Paulo C. M. Azevedo, FEUP, 2008

2. FE analysis results

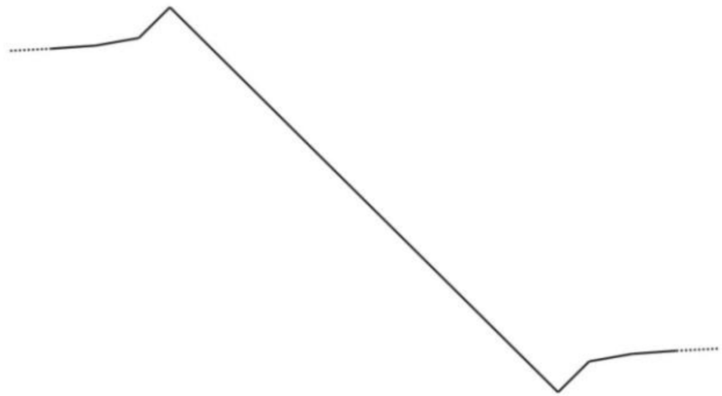

Detail of crack propagation

Analysis	φ (º)	ΔK_{eq} (Nmm$^{-3/2}$)	N
1	90.5	358	2.9E+04
2	-35.0	999	1.7E+03
3	-6.0	1106	1.3E+03
4	-0.8	1176	1.1E+03

Paulo C. M. Azevedo, FEUP, 2008

2. FE analysis results

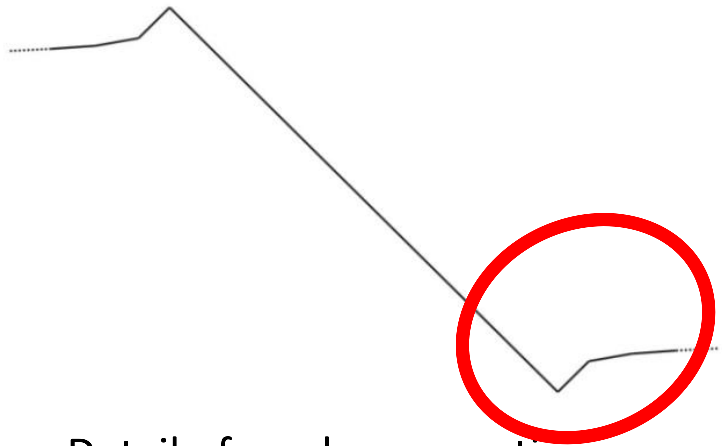

Detail of crack propagation

Analysis	φ (º)	ΔK_{eq} ($Nmm^{-3/2}$)	N
1	90.5	358	2.9E+04
2	-35.0	999	1.7E+03
3	-6.0	1106	1.3E+03
4	-0.8	1176	1.1E+03

Paulo C. M. Azevedo, FEUP, 2008

2. FE analysis results

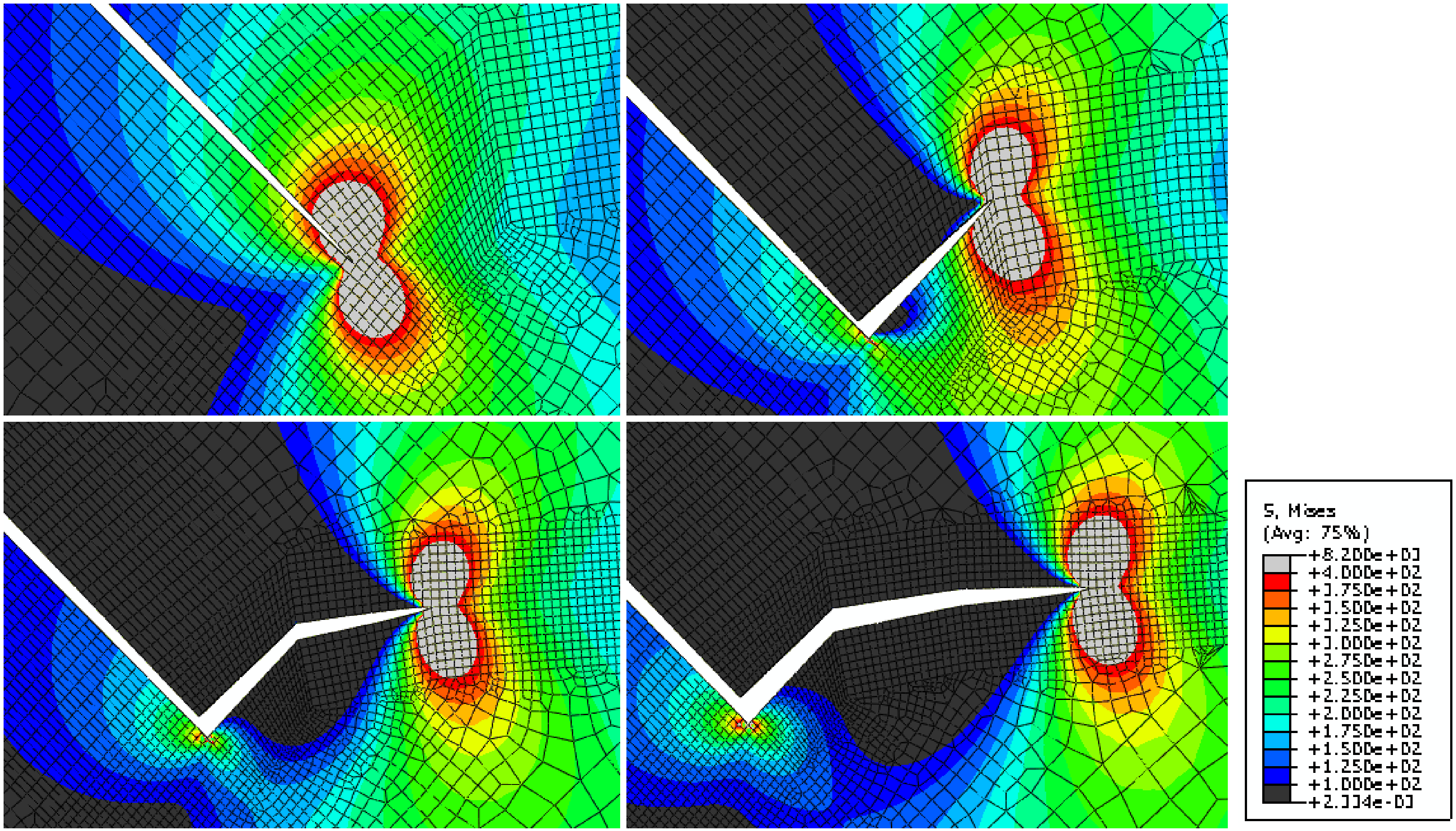

von Mises stress distribution after subsequent crack increments; zoom in the crack tip region

Paulo C. M. Azevedo, FEUP, 2008

3. DBE analysis and correction of propagation direction

Dual Boundary Element (DBE) was used to predict the crack propagation direction for the same problem. The model used is bi-dimensional (constant thickness), and consequently does not include the stiffeners. A plane stress formulation is considered.

An alternative method, based on a simple technique to correct the crack propagation direction, was tested.

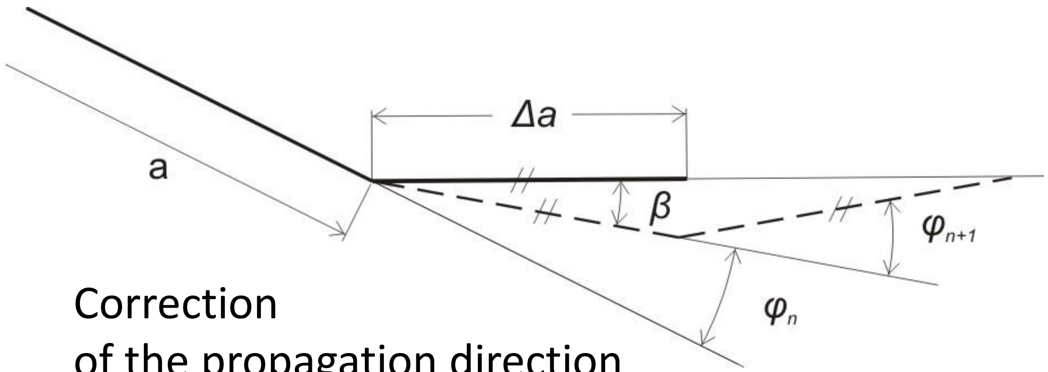

Correction of the propagation direction

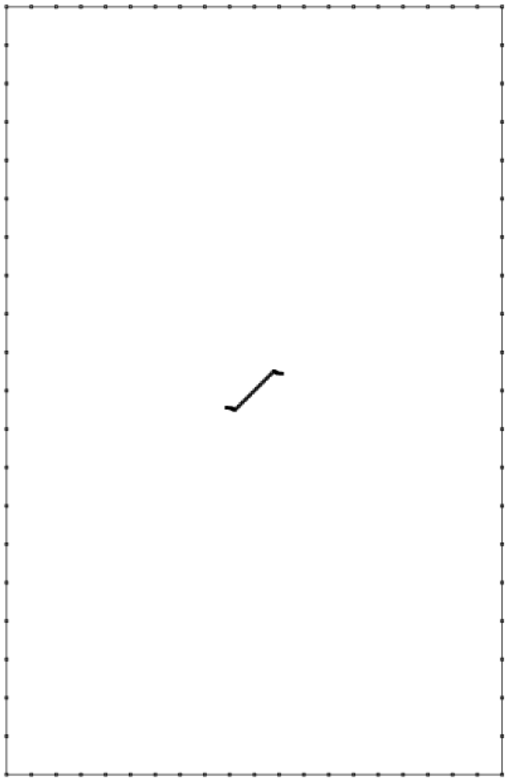

DBE mesh for third analysis (after two increments)

Paulo C. M. Azevedo, FEUP, 2008

3. DBE analysis and correction of propagation direction

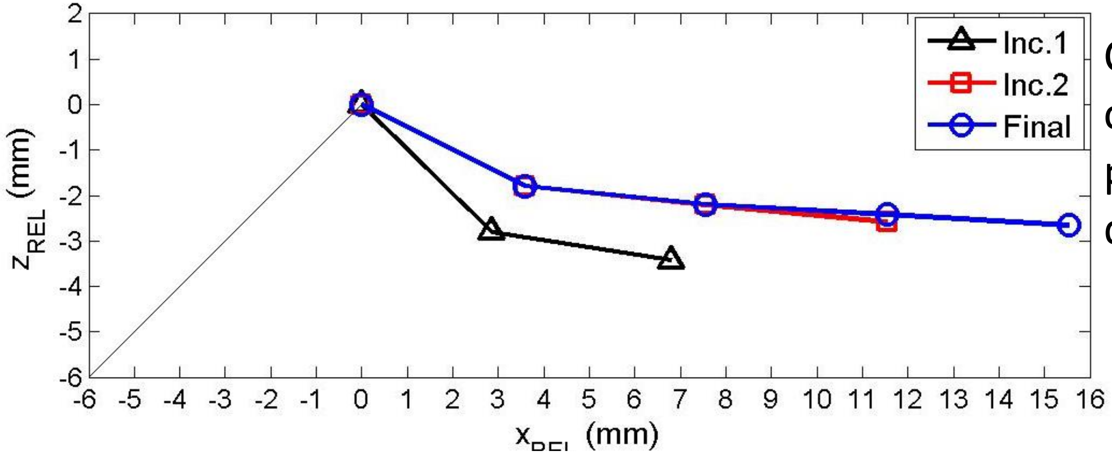

Crack path with correction of the propagation direction

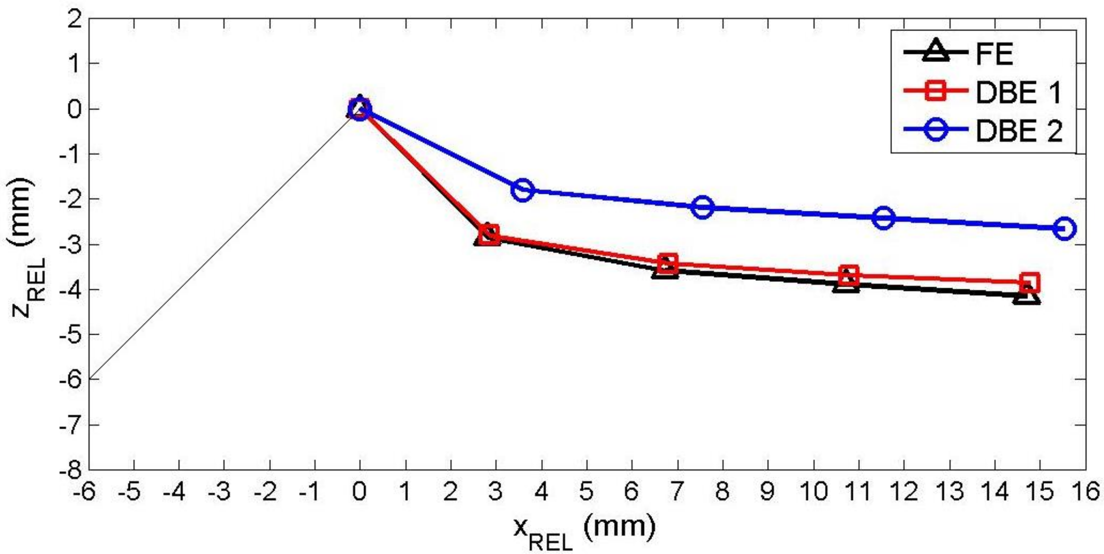

Comparison of the crack paths obtained using the different methods

Paulo C. M. Azevedo, FEUP, 2008

Concluding remarks

Under uniaxial loading, the mixed mode problem considered evolves to an almost pure mode I situation before the crack reaches the stiffeners.

The use of FEM required remeshing for crack growth modelling.

Paulo C. M. Azevedo, FEUP, 2008

Introdução – exs. de casos

- **Haste**
- **Ligação soldada**

Referência a conceitos básicos

- Bibliografia de autores do DEMec da FEUP

Propagação de fendas

- Expansão de furos

Propagação de fendas em modo misto

- O caso da flexão em 4 pontos

Métodos numéricos – o XFEM

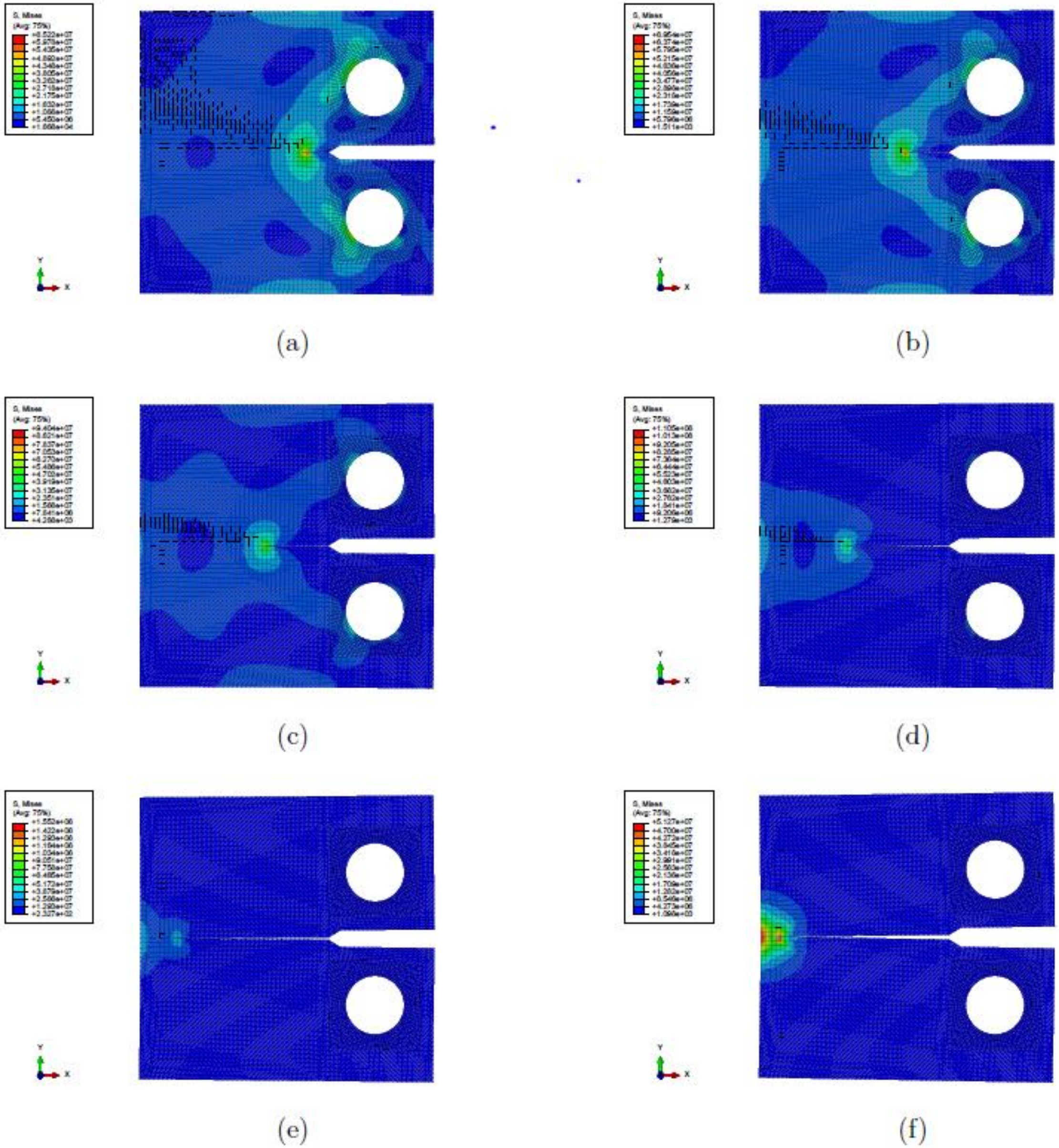

Maria Hermosilla, FEUP, 2016

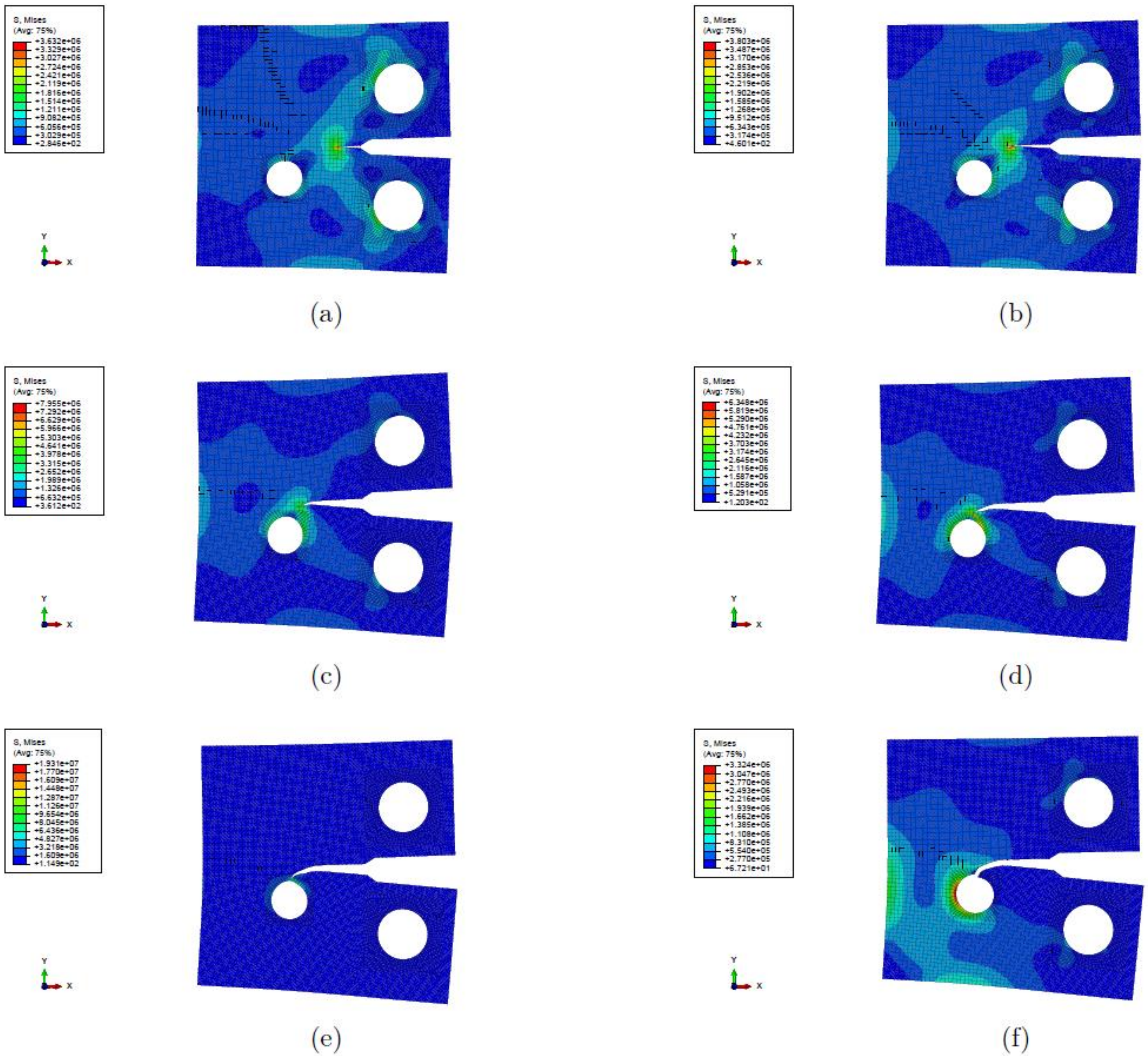

Maria Hermosilla, FEUP, 2016

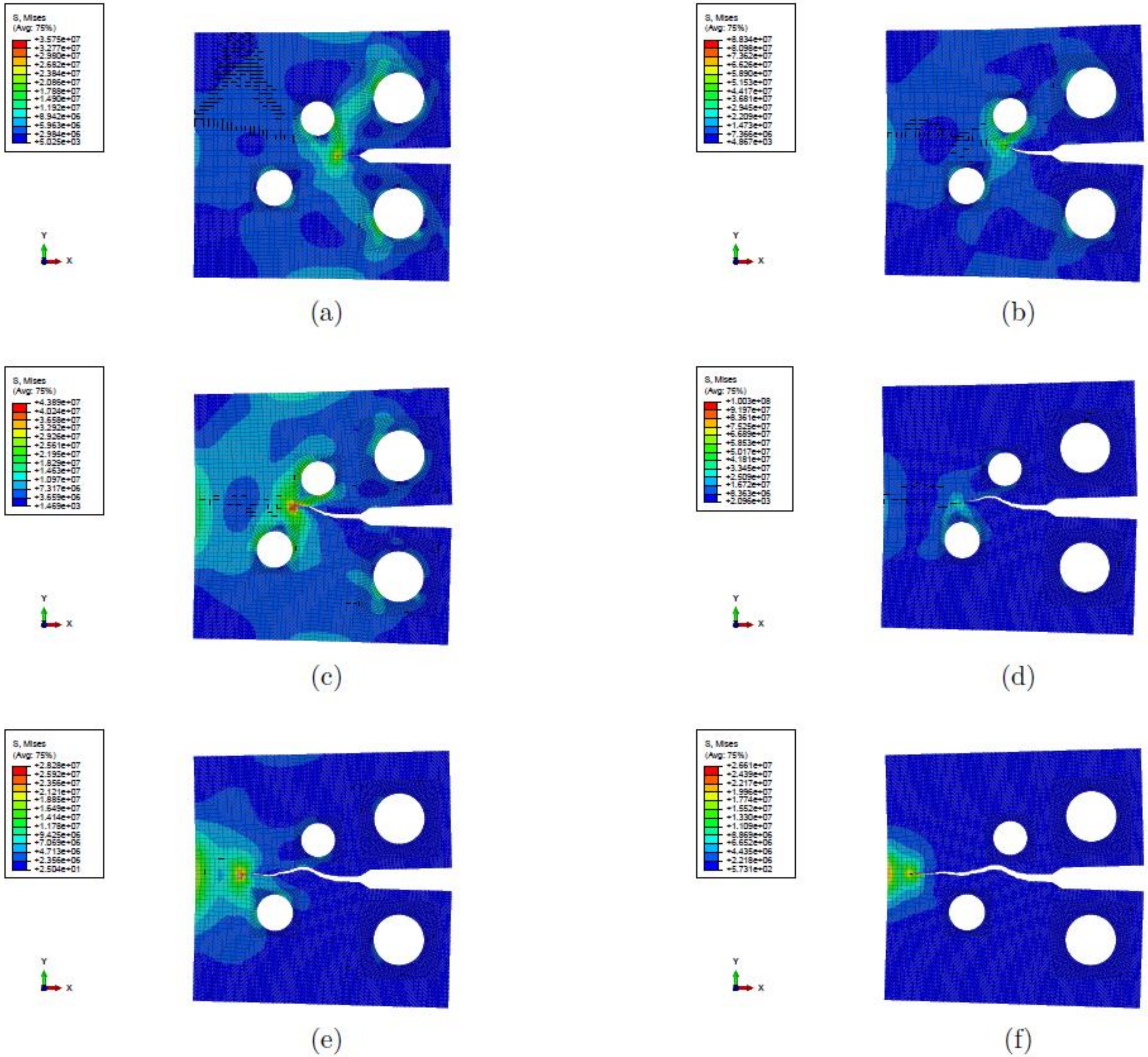

Maria Hermosilla, FEUP, 2016

$$K_I = \frac{F\sqrt{\pi a}}{WB}\frac{\cos\alpha}{1-\frac{a}{W}}\sqrt{\frac{0.26+2.65\left(a/(W-a)\right)}{1+0.55\left(a/(W-a)\right)-0.08\left(a/(W-a)\right)^2}}$$

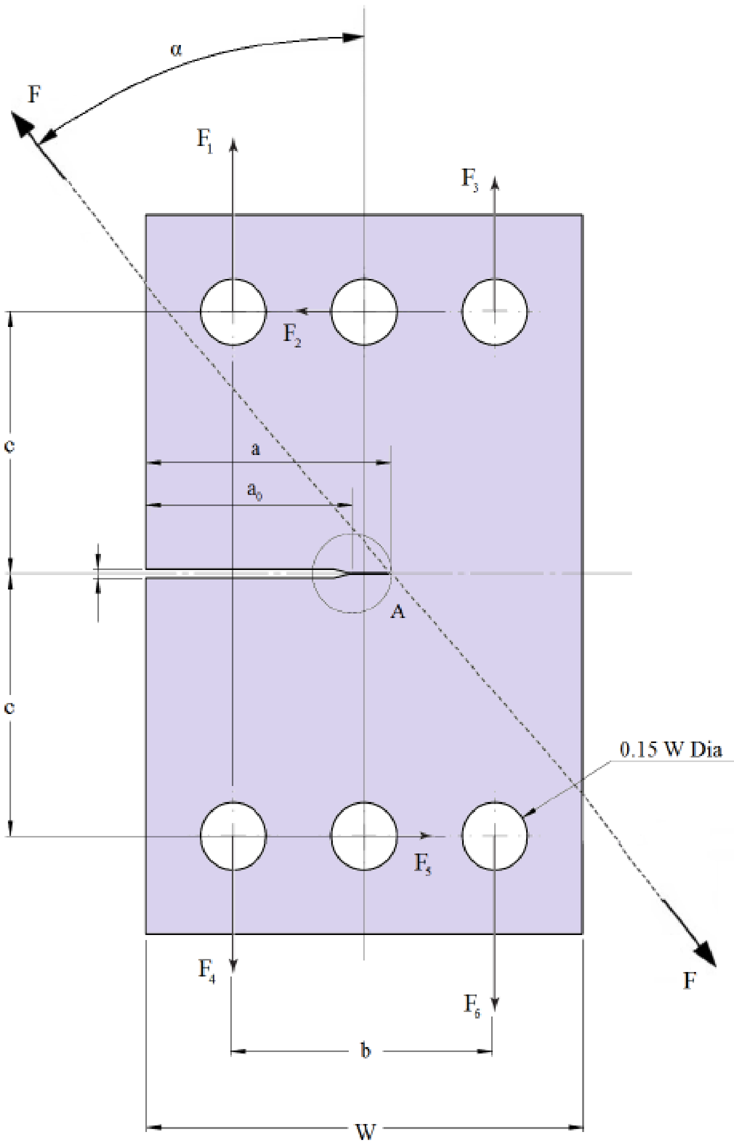

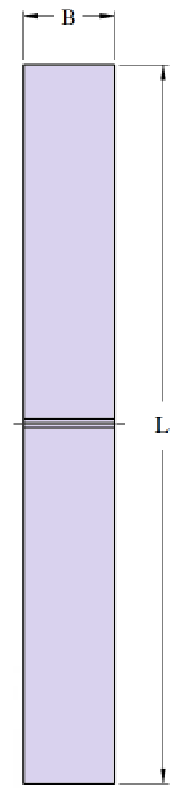

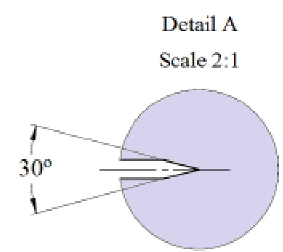

Maria Hermosilla, FEUP, 2016

$$K_{II} = \frac{F\sqrt{\pi a}}{WB}\frac{\sin\alpha}{1-\frac{a}{W}}\sqrt{\frac{-0.23+1.40\left(a/(W-a)\right)}{1-0.67\left(a/(W-a)\right)+2.08\left(a/(W-a)\right)^2}}$$

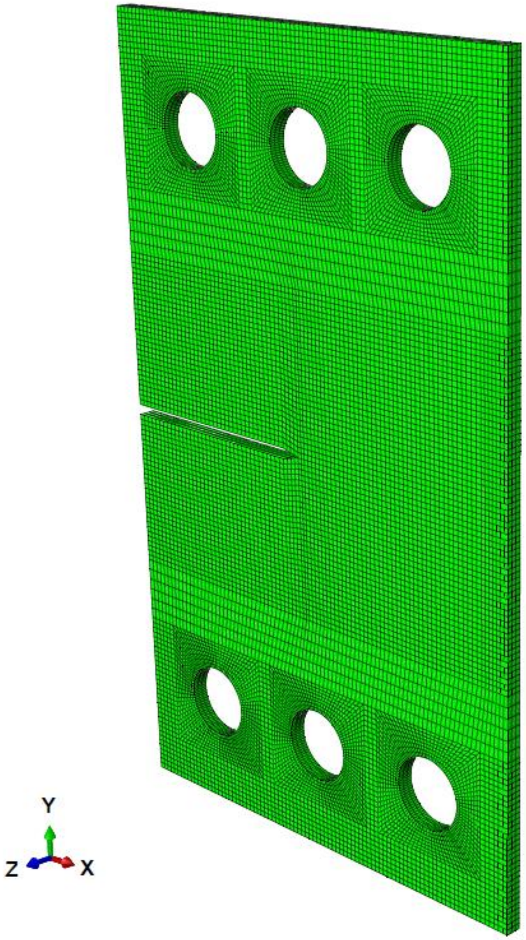

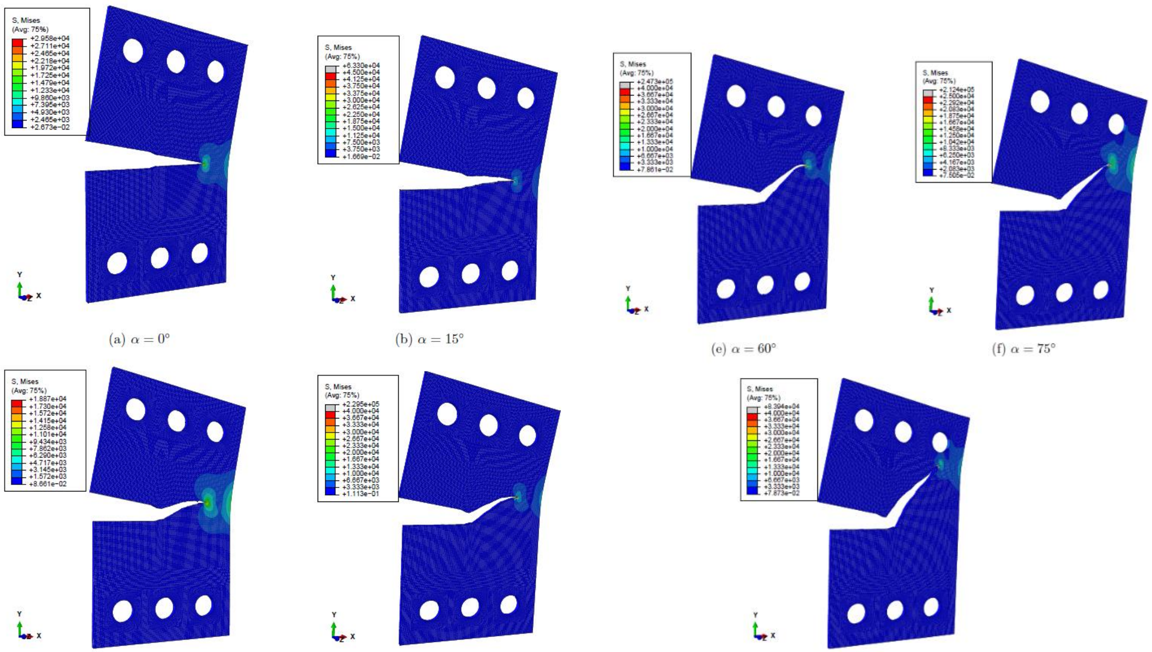

(a) $\alpha = 0°$ (b) $\alpha = 15°$ (e) $\alpha = 60°$ (f) $\alpha = 75°$

(c) $\alpha = 30°$ (d) $\alpha = 45°$ (g) $\alpha = 90°$

Maria Hermosilla, FEUP, 2016

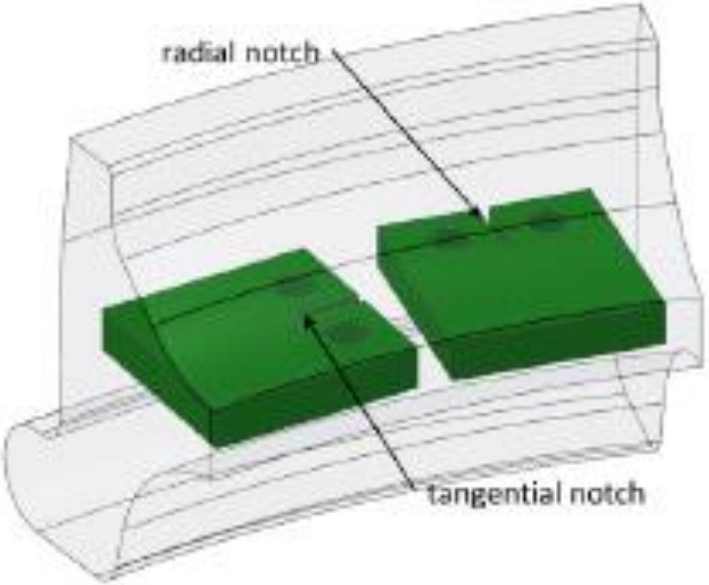

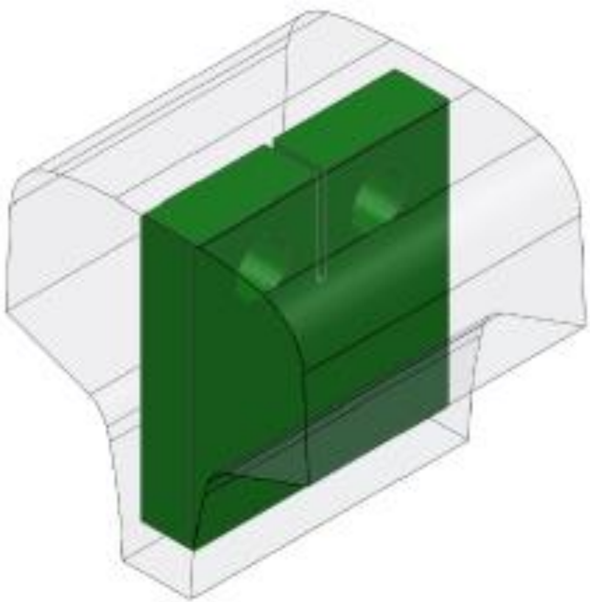

Daniel F. C. Peixoto, doutor., FEUP, 2014

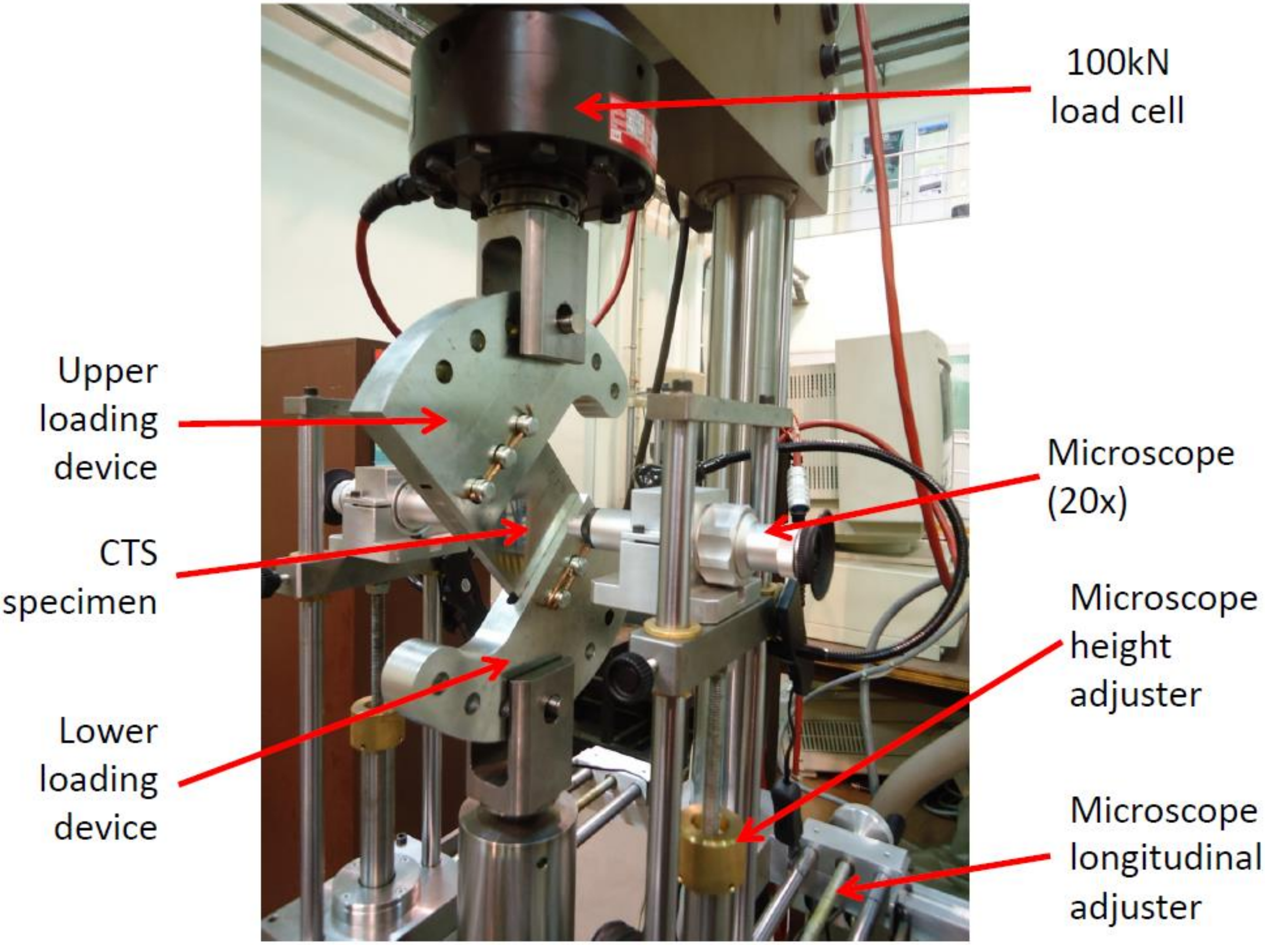

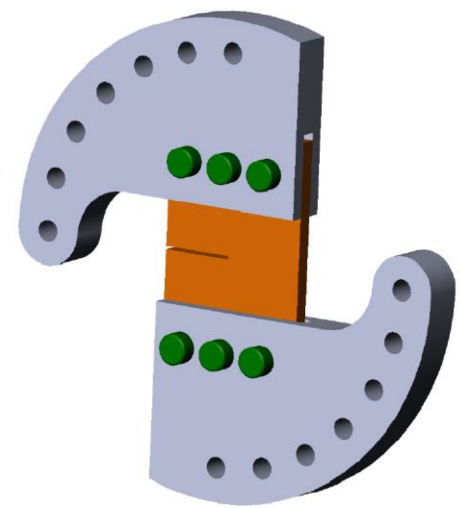

Daniel F. C. Peixoto, doutor., FEUP, 2014

4-point bending

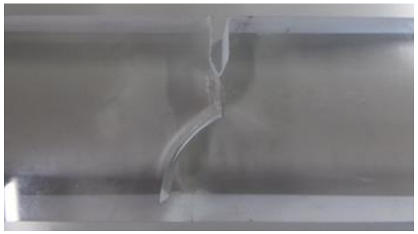

$K_I/K_{II} = 0$

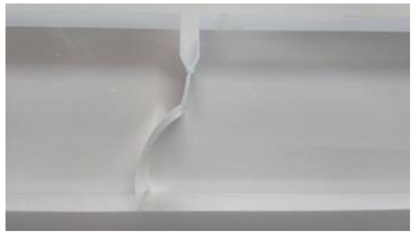

$K_I/K_{II} = 0{,}18$

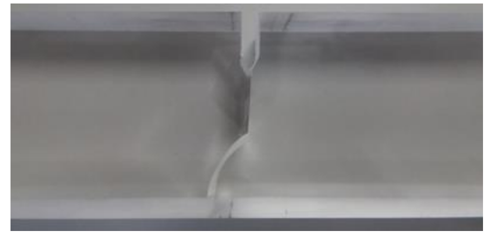

$K_I/K_{II} = 0{,}234$

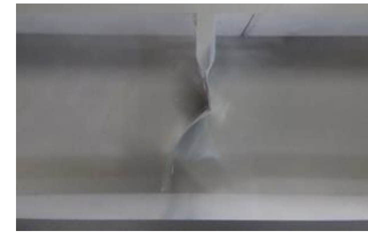

$K_I/K_{II} = 0{,}540$

$K_I/K_{II} = 0{,}899$

$K_I/K_{II} = 0{,}932$

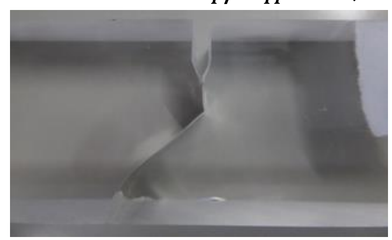

$K_I/K_{II} = 1{,}799$

$K_I/K_{II} = 1{,}857$

$K_I/K_{II} = 2{,}232$

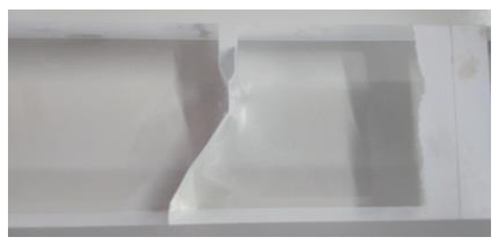

$K_I/K_{II} = 2{,}811$

$K_I/K_{II} = 3{,}749$

Sérgio A. G. Pereira, FEUP, 2018

2D crack path

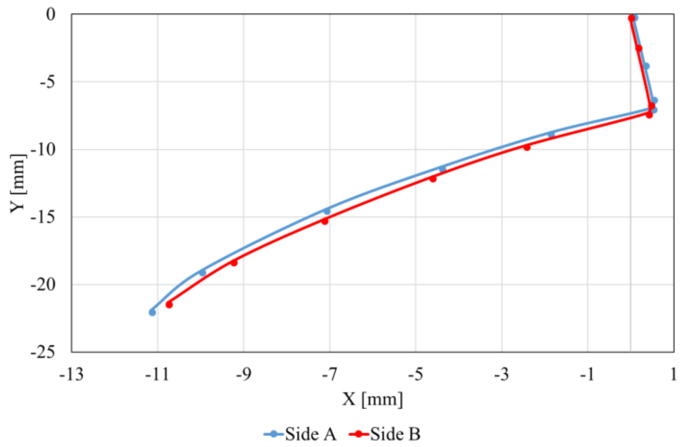

Specimen 1, comparation between both sides

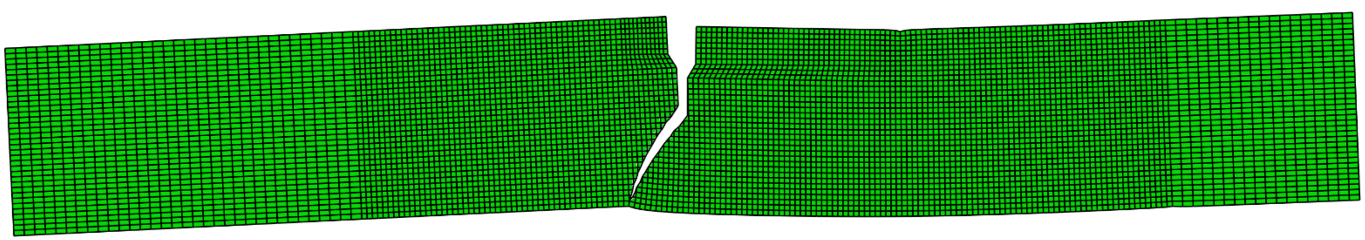

Specimen 8

Sérgio A. G. Pereira, FEUP, 2018